Staphylococcus aureus thermonuclease NucA is a pathogenicity factor for septic arthritis and rhodomyrtone resistance mechanism

Dissertation

der Mathematisch-Naturwissenschaftlichen Fakultät

der Eberhard Karls Universität Tübingen

zur Erlangung des Grades eines

Doktors der Naturwissenschaften

(Dr. rer. nat.)

vorgelegt von

Ningna Li

aus Jiangsu, China

Tübingen

2025

Gedruckt mit Genehmigung der Mathematisch-Naturwissenschaftlichen Fakultät der Eberhard Karls Universität Tübingen.

Tag der mündlichen Qualifikation:	18.07.2025
Dekan:	Prof. Dr. Thilo Stehle
1. Berichterstatter:	Prof. Dr. Friedrich Götz
2. Berichterstatter:	Prof. Dr. Andreas Peschel

Table of contents

Contents

Abbreviations and symbols

Abbreviations

aa	Amino acid
Arg	Arginine
Asp	Aspartic acid
ATP	Adenosine triphosphate
CpG	Cytosine-phosphorothioate-guanine
DMSO	Dimethyl sulfoxide
DNA	Deoxyribonucleic acid
DNase	Deoxyribonuclease
eDNA	Extracellular DNA
Fig.	Figure
Glu	Glutamic acid
h	Hour
IL	Interleukin
kDa	Kilo dalton
kb	Kilo base
LDH	Lactate dehydrogenase
min	Minute
MW	Molecular weight
NF-κB	Nuclear factor kappa B
Ni-NTA	Nickel-nitrilotriacetic acid Ni-NTA
ODN	Oligonucleotide
PBMC	Peripheral blood mononuclear cell
PBS	Phosphate-buffered saline
pH	Potential of hydrogen
PMSF	Phenylmethylsulfonyl fluoride
RNA	Ribonucleic acid
RNase	Ribonuclease
SDS	Sodium dodecyl sulphate
TSB	Tryptic soy broth
Tyr	Tyrosine
TNF	Tumor necrosis factor
WT	Wild type
µM	Micromolar

Symbols

Δ	Genetic deletion
°	Degree
°C	Degree Celsius
µ	Micro
%	Percentage
α	Alpha
β	Beta

Summary

Staphylococcus aureus is a pathogenic bacterium that expresses various pathogenic factors, including envelope-bound adhesins and secreted exoenzymes, such as exotoxins, proteases, and the thermonuclease. Thermonuclease is comprised of a signal peptide, a short pro-peptide, and mature NucA, with the ability to cleave extracellular DNA or RNA. Previous studies have demonstrated that NucA not only degrades the eDNA-based biofilm but also cleaves the NETs and promotes bacterial survival. However, little is known about its pathogenicity in sepsis and septic arthritis.

In this study, the pathogenic role of NucA was determined in a well-established mouse model of septic arthritis. The mice injected with the Δ*nuc1* mutant was much less pathogenic and the severity of clinical septic arthritis was markedly reduced, including decreased weight loss, lower kidney bacterial loads, impaired kidney abscess score, and much less IL-6 production. Notably, μCT scans revealed almost no bone erosion in the joints, suggesting a significant reduction in joint inflammation and damage.

To understand the reasons of the decreased pathogenicity observed in Δ*nuc1*-infected mice, further investigations into the *in vitro* assays were performed. Initially, the assay was performed with bacterial genomic DNA (gDNA) due to its ability to trigger immune responses via the TLR9 receptor and to induce arthritis. gDNA from *S. aureus* induced TNF-α production in a dose-dependent manner, while the stepwise degradation of gDNA by increasing amounts of NucA correlated with a stepwise decrease in TNF-α production in RAW 264.7 cells. Furthermore, live JE2Δ*nuc1* resulted in induced less IL-6 in SAOS-2 cells, and less TNF-α, IL-10, and IL-1RA in neutrophils in comparison to WT, indicating the impact of NucA in immune response.

Moreover, the JE2Δ*nuc1* mutant exhibited decreased survival within neutrophils even blocking the phagocytosis, which prompted us to explore the internalization process in other cell lines. The reduced numbers of JE2Δ*nuc1* were also observed in RAW 264.7 cells, indicating that NucA enhances *S. aureus* survival, which may contribute to an increase in the severity of septic arthritis. In further NETs formation and degradation assay, SYTOX-green screening and immunofluorescence revealed a stronger DNA signal in response to JE2Δ*nuc1* supernatants, thereby suggesting decreased NET degradation in *nuc1*-deletion strain.

In summary, the present study demonstrates that NucA plays a crucial role in the pathogenesis of *S. aureus* septic arthritis, as evidenced by Δ*nuc1*-infected mice. *In vitro* data further support these findings, demonstrating that NucA assists *S. aureus*

in killing and in the degradation of NETs, thereby promoting bacterial survival and worsening disease severity.

In a separate study on the antimicrobial compound Rom, the static and dynamic light scattering and isothermal titration calorimetry analyses demonstrated that both PG and Rom were vesicular and reacted with each other in milliseconds to form a complex. These findings indicate that PG interacts with Rom, thereby abrogating its antimicrobial activity in *S. aureus*, which is confirmed in a Rom^R mutant strain that is resistant to Rom.

Zusammenfassung

Staphylococcus aureus ist ein pathogener Erreger, der eine Vielzahl virulenter Faktoren exprimiert, darunter oberflächengebundene Adhäsine sowie sezernierte Exoenzyme wie Exotoxine, Proteasen und Thermonuklease. Letztere besteht aus einem Signalpeptid, einem kurzen Propeptid und dem reifen Enzym NucA. Thermonuklease ist in der Lage, extrazelluläre DNA (eDNA) und RNA zu spalten. Frühere Studien zeigten, dass NucA nicht nur eDNA-basierte Biofilme abbaut, sondern auch von neutrophilen Zellen freigesetzte DNA (NETs) abbaut und somit das bakterielle Überleben begünstigt. Die Rolle von NucA bei Sepsis und septischer Arthritis ist jedoch bislang kaum untersucht.

In dieser Studie wurde die pathogene Rolle von NucA in einem gut etablierten Mausmodell für septische Arthritis untersucht. Im Gegensatz zum Wildtyp *(S. aureus* Newman) war bei Mäusen, denen die Δ*nuc1*-Mutante injiziert wurde, der Schweregrad der klinischen septischen Arthritis deutlich verringert, einschließlich eines geringeren Gewichtsverlusts, einer geringeren Bakterienzahl in den Nieren, einer geringeren Anzahl von Nierenabszessen und einer wesentlich geringeren IL-6-Produktion. Insbesondere zeigten µCT-Scans fast keine Knochenerosion in den Gelenken, was auf eine deutliche Verringerung der Gelenkentzündung und -schädigung hindeutet.

Um die Gründe der deutlich abgeschwächten Pathogenität von Δ*nuc1* zu verstehen, wurden weitere Untersuchungen zu den *in vitro* Tests durchgeführt. In einem ersten Ansatz wurde genomische DNA (gDNA) von *S. aureus* näher untersucht, die bekanntermaßen über den TLR9-Rezeptor Immunreaktionen auslösen kann. Unverdaute gDNA aus *S. aureus* induzierte TNF-α-Produktion in einer dosisabhängigen Weise. Wurde jedoch gDNA durch zunehmende Menge an NucA schrittweise abgebaut, so nahm auch die TNF-α-Produktion in RAW 264.7-Zellen mit kleiner werdenden DNA-Fragmenten ab. Im Gegensatz zum Wildtypstamm, löste die Nuklease-Mutante, Δ*nuc1*, eine geringere IL-6-Produktion in SAOS-2-Zellen und eine geringeren TNF-α-, IL-10- und IL-1RA-Produktion in Neutrophilen aus, was den Einfluss von NucA auf die Immunstimulation untermauert.

Darüber hinaus wies die Nuclease-Mutante eine verringerte Überlebensrate in Neutrophilen auf, selbst unter Bedingungen, bei denen die Phagozytose blockiert ist. Dies veranlasste uns, den Internalisierungsprozess in weiteren Zelllinien zu untersuchen. Eine verringerte Anzahl von Δ*nuc1* Bakterien wurde auch in RAW 264.7-Zellen beobachtet, was darauf hindeutet, dass NucA das Überleben von *S. aureus* fördert und somit zum Fortschreiten der septischen Arthritis beiträgt. In einem

weiteren Experiment zur Untersuchung der Bildung und des Abbaus von neutrophilen extrazellulären traps (NETs) zeigten sowohl das SYTOX-Grün-Screening als auch die Immunfluoreszenzanalyse ein verstärktes DNA-Signal als Reaktion auf Überstände der Δnuc1-Mutante, was auf eine verminderte NETs-Auflösung in der *nuc1* Mutante schließen lässt.

Zusammenfassend zeigt diese Studie *in vivo* an Mäusen, und auch *in vitro* an Zelllininen dass NucA eine zentrale Rolle in der Pathogenese der septischen Arthritis durch *S. aureus* spielt, und dass NucA die Abtötung von *S. aureus* erschwert und den Abbau von NETs fördert, wodurch das bakterielle Überleben begünstigt, und der Krankheitsverlauf verschlimmert wird.

In einer separaten Arbeit über den antimikrobiellen Wirkstoff Rhodomyrtone (Rom) konnte ich mittels Analysen der statischen und dynamischen Lichtstreuung und der isothermischen Titrationskalorimetrie zeigen, dass sowohl Phosphatidylglycerol (PG) als auch Rom vesikuläre Strukturen aufweisen, und innerhalb von Millisekunden miteinander reagierten, um einen Komplex zu bilden. Mit diesen Ergebnissen wurde belegt, dass dass PG mit Rom interagiert und dadurch die antimikrobielle Aktivität gegen Gram-positive Bakterien abgeschwächt wird. In dieser Arbeit wurde der Resistenzmechanismus in der Rom^R-Mutante aufgeklärt.

List of publications and personal contributions

Publications from the current thesis

1. **Li, N.**, Deshmukh, M.V., Sahin, F., Hafza, N., Ammanath, A.V., Ehnert, S., Nussler, A., Weber, A.N.R., Jin, T., and Götz, F. (2025). *Staphylococcus aureus* thermonuclease NucA is a key virulence factor in septic arthritis. Commun Biol 8, 598. 10.1038/s42003-025-07920-4.

I performed most of the experiments in this paper. I analyzed all the experimental data. I wrote and reviewed the manuscript under the guidance of Prof. Friedrich Götz.

2. Huang, L., Matsuo, M., Calderon, C., Fan, S.H., Ammanath, A.V., Fu, X., **Li, N.**, Luqman, A., Ullrich, M., Herrmann, F., et al. (2021). Molecular Basis of Rhodomyrtone Resistance in *Staphylococcus aureus*. mBio 13, e0383321. 10.1128/mbio.03833-21.

I contributed to growth curve, static and dynamics light scattering analysis and isothermal titration calorimetry analysis and wrote up related results.

Publications <u>not</u> from the current thesis

1. Hafza, N., **Li, N.**, Luqman, A., and Götz, F. (2023). Identification of a serotonin N-acetyltransferase from *Staphylococcus pseudintermedius* ED99. Front Microbiol 14, 1073539. 10.3389/fmicb.2023.1073539.

I contributed to the method of protein purification.

2. Linnemann, C., Sahin, F., **Li, N.**, Pscherer, S., Götz, F., Histing, T., Nussler, A.K., and Ehnert, S. (2023). Insulin Can Delay Neutrophil Extracellular Trap Formation In Vitro-Implication for Diabetic Wound Care? Biology (Basel) 12. 10.3390/biology12081082.

I contributed the bacterial killing assay and bacterial sample preparation.

3. Rahmdel, S., Purkayastha, M., Nega, M., Liberini, E., **Li, N.**, Luqman, A., Bruggemann, H., and Götz, F. (2024). Diversity of Neurotransmitter-Producing Human Skin Commensals. Int J Mol Sci 25. 10.3390/ijms252212345.

I performed the screening HPLC analysis with skin-isolated bacteria.

General Introduction

Staphylococcus aureus

S. aureus was first discovered from the post-operative wound abscess of patients by Sir Alexander Ogston and was initially named Staphylococcus (Ogston 1881). Later, Rosenbach successfully isolated and cultivated this bacterium from abscesses and referred to it as *Staphylococcus aureus,* indicating its yellow-orange characterization (Rosenbach and Rosenbach 1884). Currently, *S. aureus* belongs to the genus Staphylococcus, which contains more than 30 different species.

S. aureus is regarded as both a commensal bacterium and a human pathogen, possessing the capacity to colonize many human body sites, such as the skin, nose, hands, and pharynx (Wertheim et al. 2005). This colonization leads to increased susceptibility to infections. *S. aureus* is responsible for a wide spectrum of infections with high morbidity and mortality, such as bacteraemia, infective endocarditis, skin and soft tissue infections, and osteoarticular infections (Tong et al. 2015).

Antibiotics are frequently used to treat *S. aureus* infections. However, due to inappropriate use, *S. aureus* has developed resistance to several antibiotics, such as penicillin and methicillin, resulting in methicillin-resistant *S. aureus* (MRSA) (Howden et al. 2023). MRSA has become a major concern in hospitals leading to severe and challenging infections recently. These highly pathogenic MRSA strains have been developed globally, highlighting the urgent need for effective treatment methods (Hassoun, Linden and Friedman 2017).

Virulence factors

S. aureus expresses a variety of virulence factors that assist bacterium to colonize, transmit, and invade to host cells. These virulence factors encompass secreted virulence factors, such as toxins and the extracellular enzyme, the cell surface component, and pathogen-associated molecular patterns (PAMPs) (Tam and Torres 2019).

Toxins

S. aureus secretes toxins, which comprise approximately 10% of the secretome. These toxins can be classified into pore-forming toxins (PFTs), superantigens (SAs), and exfoliative toxins (ETs).

There are two kinds of β-barrel PFTs in *S. aureus*: α-hemolysin (α-toxin, Hla) and bi-component cytotoxins. The absence of Hla in *S. aureus* LAC strain has been demonstrated the abolishment of lung infection in a pneumonia model (Bubeck Wardenburg et al. 2007). Bi-component cytotoxins are hetero-oligomeric leucocidins,

such as panton-valentine leucocidin and γ-hemolysins. Studies have identified their high cytotoxicity to neutrophils and monocytes (Loffler et al. 2010, DuMont et al. 2013).

Phenol-soluble modulins (PSMs) are a class of small peptides, which are encoded in PSMα (PSMα1- PSMα4), PSMβ operon (PSMβ1- PSMβ2) or within the sequence of RNAIII (δ-toxin) (Peschel and Otto 2013). PSMs have been investigated for their ability to lyse neutrophils via formyl-peptide receptor 2 (FPR2) and to boost excretion of cytoplasmic proteins (Rautenberg et al. 2011, Ebner et al. 2017).

SAs are nonglycosylated exoproteins with a molecular weight ranging from 19 to 30 kDa. In a mouse model, the SA-expressing strain promotes IFN-γ production and increases bacterial burden in liver when compared to the SA-deficient strain (Tuffs et al. 2022).

ETs are serine proteases, which typically cause staphylococcal scalded skin syndrome (Bukowski, Wladyka and Dubin 2010). The enzymes possess the ability to cleave the extracellular domain of desmoglein 1, thereby enabling bacteria to circulate and spread in the skin (Imanishi et al. 2019, Amagai et al. 2002).

Extracellular components

The extracellular enzymatic components comprise cofactors that activate host enzymes and enzymes that degrade host components. Staphylokinase (Sak), canonical coagulase (Coa) and von Willebrand factor binding protein (vWbp) are expressed as cofactors to activate host zymogens. Other enzymes, such as proteases, lipases, hyaluronidases and nucleases, play roles in the degradation of host components (Tam and Torres 2019).

Sak binds to the plasminogen, then cleaving the fibrin network around infected tissue and allowing the bacteria to enter (Bokarewa, Jin and Tarkowski 2006). Coa binds to prothrombin with DID2 domain while vWbp shares the homology of DID2 domain which binds to prothrombin and fibrinogen (Kroh, Panizzi and Bock 2009, Friedrich et al. 2003).

Proteases are classified into cysteines, serine proteases, and metalloproteases. *S. aureus* only has one metalloprotease, aureolysin (Aur). Aur is autocatalytic activated by its proAur via the N-terminal fungalysin-thermolysin-propeptide domain (Nickerson, Joag and McGavin 2008). Aur cleaves the antimicrobial peptide LL37, aiding *S. aureus* in its survival (Sieprawska-Lupa et al. 2004).

Staphopain A (ScpA) and Staphopain B (SspB) are two homologous cysteine proteinases. Lacking ScpA results in decreased host cell death (Stelzner et al. 2021).

SspB has the capacity to cut CD11b on phagocytes which protects *S. aureus* from phagocytosis (Smagur et al. 2009).

V8 protease and serine protease-like proteins A to F (SplA-SplF) belong to the category of serine proteases. Exogenous V8 facilitates induced adhesion to host cells (McGavin et al. 1997). Moreover, it degrades proteinase-activated receptor 1, thereby contributing to itch in the host (Deng et al. 2023). Spls share 30.4%-36.4% of aa identity with V8 proteases. In a rabbit pneumonia model, the *spl* operon deficient mutant exhibits reduced pathogenicity than WT (Paharik et al. 2016).

The lipase 1 and 2 (SAL1 and SAL2) have been identified in *S. aureus*, encoded by *gehA* and *gehB*, respectively. Deletion of both lipases leads to impaired biofilm formation (Nguyen et al. 2018a).

β-toxin (also known as β-hemolysin) and phosphatidylinositol-specific phospholipase C (PI-PLC) are two phospholipases in *S. aureus*. β-toxin promotes colonization on the skin and activates epidermal growth factor receptor via sphingomyelinase activity, which in turn induces skin inflammation (Jia et al. 2024, Katayama et al. 2013). PI-PLC plays a role in immune evasion that deletion of *plc* results in decreased bacterial survival within whole blood and neutrophils (White et al. 2014).

Hyaluronidase cleaves the hyaluronic acid polymer, which is encoded by *hysA*. The *hysA* mutant shows lower bacterial burden and lung pathology in a murine model of pulmonary infection (Ibberson et al. 2014).

Cell surface components

S. aureus expresses a spectrum of cell wall-anchored proteins, which are anchored to peptidoglycan. These proteins can be categorized into microbial surface component recognizing adhesive matrix molecule (MSCRAMM), near iron transporter (NEAT), G5–E repeat three-helical bundle motif protein, and other proteins (Foster et al. 2014).

The MSCRAMM family refers to the protein that has the ability to bind to the host cell proteins from the extracellular matrix. It contains two adjacent IgG-like folds and employs a ‘dock, lock and latch’ (DLL) mechanism for binding. For instance, fibronectin-binding proteins (FnBPs) link to integrin α5β1 for invasion, and FnBPA contributes to biofilm formation in mammalian serum (Sinha et al. 1999, Gries et al. 2020).

NEAT family, containing iron-regulated surface proteins (Isd), IsdA, IsdB, and IsdH, functions as heme transport. IsdB has the capacity to induce the TLR4 signaling pathway, initiating the immune response (Gonzalez et al. 2024).

Protein A (SpA) is a three-helical bundle motif protein capable of binding various proteins, such as von Willebrand factor, IgG Fc, and TNFR-1. *spA*-deficient strain fails to induce bone erosion and loss in osteomyelitis cases (Widaa et al. 2012, Falugi et al. 2013).

The G5-E domain family includes SasG-I and SasG-II. SasG-I mediates the adhesion to corneocytes with SasG-II binding to lectin subdomain (Mills et al. 2024). Other proteins, such as adenosine synthase A (AdsA) and surface protein X (SasX), also contribute to the pathogenicity of the bacterium. For instance, AdsA converts the adenosine monophosphate to adenosine, thereby impeding phagocytosis clearance (Thammavongsa et al. 2009).

Pathogen-associated molecular patterns (PAMPs)

The host innate immune system recognizes conserved structural of bacteria with patter recognition receptors (PRRs), known as PAMPs. These PAMPs include lipoproteins (Lpps), peptidoglycan (PGN), lipoteichoic acid (LTA), DNA, and other components (Akira and Hemmi 2003).

Lpps are anchored in the outlayer of the cytoplasmic membrane. The number of Lpps in *S. aureus* is approximately 70 with high identity, and 30% of them are involved in nutrient transport (Graf et al. 2018). The mature Lpps contain a conserved lipobox, which has a cysteine residue on it becoming lipidated and the start of aa. The modification of mature Lpps requires three distinct enzymes. The phosphatidylglycerol-pro-Lpp diacylglyceryl transferase (Lgt) puts an *sn*-1,2-diacylglyceryl group from phosphatidylglycerol (PG) to the cysteine via a thioether bond forlipidation. Afterwards, prolipoprotein signal peptidase (Lsp) cleaves the signal peptide. Apolipoprotein *N*-acyltransferase (Lnt) acts as the final enzyme to cause a mature *N*-acyl-*S*-diacylglyceryl-cysteine (Buddelmeijer 2015). *S. aureus* has a lipoprotein N-acyl transferase system (LnsA and LnsB) for *N*-acylation (Gardiner et al. 2020). In *S. aureus*, deletion of *lgt* results in the loss of lipidation in pre-Lpp, while the deletion of *lsp* leads to the missing of signal peptide processing (Kurokawa et al. 2012, Sankaran and Wu 1994).

Lpps are the predominant ligands for Toll-like receptor 2 (TLR2) pathway in *S. aureus* (Hashimoto et al. 2006). The *lgt* mutant, lacking lipidation in pre-Lpp, causes much lower cytokines production in host cells and abscess formation in a murine model (Bubeck Wardenburg, Williams and Missiakas 2006, Stoll et al. 2005). In addition, the presence of Lpps has been shown to facilitate bone erosion with increased TLR2 pathway for osteoclast differentiation, enhanced cytokines, and upregulation of RANKL expression (Kim et al. 2013).

PGN is composed of long sugar chains with multiple peptide side chains. The purified PGN induces a dose-dependent activation of the TLR2 pathway (Dziarski and Gupta 2005). LTA comprises a diglucosyl diacylglycerol glycolipid that anchored to the cytoplasmic membrane and the polymeric backbone (Fischer, Mannsfeld and Hagen 1990). In immune response, LTA has been observed to activate the CD14, LBP, and TLR2 pathway, while inhibit the T-cell activation in a TLR2-independent manner (Schroder et al. 2003, Hattar et al. 2017, Kaesler et al. 2016).

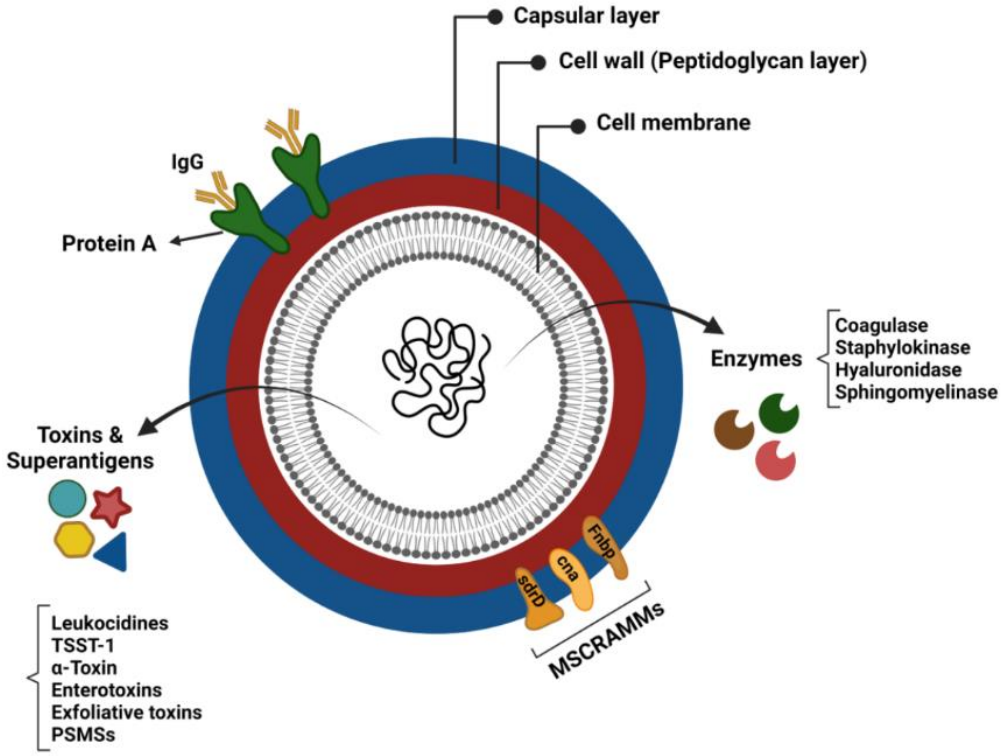

Fig. 1.1 Schematic representation of virulence factors in *S. aureus*. Adapted with permission from (Shaghayegh et al. 2022). Reuse followed the Creative Commons Attribution (CC BY) license (https://creativecommons.org/licenses/by/4.0/).

Nuclease

Nuclease is an enzyme that cleaves the phosphodiester bonds in nucleic acids. These enzymes encompass DNase, RNase, recombinase, and ribozymes.

Catalytic reaction

Nucleases cleave the bridging P–O bonds at the 3′ or 5′ position in nucleic acids. This reaction consists of nucleophilic attack, formation of penta-covalent bipyramid intermediate, and breakage of scissile bond. They produce the 5′-phosphates and 3′-OH groups mostly, with the exception of Tyr-dependent site-specific recombinases, Type IB topoisomerases (TopIBs), and RNase, which use a 2′,3′-cyclic phosphodiester intermediate (Yang 2011).

Nuclease classification

Nucleases can be classified in many ways. One classification is dependent on their substrate preference, which is divided into DNase and RNase. Exo- and endonucleases are distinguished based on their substrate recognition whether they identify a 5′ or 3′ end or whether they process a single or oligo- nucleotides. Endonucleases cut within the molecule, while exonucleases cut at the end (Chase and Richardson 1974). However, it is notable that some nucleases exhibit characteristics of both exo- and endonucleases (Shen et al. 2005). Additionally, based on their catalytic mechanism, they use different ions for the reaction, normally with Mg^{2+}, Ca^{2+}, and Zn^{2+} (Ivanov, Tainer and McCammon 2007). However, certain nucleases, such as recombinase, RNase T1, and T2 catalyse molecules without ions (Deshpande and Shankar 2002).

S. aureus nucleases

The secreted nuclease was first identified in *S. aureus* by Cunningham in 1956 (Cunningham, Catlin and De Garilhe 1956). This nuclease (NucA) displays both ribonuclease and deoxyribonuclease activities and is classified as a member of the sugar-nonspecific class (Tucker, Hazen and Cotton 1978). NucA is a 5′-phosphodiesterase, catalysing the nucleic acids to generate 3′-nucleotides, dinucleotides, and phosphates (Anfinsen 1968). It utilizes Ca^{2+} as a cofactor but is inhibited by the presence of Hg^{2+}, Zn^{2+}, and Cd^{2+} (Cuatrecasas, Fuchs and Anfinsen 1967). It prefers DNA as a substrate over RNA. The optimal pH for NucA is pH 9.2 and its optimal temperature is 55 ^{o}C (Hu et al. 2013). NucA is considered as a thermostable nuclease that still has 10% activity left even after being kept to 120 ^{o}C for 34 min (Erickson and Deibel 1973). Due to its thermal unfolding and lacking disulfide bridges, it is regarded as a model for protein-folding (Chen et al. 2000).

The mature form of NucA contains 149 aa. The crystal structure reveals that the Tyr-113 and Tyr-115 form a binding pocket for nucleotide and Ca^{2+} links to the Asp-21, Asp-40, and Glu-43 (Hynes and Fox 1991). The complex structure with thymidine 3',5'-bisphosphat shows a proposed mechanism in which Glu-43 and the water molecule help for the nucleophilic attack, further promoted by Ca^{2+} and hydrogen bonds from Arg-35 and Arg-87 (Cotton, Hazen and Legg 1979).

In the *S. aureus* USA300 genome, NucA is encoded by nuc (SAUSA300_0776 or SAUSA300_RS04185). The *nuc* gene encodes the nuclease (Nuc1), a protein comprising 228 aa. The Nuc1 consists of a signal peptide (60 aa long), a pro-peptide (19 aa long), and the mature part (NucA) (Davis et al. 1977). NucA is secreted outside. During the secretion process, the signal peptide is cleaved, generating NucB which contains pro-peptide (Suciu and Inouye 1996). The NucB can be

cleaved by PMSF-sensitive extracellular protease *in vivo* or a protease from strain V8 *in vitro* to get NucA (Davis, Parr and Taniuchi 1979, Miller, Kovacevic and Veal 1987). In *S. aureus*, the pro-peptide is not necessary and the kinetic assay for refolding indicates similar activity in NucA and NucB (Davis et al. 1979).

Based on the whole genome sequence, the second thermonuclease has been identified. It is encoded by *nuc2* (SAUSA300_1222 or SAUSA300_RS06625) in USA300, referred to as Nuc2 (Diep et al. 2006). It is a sugar non-specific endonuclease. Further sequence alignments show that both Nuc1 and Nuc2 have a conserved active site, a DTPE motif, and a metal-binding site (Kiedrowski et al. 2014).

However, many differences exist between Nuc1 and Nuc2. Nuc2 contains 177 aa and only shares 34.6% sequence identity with Nuc1. Unlike the secreted Nuc1, Nuc2 is anchored in the cell surface, facing the extracellular environment (Kiedrowski et al. 2014). In a phylogenetic analysis of thermonucleases, Nuc2 belongs to the *Staphylococcus* cluster, while the Nuc1 is classified with other bacteria, such as *Enterococcus faecalis*, *Bacillus. Subtilis*, and *Listeria monocytogenes* (Hu et al. 2013). Additionally, the expression of those two also varies. The transcript of *nuc1* starts from the early exponential phase and reaches the maximum in the post-exponential growth phase. Conversely, the *nuc2* is expressed from the beginning and starts to decline at the early exponential phase (Hu et al. 2012). Moreover, the optimal pH for Nuc2 is 10 for catalytic activity, and its optimal temperature is 70 ^{o}C. Nuc2 has been detected in much lower activity compared to Nuc1 (Kiedrowski et al. 2014). In addition, the biofilm formation in Δ*nuc2* mutant was not significantly affected compared to the Δ*nuc1* mutant. In a hematogenous mice model, the Δ*nuc2*-infected mice exhibit comparable phenotypes to WT strain while the Δ*nuc1* is less pathogenic to mice, indicating Nuc2 does not contribute significantly to virulence like Nuc1 (Yu et al. 2021). Consequently, the discussion will focus on Nuc1.

Due to the specificity of thermonuclease Nuc1, molecular approaches have been developed to detect *S. aureus* based on it. These approaches include phosphorescent-based, fluorescent-based, and colorimetric-based nuclease sensors (Samani et al. 2021). For example, the synthetic oligonucleotides with chemical modifications and fluorophore and quencher, TT probe, have been investigated to be activated by Nuc1 cleavage, which has been confirmed in a mouse model (Hernandez et al. 2014, Burghardt et al. 2016).

Biological functions

Recent studies have reported that the *nuc* gene is regulated by the SaeRS two-component system. SaeR is a two-component system comprising a histidine kinase

(SaeS) and a regulator (SaeR). This system functions as a global regulator to mediate the gene expression (Voyich et al. 2009). In the *sae* mutant, the *nuc* gene expression is significantly reduced. Further experiments have confirmed that SaeR binds to *nuc* protomer in a dose-dependent way, indicating the mediation of *nuc* by Sae (Olson et al. 2013).

Nuclease has been described with a variety of biological functions, including degradation of eDNA/RNA of biofilm and interruption of DNA backbone of neutrophils extracellular traps (NETs). These will be discussed in the following text.

S. aureus biofilm is the bacterial community that produces a membrane-like extracellular matrix (ECM). ECM refers to the extracellular polymeric substances including secreted proteins, polysaccharides, eDNA, and components of host factors. The process of biofilm formation involves several stages, including adhesion to the surface, formation of microcolony, maturation of the biofilm, and dispersal process. The early stage of biofilm development is sensitive to DNase treatment. In the *nuc1*-deficient mutant, enhanced eDNA and biofilm formation are detected (Kiedrowski et al. 2011). The exodus of biofilm has been abrogated in this mutant, leading to the hyperproliferation of biofilm (Moormeier et al. 2014). In addition, during the process of biofilm sloughing, Δ*nuc1* mutant has been observed to release more cells and bigger particles from detachment of large particles of biofilm (Kaplan and Horswill 2024). It has been also found that the biofilm thickness is influenced by different solid surfaces, and no significant differences are observed between WT and Δ*nuc1* mutant on glass, silanized glass, or Pluronic F-127-coated silanized glass, but elicited differences in biomass accumulation (Forson, van der Mei and Sjollema 2020).

Neutrophils represent the primary line of defence within innate immune cells, which generate NETs and engage in phagocytosis to defend against bacterial infections. NETs consist of a DNA backbone and a variety of proteins. Previous work has indicated that *S. aureus* triggers the formation of NETs within a short time (Pilsczek et al. 2010). After being stimulated by *S. aureus*, NETs can be eliminated by extracellular DNase and even can be degraded by *nuc1*-producing strains. Moreover, the *nuc*-producing strain has been less entrapped and killed in neutrophils compared to the *nuc*-deficient strain, suggesting that Nuc1 helps to evade killing (Berends et al. 2010). Immunoglobulin and sub-clindamycin have been observed to inhibit the nuclease activity in a concentration-dependent manner in a clindamycin-susceptible MRSA strain. Incorporating immunoglobulin or sub-clindamycin decreases NET degradation but amplifies the bacterial clearance in neutrophils (Schilcher et al. 2014).

Further work has extended the investigation on macrophages and neutrophils together. The mutant strains lacking *nuc* or adenosine synthase A (*adsA*) have been found that staphylococci exist within the neutrophils cuff in infiltrated macrophages, while the completed strain restores to WT phenotype that the staphylococci located in the neutrophils cuff far away from macrophages. In vitro assay has identified that the DNA converts into deoxyadenosine (dAdo) after the NETs degradation, which is toxic to macrophages. This process needs both nuclease and AdsA (Thammavongsa, Missiakas and Schneewind 2013). The dAdo is transported by the hENT1(human equilibrative transporter) through the plasma membrane. Furthermore, the purine salvage pathway kinases, containing the kinase (ADK) and deoxycytidine kinase (DCK), convert the dAdo to dAMP, dADP, and dATP. This leads the caspase-3 activation and subsequent cell apoptosis (Winstel, Missiakas and Schneewind 2018). Besides, AdsA has been found to combine the nuclease to convert the degraded DNA to deoxyguanosine (dGuo). This process is also mediated by hENT1, facilitating the transfer of dGuo to dGMP, dGDP, and dGTP, thus inducing cell death. These findings demonstrate that the combination of nuclease and AdsA results in the synthesis of dGuo and dAdo, promoting cell death (Tantawy et al. 2022). Additionally, the biofilm-formed *nuc1* mutant treated with neutrophils has been observed to cause more NETs release than WT. The extracellular bacteria are reduced compared to the neutrophils-associated bacteria in the *nuc1* mutant, indicating the Nuc1 is independent of phagocytosis for survival in a biofilm-formed environment (Bhattacharya et al. 2020).

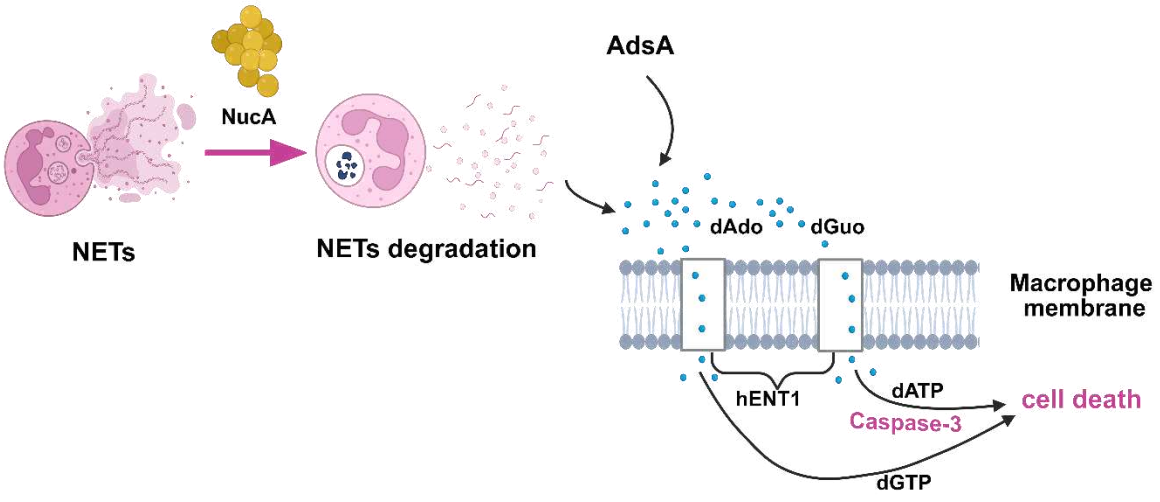

Fig. 1.2 Function of NucA in neutrophils and macrophages. NucA degrades the DNA backbone of NETs and then combines with AdsA to convert fragments into dAdo and dGuo. dAdo and dGuo are transferred into macrophages via hENT1 and convert to dATP and dGTP separately, thereby inducing Caspase3-activated cell death. Created in https://BioRender.com.

Many studies have also shown the role of Nuc1 in murine models and clinical cases. In a murine implant infection model, the existence of Nuc1 has been found to be associated with higher survival, increased biofilm formation, and elevated production of myeloperoxidase with citrullinated histones. The presence of Nuc1 also induces the apoptosis of immune cells (Forson et al. 2021). In a peritonitis model, the bacteria burden in the heart, kidney, and peritoneum is reduced in Δ*nuc1*-infected mice after 8 h of infection, indicating a lower degree of pathogenesis (Olson et al. 2013). In the exogenous Implant-Associated Infections (IAI) mouse model, IAI Δ*nuc1/2*-injected mice have also been found with higher survival and enhanced viability in THP-1 cells (Yu et al. 2021). In clinical cases, long-persistence *S. aureus* has a significantly higher nuclease activity, which accordingly has better growth in comparison to lower nuclease activity isolates in neutrophils (Herzog et al. 2019, Ludwig et al. 2023).

Other nucleases

It has been demonstrated that other bacteria can produce nucleases that play similar biological roles to that of Nuc1. Group A *Streptococcus* (GAS) is a pathogenic bacterium that expresses several extracellular DNases (Sumby et al. 2005). In a murine model, the three-DNase-deficient strain exhibits faster clearance and lower infection. Sad1 is one of the potent DNases in GAS. It can degrade genomic DNA which aborted TLR9-stimulated IFN-α and TNF-α production in murine macrophages, and both cytokines are reduced in *sad1*-deficient GAS-infected mice (Uchiyama et al. 2012). Moreover, Sad1 has been identified to promote NETs degradation and reduce survival in neutrophils, a function analogous to that of Nuc1 (Buchanan et al. 2006). *Streptococcus suis* has also been observed to degrade NETs via nuclease A (SsnA) and endonuclease A (de Buhr et al. 2015).

The immune response

The immune response induced by *S. aureus* includes innate and adaptive immune systems. Normally, the innate immune response is regarded as a non-specific response, which requires macrophage, neutrophils, or other cells, while the adaptive immune response is considered as a specific response, which is recognized by B and T cells (Krishna and Miller 2012).

Innate immune response

The innate immune response is initiated at the epithelial barrier, tissue-resident cells, blood, and lymph nodes (macrophages, neutrophils, keratinocytes, and monocytes, etc.) (Bekeredjian-Ding, Stein and Uebele 2017). They recognize *S. aureus* PAMPs through pattern recognition receptors (PRRs) and induce the expression of proinflammatory mediators, including antimicrobial peptides, cytokines, and

chemokines, to regulate the early defense against infection (Takeuchi and Akira 2010).

Neutrophils

Neutrophils are professional phagocytes with a short life, which are abundant in the innate immune system. They are widely regarded as the primary phagocytic defense against *S. aureus* infection (Segal 2005). *S. aureus* is initially recognized by PRRs located on the epithelial barrier. This recognition elicits cytokines production and adhesion molecules upregulation on the endothelium. The adhesion compounds, including L-selection, E-selection, and P-selection, regulate the capture, rolling, adhesion, and crawling of neutrophils (Petri, Phillipson and Kubes 2008). After this phase, cell adhesion proteins, integrins, and junctional proteins facilitate neutrophils to transmigrate through the venular wall to the infection sites (Ley et al. 2007, Sadik, Kim and Luster 2011). In this way, the neutrophils rapidly accumulate in the infection tissue.

Once arriving at the site of infection, neutrophils initiate phagocytosis, which involves binding and invading pathogens. Neutrophils detect *S. aureus* via PRRs(Kawai and Akira 2011). Involvement of these receptors not only triggers cytokines expression but also stimulates the production of reactive oxygen species (ROS), which in turn enhances the bactericidal activity, cytokines expression, and phagocytosis (Kanneganti, Lamkanfi and Nunez 2007). However, PRRs recognition alone is insufficient to stimulate the phagocytosis. Studies have demonstrated that this process can be accelerated when pathogen is opsonized by host serum factors (complement, antibody, and receptors). Notably, the phagocytosis process itself also induces other immunomodulatory effectors that recruit additional neutrophils and activate other cells (McGuinness, Kobayashi and DeLeo 2016).

After *S. aureus* invades, neutrophils employ both oxygen-dependent and oxygen-independent mechanisms to eliminate the microorganism. The oxygen-dependent process relies on the generation of ROS. Studies have shown that high levels of ROS are produced by NADPH oxidase (NOX2) in phagosomes. NOX2 functions to transfer the electrons from the cytosolic NADPH to inside molecular oxygen, thereby releasing superoxide (Winterbourn and Kettle 2013). The resulting superoxide has strong antimicrobial activity and has been found to produce other secondary antimicrobial oxygen derivatives, such as H2O2, HOCl, and ONOO− (Rigby and DeLeo 2012). H2O2 is catalyzed by myeloperoxidase (MPO) with chloride to HOCl, thereby contributing to antimicrobial activity (Nauseef 2014). The oxygen-independent system requires antimicrobial peptides and proteins, which are fused in

granules with phagosomes (Hirsch and Cohn 1960). Taken together, the combination of both systems ensures efficient clearance of pathogens by neutrophils.

Another significant antimicrobial mechanism is NETs. NETs consist of a DNA backbone with mitochondrial DNA and nucleus DNA, proteases, granular proteins, and peptides (Brinkmann et al. 2004, Lood et al. 2016). Previous work has demonstrated that more than 20 proteins are composite in NETs, such as histones, neutrophil elastase (NE), MPO, actin, and calprotectin (Urban et al. 2009). Two distinct forms of NETs have been identified: one is suicidal NETosis, which leads to neutrophil death within 3-8 hours; another is vital NET formation, which entraps bacteria in a short time within NETs vesicle (Papayannopoulos 2018). The formation of vital NETs is typically associated with TLR pathway or opsonized bacteria, which develop when first neutrophils migrate to the infection sites (Yipp et al. 2012, Pilsczek et al. 2010). This process involves the decondensation of the nucleus to form chromatin and granule contents, followed by blebbing to DNA-containing vesicles. ROS initiates the MPO to induce translocation of NE to nucleus, leading to decondensation of chromatin (Papayannopoulos et al. 2010). The MPO-NE pathway is responsible for chromatin decondensation, while MPO-deficiency abolishes the ability to form NETs (Metzler et al. 2011). Histone deamination, contributing to chromatin modification, is regulated by peptidylarginine deiminase 4 (Wang et al. 2004). Following the decondensation of chromatin, antimicrobial contents are transferred to the extracellular space without damaging the plasma membrane (Fuchs et al. 2007, Yipp et al. 2012). Till now, this whole process remains unclear and need further investigation.

Macrophages

Macrophages are professional phagocytic cells, which ingest pathogens and induce immune response to facilitate their death. Macrophages are originated from monocytes, dendritic cells, and precursor cells. Like neutrophils, macrophages recruit to the infection site and engage in phagocytosis. However, macrophages have longer lifetime, ranging from weeks to month while neutrophils only have several hours (Davies et al. 2013). Furthermore, they exhibit a more limited inflammation response.

The epithelial PRRs recognize *S. aureus* and produce pro-inflammatory cytokines and chemokine, leading to the recruitment of macrophages to the infection site. Upon encountering the pathogens, macrophages use macropinocytotic, receptor-regulated endocytosis, and phagocytosis mechanisms to invade pathogens. *S. aureus* invades through a receptor-regulated phagocytosis process with Fc receptors (FcRs), complement receptors, and scavenger receptors (SRs). After the initial

internalization process, macrophages construct a cup-like structure with the actin cytoskeleton to form the phagosome (Swanson 2008).

Once *S. aureus* has been internalized, multiple responses are generated by macrophages to clear pathogens. These responses encompass producing ROS, reactive nitrogen species (RNS), nutrition restriction, antimicrobial peptides and enzymes, and autophagy (Flannagan, Heit and Heinrichs 2015).

Recent studies have also identified that macrophages elicit the formation of extracellular traps (mETs), which consist of a DNA-backbone structure analogous to NETs (Aulik, Hellenbrand and Czuprynski 2012). Previous studies have shown that pretreatment of human macrophages with statins boosts the expression of mETs, thereby helping the clearance of *S. aureus* (Chow et al. 2010).

TLR signaling pathway

Toll-like receptors (TLRs) are proteins that first identified in the context of dorsoventral axis formation and then are continued by other researcher to elucidate their biological functions (Lemaitre et al. 1996, Janeway 1989). TLRs are classified as type I transmembrane proteins and share high similarity in their domains. They all possess an N-terminal domain with leucine-rich repeat (LRR) to bind ligands, a C-terminal signaling domain, and a transmembrane helix domain (Bell et al. 2003). There are 10 TLRs in humans, whereas 13 in mice. Notably, TLR1-9 are conserved in both species, while TLR10 functions in human and TLR11 functions in mice (Yarovinsky et al. 2005). Each TLR is in a distinct position and recognizes specific PAMP ligands, causing immune response. Based on PAMP ligands and cellular locations, TLRs are divided into two groups. The first group, comprising TLR3, TLR7, TLR8, TLR9, TLR11, TLR12, and TLR13, recognizes microbial nucleic acid and is expressed in intracellular endosomes. The second group, including TLR1, TLR2, TLR4, TLR5, TLR6, and TLR10, is located on the plasma surface and detects the cell surface compounds (Duan et al. 2022, West, Koblansky and Ghosh 2006). These TLRs detect the PAMPs of *S. aureus*, mediating host-pathogen interaction. For instance, TLR2, along with TLR6, recognizes diacylated lipopeptides and LTA, while combining with TLR1, it targets triacylated lipopeptides (Fitzgerald and Kagan 2020). TLR8 is responsible for RNA and triggers the expression of IFN-β (Bergstrom et al. 2015). TLR9 is activated by unmethylated CpG-DNA motifs from bacteria and functions in macrophages, B cells, and dendritic cells (Parker and Prince 2012).

TLR2 has been identified as the main signaling pathway for *S. aureus*, with lipoprotein being the predominant ligand (Hashimoto et al. 2006, Nguyen et al. 2018b). The *lgt*-deletion mutant, in the absence of lipidation of lipoprotein, has been investigated to exhibit a significant reduction of cytokine production (Stoll et al.

2005). The vSaα island in *S. aureus* encodes the lipoprotein-like lipoproteins (*lpl*), which have been identified to function on TLR2-dependent immune stimulation and internalization within the host (Nguyen et al. 2015). Furthermore, Lpp mutant has been investigated to decrease the skin abscess development in murine models (Mohammad et al. 2021).

TLR9 detects the non-methylated CpG-motifs from verses or bacteria, and CpG-containing synthetic oligodeoxyribonucleotides (ODNs). Mammalian DNA typically contains methylated CpG at cytosine. Additionally, the host cell is susceptible to degradation by host nucleases, while bacterial DNA is resistant to this process (Ewald and Barton 2011). The functional TLR9 is expressed in B cells, dendritic cells, and macrophages (Parker and Prince 2012). Previous studies have demonstrated that the full-length TLR9 is expressed in the endoplasmic reticulum, transferred to Golgi via UNC93B1, and finally translocated to the endolysosome. Then, TLR9 is cleaved by endosomal proteases for future activation of the MyD88 pathway (Ewald et al. 2008). This proteolysis process requires asparagine endopeptidase and cathepsins (Ewald et al. 2011). Thus, the subsequent recognition process accurses only on the endolysosome, rather than cell surface.

The truncated TLR9 is a monomer, and CpG DNA with phosphorothioate (PS) backbones binds to TLR9 to form a dimer (Li, Berke and Modis 2012). When it comes to natural phosphodiester (PD) DNA, TLR9 has been found to recognize the sugar backbone with base-free 2′ deoxyribose of PD (Haas et al. 2008). The structure of TLR9 with CpG-DNA has revealed that they form a 2:2 stoichiometric complex. Additionally, the agonistic DNA inserts to build a bridge between two TLR9 proteins (Ohto et al. 2015). Other studies have demonstrated that DNase II is necessary for TLR9 activation. DNase II is responsible for degrading longer fragments into shorter ones to stimulate TLR9. For example, CpG-A ODN needs to be digested to the fragments with 3′11-13-mer for activation (Chan et al. 2015). Furthermore, the recognition of TLR9 is both length-dependent and CpG frequency-dependent. Higher frequencies of CpG genomic DNA have been investigated to induce a more robust immune response via TLR9 (Dalpke et al. 2006, Roberts et al. 2005). In addition, ODNs with more than 21 CpG nucleotides and CpG positioned 4–6 nt from the 5′-end are necessary for activating human TLR9 (Pohar et al. 2015). It has also been found TLR9 can be enhanced by shorter DNA as few as 2 CpG-containing nucleotides, even though no stimulation has directly been detected and a much weaker binding affinity compared to longer one (Pohar et al. 2017).

After the activation the TLR9 pathway, the subsequent immune response occurs. The ODN itself activates the HUVEC cells, which leads to increased β2 integrin and

E-selectin-mediated neutrophil adhesion (El Kebir et al. 2009). *S. aureus* induces type I IFN cascade in dendritic cells through the TLR9 pathway (Parker and Prince 2012). Pre-treatment of SAOS-2 cells with ODN has been shown to induce ROS production, which in turn reduces the *S. aureus* survival within the cells (Mohamed et al. 2016). Additionally, pretreatment of the RAW 264.7 cells or primary peritoneal macrophages with ODN has been identified to increase the c-Jun N-terminal kinase and P38 levels, thereby enhancing the phagocytosis of *S. aureus* (Wu et al. 2016). In the MRSA pneumonia mice model, *Tlr9*−/− mice exihibit lower cytokines production, bacterial clearance, and enhanced lung consolidation (van der Meer et al. 2016). Knock-out TLR9 in macrophage RAW 264.7 cells or mice has been shown to impair the NLRP3 inflammasome activation and oxidative stress in response to *S. aureus* (Zhao et al. 2020).

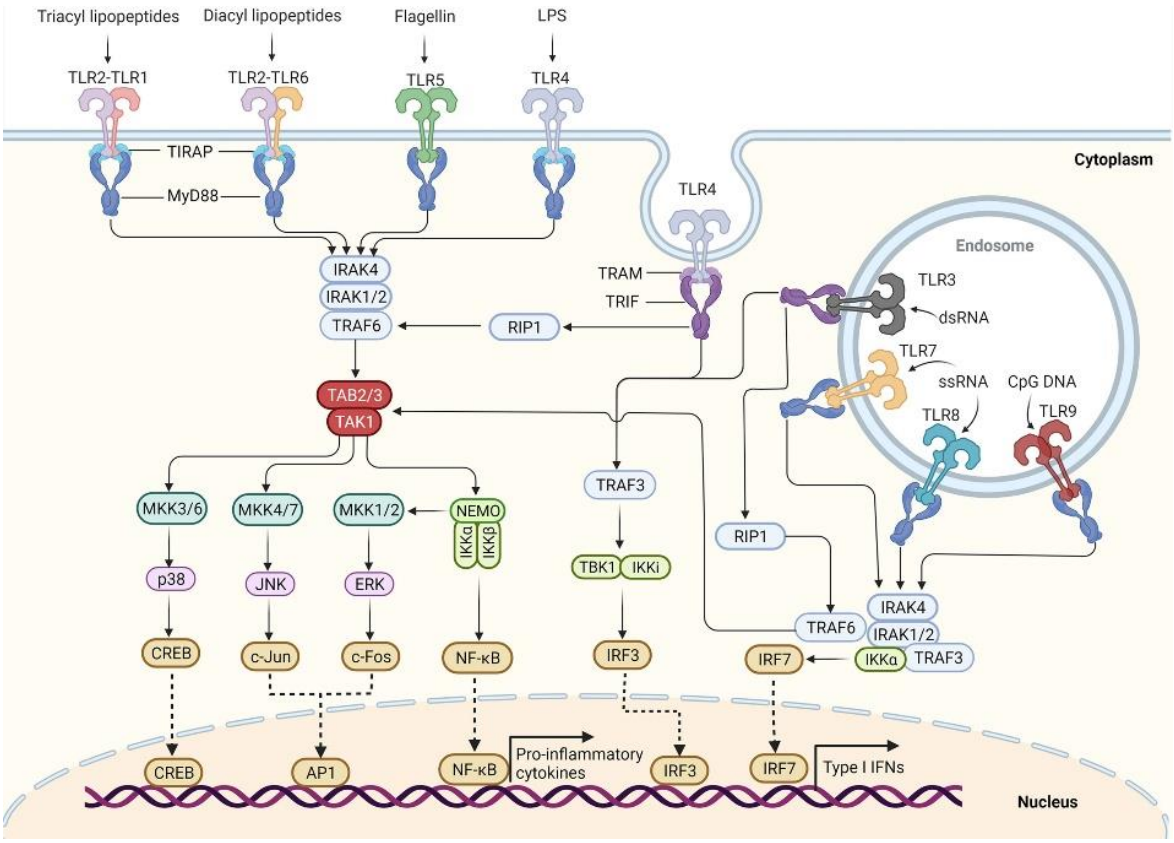

Fig. 1.3 TLR signaling pathway. TLR1, TLR2, TLR4, TLR5, and TLR6 are located on the plasma surface and detect the cell surface compounds. TLR3, TLR7, TLR8, and TLR9 are expressed in intracellular endosomes and recognize microbial nucleic acid. Adapted from (Duan et al. 2022). Reuse followed the Creative Commons Attribution (CC BY) license (https://creativecommons.org/licenses/by/4.0/).

Cytokines

During the process of the immune system's defense against pathogens, various cytokines are produced. They are typically expressed by immune cells and be also released in response to cellular damage. These include proinflammatory cytokines,

such as TNF-α, IL-6, and IL-8, and anti-inflammatory cytokines, such as IL-1ra, IL-10, and Transforming growth factor beta (TGF-β). In human immune systems, there is always a balance between pro-inflammatory and anti-inflammatory cytokines to regulate the infection (Opal and DePalo 2000, Wang and He 2018). This chapter will focus on the functions of some classical cytokines.

TNF-α is expressed by macrophages, neutrophils, osteoblasts and other cells. Following its binding to receptor TNFR1 or TNFR2, TNF-α displays specific biological functions. Studies have shown that peptidoglycan from *S. aureus* trigger a dose-dependent TNF-α expression in whole blood (Wang et al. 2000). Protein A in *S. aureus* binds to TNFR1, tiggers NF-κB activity on epithelial cells, leading to the PMN recruitment in an *in vivo* murine model (Gomez et al. 2004). Lpl increases TNF-α and IL-6 production via TLR2 pathway (Nguyen et al. 2015). Furthermore, the knockout TNF-α in mice leads to lower survival rates, significant weight loss and faster bacteria detection, suggesting the role of pathogens infection in the brain abscess mouse model (Kielian et al. 2004).

IL-6 is a pro-inflammatory cytokine produced by monocytes, osteoblasts, fibroblasts, T cells, and other cells. Previous work has found that both PepG and LTA purified from *S. aureus* induce IL-6 production in monocytes and T cells (Wang et al. 2000). Furthermore, *S. aureus* induces IL-6 production in keratinocytes, which reduces the terminal differentiation expression (Son et al. 2014). In a murine model of osteomyelitis, IL-6 is produced by osteoblast infected in response to *S. aureus (Marriott et al. 2004)*. Additionally, IL-6-deficient mice have exhibited enhanced bacteria burden in the skin when infected with *S. aureus* in comparison to the WT mice (Hruz et al. 2009).

IL-8 is a pro-inflammatory cytokine that is secreted by various cells such as monocytes, macrophages, and epithelial cells. It can be rapidly expressed and persistent in inflammation sites (Remick 2005). Numerous *S. aureus* PAMP induce IL-8 production, such as enterotoxin and lipoproteins (O'Brien et al. 2006, Kang et al. 2015). It has also been found to recruit neutrophils to the infection sites and help to release the granule components (Schroder 1989).

IL-10 is an anti-proinflammatory cytokine that is produced by monocytes, T cells, and neutrophils. Research has investigated that IL-10 regulates the neutrophils function on ROS, oxidative burst, and Mac-1 expression (Dang et al. 2006, Menezes et al. 2009). The concentration of IL-10 has been observed to be associated with host mortality that high concentration predicts high mortality, while moderate concentration indicates low mortality (Osuchowski et al. 2006).

IL-1Ra, belonging to the IL-1 family, functions as an IL-1 receptor antagonist. It is expressed in many cells, including neutrophils, macrophages, and monocytes (Arend 2002). Elevated IL-1Ra concentrations in blood are associated with sepsis (Fischer et al. 1992). In a murine infection model, *S. aureus* induces IL-1Ra production in the early stage of infection (Giai et al. 2016). Furthermore, pretreatment of mice with IL-1Ra prior to *S. aureus* infection has been shown to lead to a higher frequency of sepsis, increased histological and radiological signs, along with increased mortality (Ali et al. 2015).

Septic arthritis

Septic arthritis (SA) is a disease that has infections in the bone or joints with a high mortality and morbidity rate. The incidence of SA ranges from 4 to 10 cases per 100,000 patients, with the prevalence of post-arthroscopy SA approximately 0.14% in Iceland (Geirsson, Statkevicius and Vikingsson 2008). While SA predominantly occurs in the elderly and young children, osteoarthritis, diabetes, needle insertions, and surgeries are additional risk factors (Mathews et al. 2010). The SA is primarily caused by severe bacterial infection with the main causative bacterial strain being *S. aureus*, followed by *Streptococcus*, *Pseudomonas aeruginosa*, and *Escherichia coli* (Garcia-Arias, Balsa and Mola 2011). *S. aureus* expresses various virulence factors to promote colonization and invasion, resulting in joint damage in SA (Tam and Torres 2019).

Bacterial factors

S. aureus produces toxins, enzymes, and proteins to damage the host cells. These virulence factors have been discussed in the previous chapter.

The cell wall components, such as PGN, collagen, and Lpps, have been identified as pathogenic factors in SA. Lpps function as a dual mediator in SA. On one hand, the joint that is directly injected with purified Lpp develops destructive bone damage through the monocytes/macrophages-mediated TLR2 pathway in the SA murine model. Conversely, the live *lgt* mutant induces reduced sensitivity to host clearance, leading to enhanced bacterial burden and joint damage in sepsis mice model (Mohammad et al. 2019).

Toxins, including PSMs and Hla, also function in tiggering arthritis. Murine model studies demonstrate the opposite roles for PSM subtypes, with the PSMα-deficient strain inducing reduced weight loss and lower bacterial load while the PSMβ-deletion strain causes higher IL-6 production and symptoms of arthritis (Hu et al. 2022).

Secreted enzymes and proteins are also risk factors for SA. The *vwb*-mutant *and vwb-coa*-mutant show decreased clinical arthritis frequency and bone erosion score

in SA model, but not in *coa*-mutant, suggesting that vWbp has an impact on bone damage (Na et al. 2020).

Bacterial DNA or unmethylated CpG ODNs stimulate immune response. Direct injection of these molecules into joints causes arthritis in a short time, even lasting up to 2 weeks (Deng and Tarkowski 2000, Deng et al. 1999). This process is accompanied by immediate production of TNF-α and septic toxin. But this can be abolished in TNF receptor-lacking mice or pretreated with anti-TNF-α antibody (Sparwasser et al. 1997). Furthermore, pre-treated collagen-induced mice with CpG DNA exacerbate arthritis severity via the Th1-type pathway (Miyata et al. 2000).

Host immune response

When *S. aureus* invades, colonizes, and proliferates in the host, it induces an immune response in host cells. Both innate and adaptive immune cells contribute to defense and clearance of pathogen. The innate immune cells, such as neutrophils, macrophages, and natural killer (NK) cells, act as the first defense line, while the adaptive immune cells include T cells, B cells, and NKT cells, and other cell types mediate pathogens killing (Jin et al. 2021).

Neutrophils are rapidly recruited to infection sites, as we discussed in the previous chapter. Photodynamic therapy has shown that neutrophils are recruited to the infectious joint site and play a protective role (Tanaka et al. 2012). Depleting granulocytes via antibody RB6-8C5 in mice leads to higher severity in arthritis and mortality, demonstrating critical role of neutrophils in arthritis control (Verdrengh and Tarkowski 1997).

Macrophages are immune cells that can be activated. Recent studies have demonstrated that patients with arthritis show elevated cytokines levels, including CXCL4, CXCL7, IL-1β, IL-29, and TNF-α, which are expressed by synovial macrophages (Takano et al. 2016, Yeo et al. 2016). Additionally, the level of synovial macrophages has been known as an indicator of the severity of joint inflammation (Hamilton and Tak 2009).

Other cell types, such as osteoblasts, osteoclasts, and osteocytes, have also been identified to participate in bone damage. Osteoclast cells are located in the synovial and bone surfaces. They are differentiated from bone marrow monocytes through exposure to receptor activator of nuclear factor κB ligand (RANKL) and macrophage colony-stimulating factor 1 (M-CSF) (Schett and Gravallese 2012). *S. aureus* has been studied to induce the production of RANKL in stromal cells, leading to osteoclasts formation and bone erosion. Inhibition of RANKL with denosumab antibody has been shown to completely abrogate bone erosion in *S. aureus*-infected

mice model (Campbell et al. 2024). Osteoblast cells are responsible for the synthesis of bone extracellular matrix that constitute the bone tissue (Josse, Velard and Gangloff 2015). Osteoblasts produced cytokines, such as IL-6 and TNF-α, and chemokines, such as CCL2 (MCP-1) and CXCL2 when infected with *S. aureus* (Ning et al. 2011). Additionally, *S. aureus* can be internalized into osteoblasts with FnBP or be affected by SigB (Ahmed et al. 2001, Nair et al. 2003).

When infected with pathogens, cytokines are released by various cells and promote inflammation. In the clinical assay, high concentrations of IL-6 and TNF-α production are highly detected even after treatment in non-gonococcal septic arthritis patients, while IL-1β is decreased after treatment (Osiri et al. 1998). Consequently, elevated IL-6 concentrations in synovial fluid have been considered as a potential biomarker for joint infection (Lenski and Scherer 2014). IL-10, acting as an anti-inflammatory cytokine, has been identified to promotes elimination of pathogen and protect host from sepsis (Gjertsson, Hultgren and Tarkowski 2002). The expression of TNFα and IL-6 has been found to trigger osteoclast-like cell formation in a dose-dependent manner, while TNFα and IL-1β also induce osteoclast differentiation in macrophages. However, both processes are in a RANKL-independent way (Yokota et al. 2014). Other studies have shown that IL-6 not only binds to RANKL inducing osteoclast differentiation but also acts in an opposite way that suppresses the IκB degradation and JNK activation pathway (Yoshitake et al. 2008).

Antibiotics

S. aureus causes a wide range of clinical infectious diseases, such as skin and soft infection, arthritis, and lung infections (Tong et al. 2015). To treat those infections, antibiotics including penicillin and daptomycin, are commonly used to reduce the risk of morbidity (Silver 2011). However, *S. aureus* has evolved resistance to these classical antibiotics: penicillin-resistant and methicillin-resistant *S. aureus* (MRSA), compromising the treatment efficacy at infection sites (Lowy 2003). Thus, finding new antibiotics is an urgent need for combating bacterial infection.

Many classic antibiotics are derived from fungal, protozoan, bacterial, and plant sources. Recently, plant-derived antibiotics have gained attention in the scientific community, with these natural products being identified as promising candidates (Angelini 2024). For instance, methanolic extracts from duzhong and yerba mate have been observed to have antibiotic activity against *Propionibacterium acnes* (*P. acnes*), and co-incubation with *P. acnes* triggers decreased pro-inflammatory cytokine production in monocytes THP-1 cells (Tsai TsungHsien et al. 2010). Pulsaquinone 1, the quinone group compound isolated from *Pulsatilla koreana*, has also been found to suppress the growth of *P. acnes* (Cho, Sultan and

Moon 2009). Benzyl isothiocyanate, a component derived from *Salvadora Persica* root extracts, has been shown to inhibit Gram-negative pathogens, such as *Aggregibacter. actinomycetemcomitans* and *Porphyromonas. gingivalis.* (Sofrata et al. 2011). Allyl isothiocyanate, a secondary plant metabolism from the *Brassicaceae* family, is known to exhibit antimicrobial activity against *S. aureus* and *E. coli* (Lu et al. 2016). These findings highlight the potential of medicinal plants acting as a source for infectious diseases, which have low side effects and high accessibility.

Rhodomyrtone

Rhodomyrtone (Rom) is a bioactive compound isolated from *Rhodomyrtus tomentosa* (Aiton) leaves (Salni et al. 2002). It is known to inhibit the growth of Gram-positive bacteria, including *S. aureus*, *Streptococcus pneumoniae*, *Enterococcus faecalis*, and *P. acnes*, with a minimum inhibitory concentration (MIC) of ~0.5 µg/ml for *S. aureus* (Limsuwan et al. 2009, Leejae, Taylor and Voravuthikunchai 2013, Saising and Voravuthikunchai 2012), At this concentration, there is no cytotoxicity for keratinocytes, fibroblast and even Zebrafish. In a murine model, the tolerated dose could be up to 5 g/kg (Siriyong et al. 2020). While it is not toxic to the host at low concentrations, Rom is found to impede proliferation, induce apoptosis, and delay wound healing in keratinocytes at high concentrations (Chorachoo et al. 2016).

It remains unclear how Rom inhibits the Gram-positive pathogens. To investigate the mechanism, *Bacillus subtilis* and *S. aureus* have been exposed to Rom and subsequently analyzed via proteomic profiling or fluorescent microscopy (Saising et al. 2018). In *Bacillus*, the repeated binding and release of Rom from the bacterial membrane triggers various events. These events include the gathering of phospholipid head groups in the outlet membrane and the spreading of fatty acids in the inner membrane, which then forms a highly fluid domain that traps the proteins in vesicles (Saeloh et al. 2018). This process promotes membrane destruction and inhibits the growth of *Bacillus*. In the case of *S. aureus*, fluorescence microscopy reveals that treating Rom decreases membrane potential and affects topology, leading to higher ATP release. Surprisingly, addition of limited saturated fatty acids (pentadecyclic acid, palmitic acid, and stearic acid) has been observed to abolish the inhibition and rescue the growth of Rom-treated *S. aureus* (Saising et al. 2018).

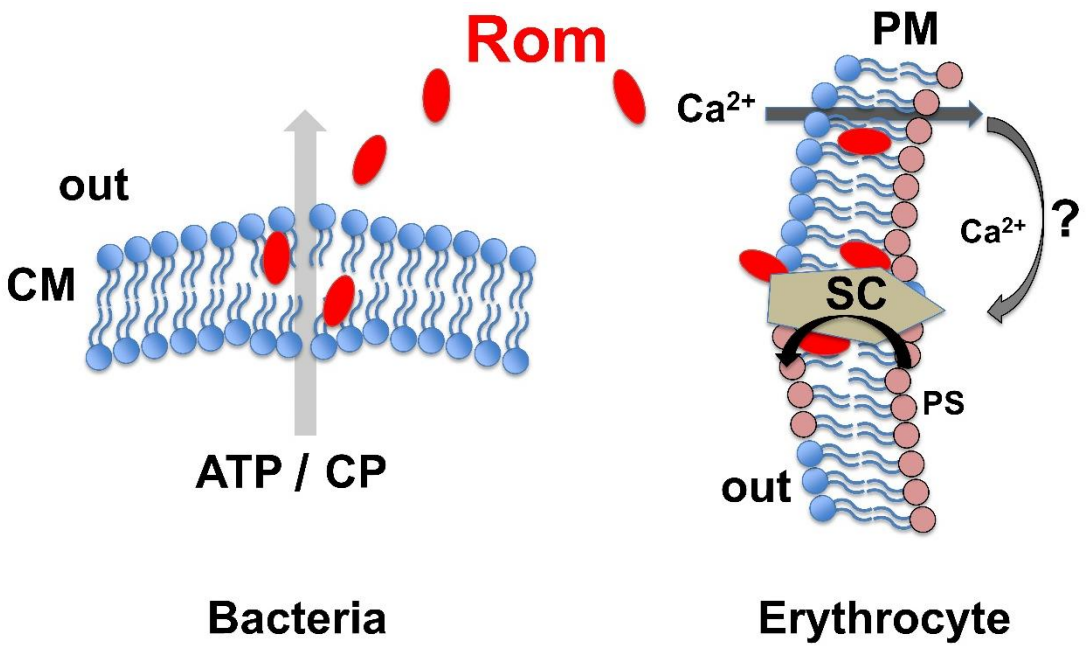

Fig. 1.4 Model of Rom's membrane activities. Rom does not form pores Gram-positive bacteria but appears to intercalate between the membrane phospholipids thus causing release of ATP and cytoplasmic proteins (**CP**). In erythrocyte membrane it induces eryptosis accompanied by activation of the scramblase (**SC**) and phosphatidylserine (**PS**) translocation to the outer leaflet of the plasma membrane (**PM**). In theory, SC may be activated directly and/or indirectly, e.g. via increased influx of Ca^{2+} ions.

To further understand the mechanism, a Rom-resistance *S. aureus* (Rom^R) strain was developed in HGOO1 with an MIC greater than 128 µg/ml (Nguyen et al. 2019). A subsequent comparison of the whole genome sequence reveals that the resistance comes from a point mutation in the *farR* gene. Transcriptomic analysis and RT-PCR show increased *farR*, *farE*, *psm*, and *agr* expression in the mutant. FarE is responsible for pumping linoleic and arachidonic acids. Accordingly, the mutant exhibits increased levels of fatty acids in the mutant in comparison to wild-type strain. Additionally, overnight cultural supernatant of Rom^R is more cytotoxic. The increased fatty acids and other toxins, such as PSM, lead to an elevated pathogenicity in the mouse model (Nguyen et al. 2019).

Chapter 1. *Staphylococcus aureus* thermonuclease NucA is a key virulence factor in septic arthritis

Aim of the study

Thermonuclease, Nuc1, is composed of a signal peptide, a short pro-region, and fully mature NucA. It is normally secreted as NucA and functions to degrade extracellular DNA/RNA. In addition to promoting the dispersal and destabilization of biofilms via degrading extracellular DNA, NucA also contributes to the degradation of NETs degradation and enhances bacterial survival within neutrophils. However, there are still questions about its pathogenicity in the host and its role in arthritis.

In this study, we aim to investigate the role of NucA in a well-established mouse model of septic arthritis. Our data present that in the hematogenous septic arthritis mouse model, Δ*nuc1*-infected mice exhibit severe bone destruction, rapid weight loss, and high proinflammatory cytokine production. To further investigate the reason why there was higher pathogenicity in *nuc1*-expressing strain infected mice, we conducted the *in vitro* assays. The results suggest that the reduced killing by neutrophils as well as the NET degrading activity of NucA, and its induction of proinflammatory cytokines in certain host cells could be responsible for the enhanced pathogenicity.

Results

The *S. aureus* Newman Δ*nuc1* mutant is much less pathogenic in the mouse model of septic arthritis

To investigate the role of NucA, *S. aureus* Newman wild type (NWT) and its Δ*nuc1* mutant were constructed and evaluated in a mouse model of *S. aureus* septic arthritis. Naval Medical Research Institute (NMRI) mice were employed in this study. Mice received intravenous inoculations with either NWT or Δ*nuc1*, and were observed for 7 days to monitor the infection process and immune response. Remarkably, Δ*nuc1*-infected mice exhibited minimal weight loss until day 7, whereas NWT-infected mice continued to lose weight up to 20% by the experiment's termination on day 7 (**Fig. 2.1a**). The severity of septic arthritis was assessed by clinical arthritis frequency and clinical arthritis score (see Materials and Methods for details). Here, Δ*nuc1*-infected mice displayed significantly lower clinical arthritis symptoms than NWT-infected mice. Twenty percent of Δ*nuc1*-infected mice developed mild clinical arthritis symptoms up to day 7. In contrast, 40% of NWT-infected mice exhibited clinical arthritis symptoms as early as day 3, and by day 5, all animals had developed severe septic arthritis (**Fig. 2.1b**). Not only was the frequency of arthritis higher, but the clinical arthritis score was also elevated in mice infected with the NWT strain compared to the mutant strain (**Fig. 2.1c**). The frequency of polyarthritis, which is associated with chronic illness and a higher rate of mortality, was developed in NWT-infected mice from day 4, while it was not detected in Δ*nuc1*-infected mice (**Fig. 2.1d**). Moreover, both the kidney bacterial load (**Fig. 2.1e**) and kidney abscess scores (**Fig. 2.1f**) were significantly lower in the mice infected with the Δ*nuc1* mutant compared to those infected with its parental strain. **Fig. 2.1g** illustrates the clear differences in kidney abscess formation between NWT and Δ*nuc1*-infected mice.

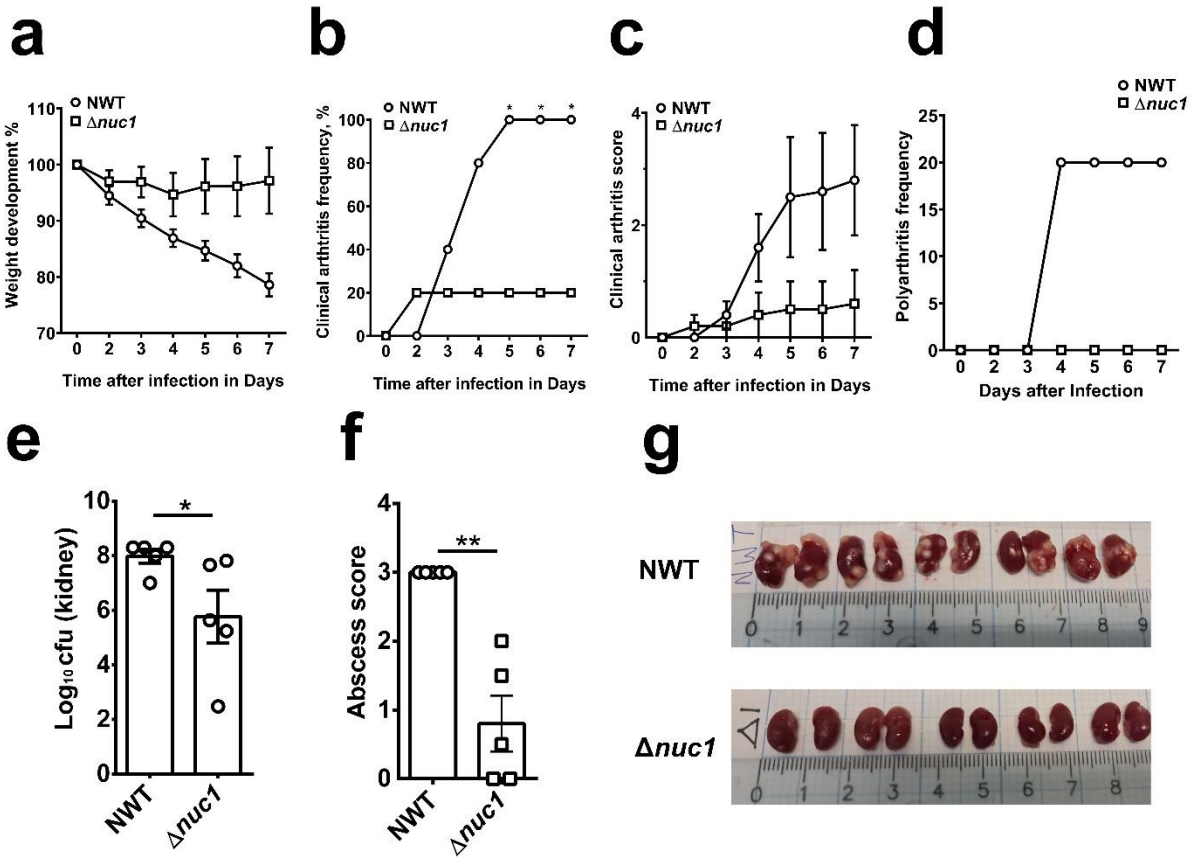

Fig. 2.1 *S. aureus* Newman wild-type strain (NWT) imparts more severe arthritis and virulence than its Δ*nuc1* mutant during infection in NMRI mice. (**a**) Weight development, (**b**) clinical arthritis frequency, (**c**) score, and (**d**) polyarthritis frequency were measured from mice infected with either NWT or Δ*nuc1* mutant for 7 days. (**e**) Bacterial counts in the kidney, (**f**) kidney abscess score, and (**g**) representative kidney abscess images from mice were investigated on day 7 post-infection. Statistical analyses were performed using the Mann-Whitney U test (**a** and **c**), where the data were presented as the mean ± SEM (standard error of the mean). Statistical significance: not significant, $p>0.05$; *$p<0.05$; **$p<0.01$.

To further confirm our clinical observations, we conducted µCT scans on all joints from mice inoculated with *S. aureus*. Intravenous injection of *S. aureus* NWT in NMRI mice resulted in severe bone destruction in 12% of joints after 7 days post-infection, whereas mice infected with the Δ*nuc1* mutant showed almost no sign of bone erosion (**Fig. 2.2a, b**). **Fig. 2.2c** shows representative 3D images of a wrist, a knee, and a shoulder from mice infected either with the Δ*nuc1* mutant or NWT strain.

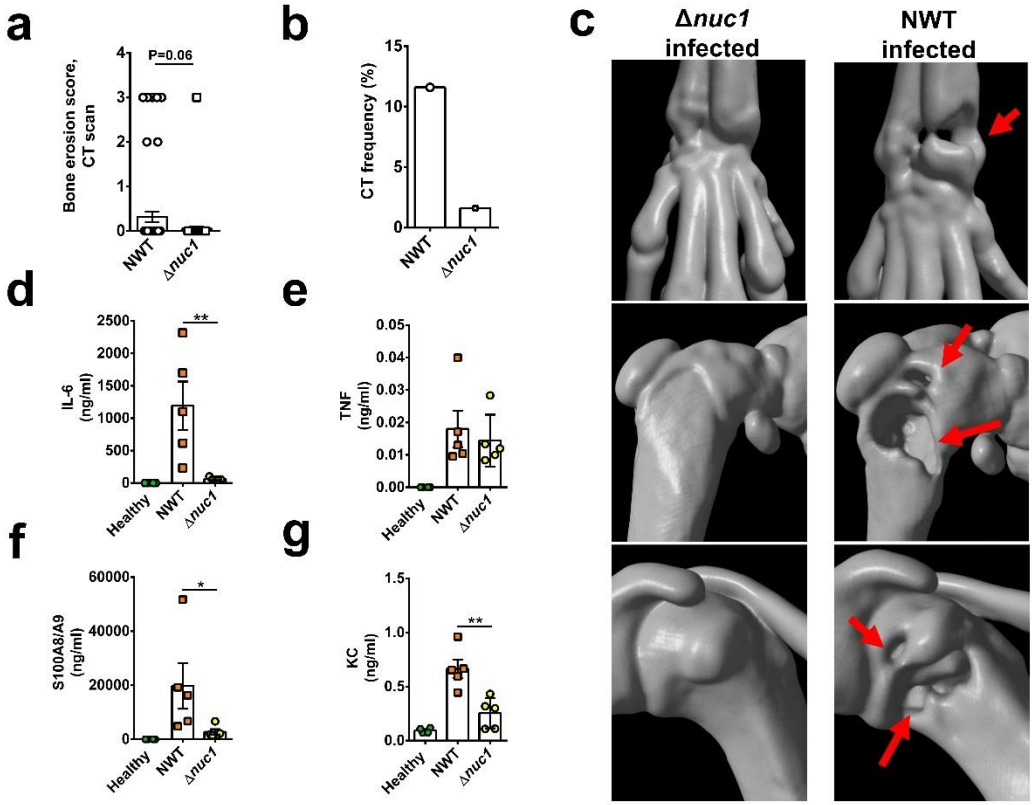

Fig. 2.2 Monitoring bone erosion by microcomputed tomography (µCT) and cytokine levels in mice infected with NWT or Δ*nuc1*. (**a**) Bone erosion frequency in joints evaluated using µCT in NMRI mice. (**b**) CT frequency of the joints in NMRI mice intravenously injected with *S. aureus* NWT or its Δ*nuc1* mutant on day 7 post-infection. (**c**) Representative images of micro-computed tomography (µCT) scanning of the mice joints (hand, knee, shoulder) after infection. Upper panel: NWT; lower panel: Δ*nuc1*; arrow indicates bone erosion. (**d-g**) Levels of IL-6, TNF-α, KC, and S100A8/A9 were measured in plasma derived from NMRI mice intravenously injected with NWT or Δ*nuc1*. Statistical analyses were performed using the Mann-Whitney U test **(a** and **c)**, where the data were represented in mean ± SEM. Statistical significance: not significant, p>0.05; *p<0.05; **p<0.01.

Infection with wild type *S. aureus* results in a massive increase in the levels of IL-6 and S100A8/A9

On day 7 post infection we collected blood samples from the infected mice and measured the levels of selected pro-inflammatory cytokines, including IL-6, TNF, KC (CXCL1), and S100A8/A9. As shown in **Fig. 2.2d**, the levels of IL-6, KC (CXCL1), and S100A8/A9 were markedly reduced in Δ*nuc1*-infected mice as compared to NWT-infected mice. While the TNF levels tended to be lower in Δ*nuc1*-infected mice, the difference did not reach statistical significance. Collectively, our results indicate that NucA is a crucial virulence factor in the pathogenicity of *S. aureus* in an infection model of septic arthritis. We further investigated possible reasons of the lower pathogenicity of the Δ*nuc1* mutant in the septic mouse model using different host cells.

NucA digestion of gDNA decreased TNF-α production in mouse macrophages

Previous research found that the DNA from *S. aureus*, containing unmethylated CpG motifs, acts as a factor that triggers arthritis and septic shock. Unmethylated bacterial DNA and CpG motifs are recognized by the TLR9, which is expressed in immune cells such as macrophages and dendritic cells, triggering host immune respnse. SA113Δ*lgt* and JE2Δ*lgt* lacks the phosphatidylglycerol: prolipoprotein *diacylglyceryl transferase* Lgt, and therefore no lipidation of lipoproteins takes place and no TLR2 response can be triggered by this mutant. By including this mutant and the double mutant JE2Δ*nuc1*Δ*lgt* together with JE2 and JE2Δ*nuc1* in the comparative immunostimulation studies, it is possible to specifically detect NucA-induced cytokine induction.

The mouse macrophage-like RAW 264.7 cells were treated with increasing concentrations of gDNA from JE2Δ*lgt* and RAW 264.7 (negative control). The standard CpG oligonucleotides ODN2006 and the non-CpG oligonucleotides ODN2137 were used as positive and negative controls, respectively (**Fig. 2.3c**). gDNA from *S. aureus* JE2Δ*lgt* increased the production of the proinflammatory cytokine TNF-α in mouse macrophage-like RAW 264.7 cells in a concentration-dependent manner, while gDNA from RAW 264.7 cells did not (**Fig. 2.3c**). At a dose of 10 ng/ml, *S. aureus* gDNA induced the release of high TNF-α levels, as did exposure to 1 µM ODN2006, indicating a high immunostimulatory activity of the staphylococcal DNA. The degradation of eDNA by recombinant NucA, which was expressed and purified from *Escherichia coli* (**Fig. 2.3a, b)** suggested that NucA plays a role in controlling DNA/RNA-dependent immune stimulation. Indeed, the stepwise degradation of *S. aureus* gDNA by increasing amounts of NucA (from 46 pM to 3 nM) correlated with a stepwise decrease in TNF-α production in RAW 264.7(**Fig. 2.3d, e**). However, gDNA from SA113Δ*lgt* caused little stimulation and stepwise degraded-gDNA did not result in differences in TNF-α expression in PBMC (**Fig. 2.3f**).

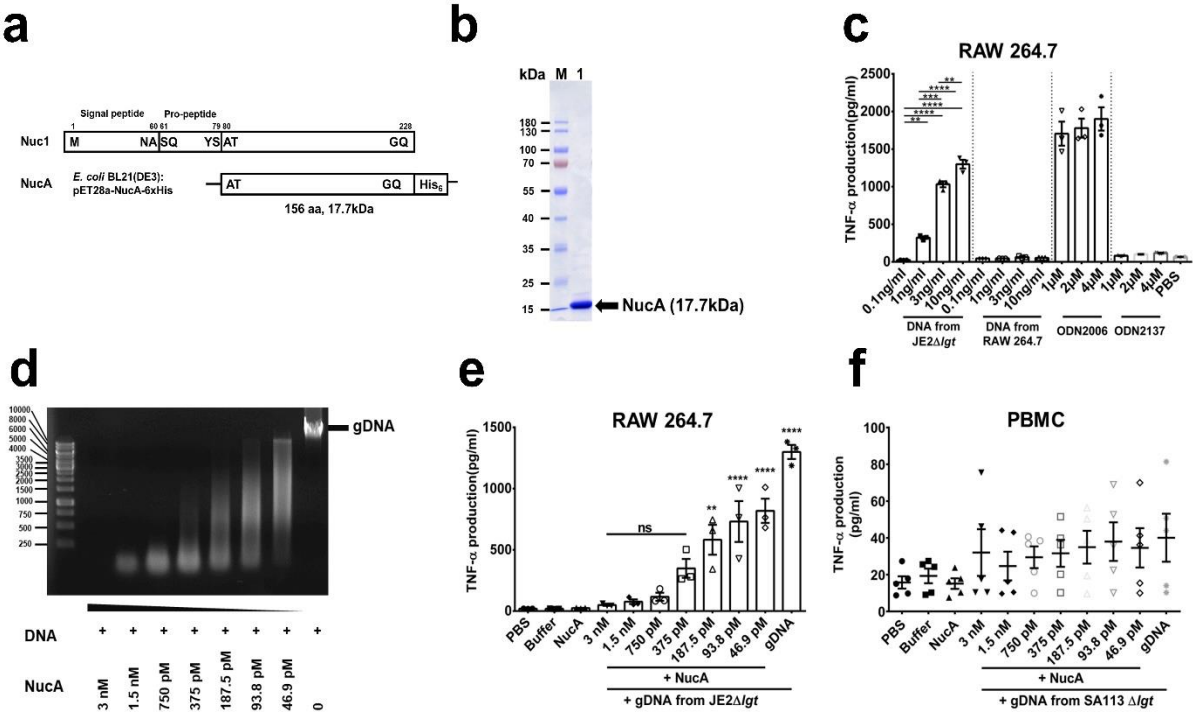

Fig. 2.3 Induction of TNF-α by macrophages upon exposure to diverse DNA. (**a**) Nuc1 is organized as a pre-pro-enzyme. The pre-pro-enzyme is processed to the mature nuclease NucA. Sequence of the mature NucA that was expressed in *E. coli* BL21(DE3) (pET28a-NucA-6x-His) as a C-terminal His-tag fusion protein. (**b**) Demonstration of Ni-NTA purified NucA in SDS-PAGE. NucA was used in gDNA hydrolysis assays. (**c**) Stimulation of mouse macrophage RAW 264.7 cells with JE2Δ*lgt* gDNA, mammalian gDNA, ODN2006 (CpG oligonucleotide), and ODN2137 (GpC dinucleotides) at varying concentrations for 18 h, followed by TNF-α measurements. (**d**) Agarose gel analysis showed the degradation of JE2Δ*lgt* gDNA by gradually decreasing NucA concentration. (**e, f**) Undigested and digested JE2Δ*lgt* gDNA were incubated with RAW 264.7 cells for 18 h and PBMC for 5 h. Released TNF-α in cellular supernatants was quantified by ELISA. Data represents the mean ± SEM from three independent experiments; ns (not significant), $p>0.05$; *$p<0.05$; ****$p<0.0001$, one-way ANOVA with Dunnett's posttest.

The *nuc1* deletion mutant loses activity in DNA degradation

S. aureus USA300 LAC JE2 and Newman strain were selected to verify the function of NucA *in vitro*. Both strains express NucA and the corresponding Δ*nuc1* mutants could be complemented by pRB473-*nuc1* (**Fig. 2.4a**). In *S. aureus*, NucA is secreted into the supernatant and degrades extracellular DNA and RNA. This was demonstrated when we incubated the supernatant of JE2 and its mutants JE2Δ*nuc1*, JE2Δ*lgt*, and JE2Δ*nuc1*Δ*lgt* with *S. aureus* gDNA for 1 h to evaluate the nuclease activity. In all mutants in which *nuc1* was deleted, the gDNA remained intact, whereas in JE2 and the JE2Δ*lgt* mutant, the gDNA was completely degraded, indicating that NucA is responsible for gDNA degradation (**Fig. 2.4b**). Additionally, the generated

mutants showed hardly any difference in growth and hemolytic activity compared to the parent strain (**Fig. 2.4c, d**).

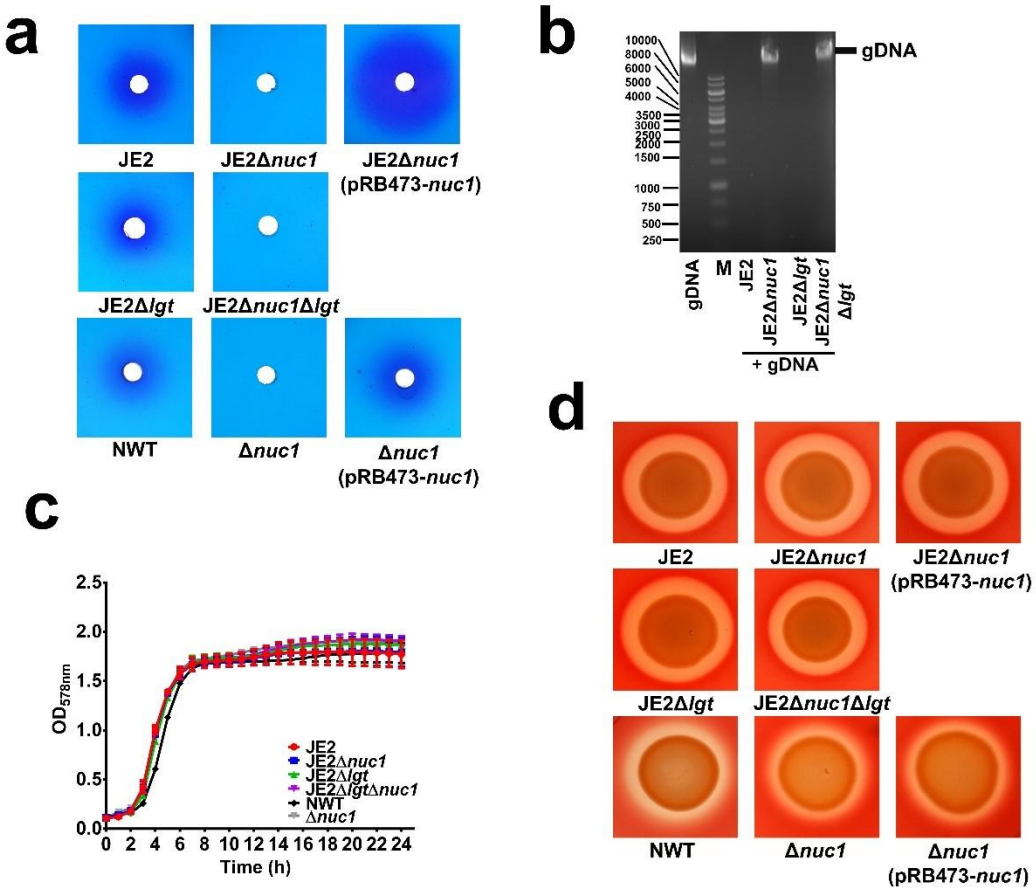

Fig. 2.4 Characteristics of JE2, Newman and their mutants. (**a**) JE2Δ*lgt* gDNA was incubated with overnight cultural supernatant from JE2, JE2Δ*nuc1*, JE2Δ*lgt*, and JE2Δ*nuc1*Δ*lgt* for 1 h at 37°C. The degradation of DNA was visualized through agarose gel electrophoresis. (**b**) Growth in TSB medium, (**c**) hemolytic activity and (**d**) nuclease activity of JE2 JE2Δ*nuc1*, JE2Δ*lgt*, JE2Δ*nuc1*Δ*lgt,* JE2Δ*nuc1*(pRB473-*nuc1*), Newman (NWT), Δ*nuc1* and Δ*nuc1*(pRB473-*nuc1*).

The *S. aureus nuc1* deletion mutants have an impact on cytokines production

We investigated whether the immune stimulation of JE2 and its mutants differed. We incubated live *S. aureus* JE2 and its JE2Δ*nuc1*, JE2Δ*lgt*, and JE2Δ*nuc1*Δ*lgt* mutants for 18 h with RAW 264.7, SAOS-2*, and chondrocytes,* and 5 h with PBMC and neutrophils. There was no difference in IL-6 and TNF-α production between JE2 and JE2Δ*nuc1* stimulation in RAW 264.7, chondrocytes, and PBMCs (**Fig. 2.5a, c, d**). In SAOS-2 *cells,* IL-6 production was slightly decreased in response to all mutants, while in neutrophils the production of TNF-α, IL-10, and IL-1Ra was significantly decreased in response to all the mutants (**Fig. 2.5b, e**), particularly those in which *lgt* was deleted (JE2Δ*lgt* and JE2Δ*nuc1*Δ*lgt)*. The results show that Nuc1 plays little impact on immune

response. However, at the bacterial level not so much bacterial DNA but the TLR-2 activating lipoproteins are the prominent immune stimulants.

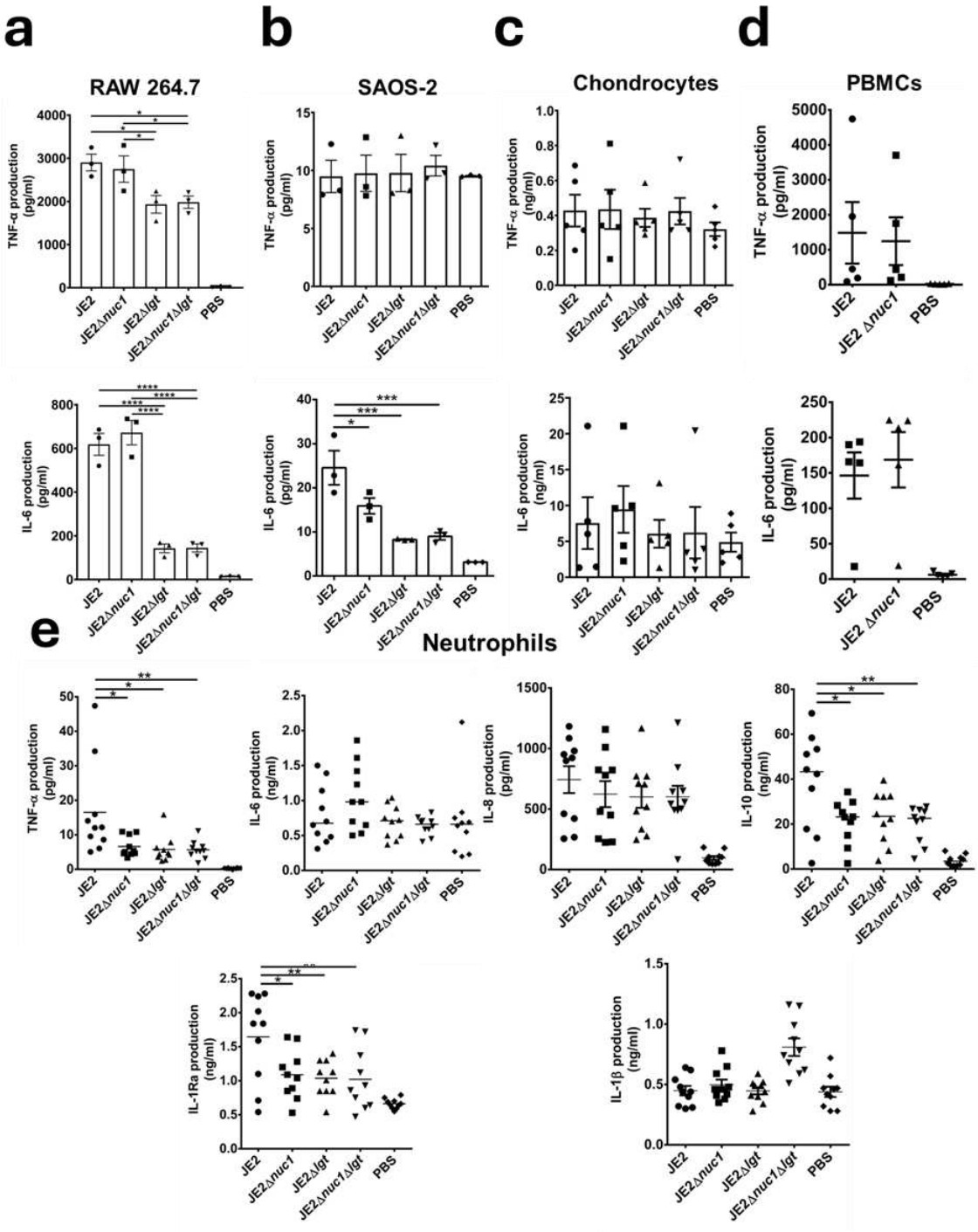

Fig. 2.5 Induction of cytokines by various host cells upon exposure to live JE2, JE2Δ*nuc1*, JE2Δ*lgt*, and JE2Δ*nuc1*Δ*lgt*. The PBS-washed bacteria were incubated with (**a**) RAW 264.7 at a MOI=30, (**b**) SAOS-2 cells at a MOI=3, (**c**) chondrocytes at a MOI=30 and (**d, e**) with PBMCs neutrophils at a MOI=50. Cellular supernatants were collected after 18 h for RAW 264.7, SAOS-2 cells and chondrocytes, and after 5 h for PBMC and neutrophils to measure various cytokines by ELISA assay. For PBMC and neutrophils, the experiments were displayed from n=5 and n = 10 donors, respectively.

Triplet experiments were conducted; error bars indicate ± SEM; not significant, p>0.05; *p<0.05; **p<0.01; and ****p<0.0001, one-way ANOVA with Dunnett's posttest.

As NucA is secreted extracellularly, further investigation was performed to assess whether there were differences in the immune response on the cultural supernatant of the mutants and WT. The bacterial overnight supernatants were collected from JE2 and its mutants, subsequently incubated with RAW 264.7, SAOS-2*, and chondrocytes for* 18 h*,* and with PBMC and neutrophils for 5 h. No significant differences were observed between JE2 and JE2Δ*nuc1*, while only TNF-α was slightly reduced in RAW264.7 in JE2Δ*nuc1* compared to the parent strain (**Fig. 2.6**).

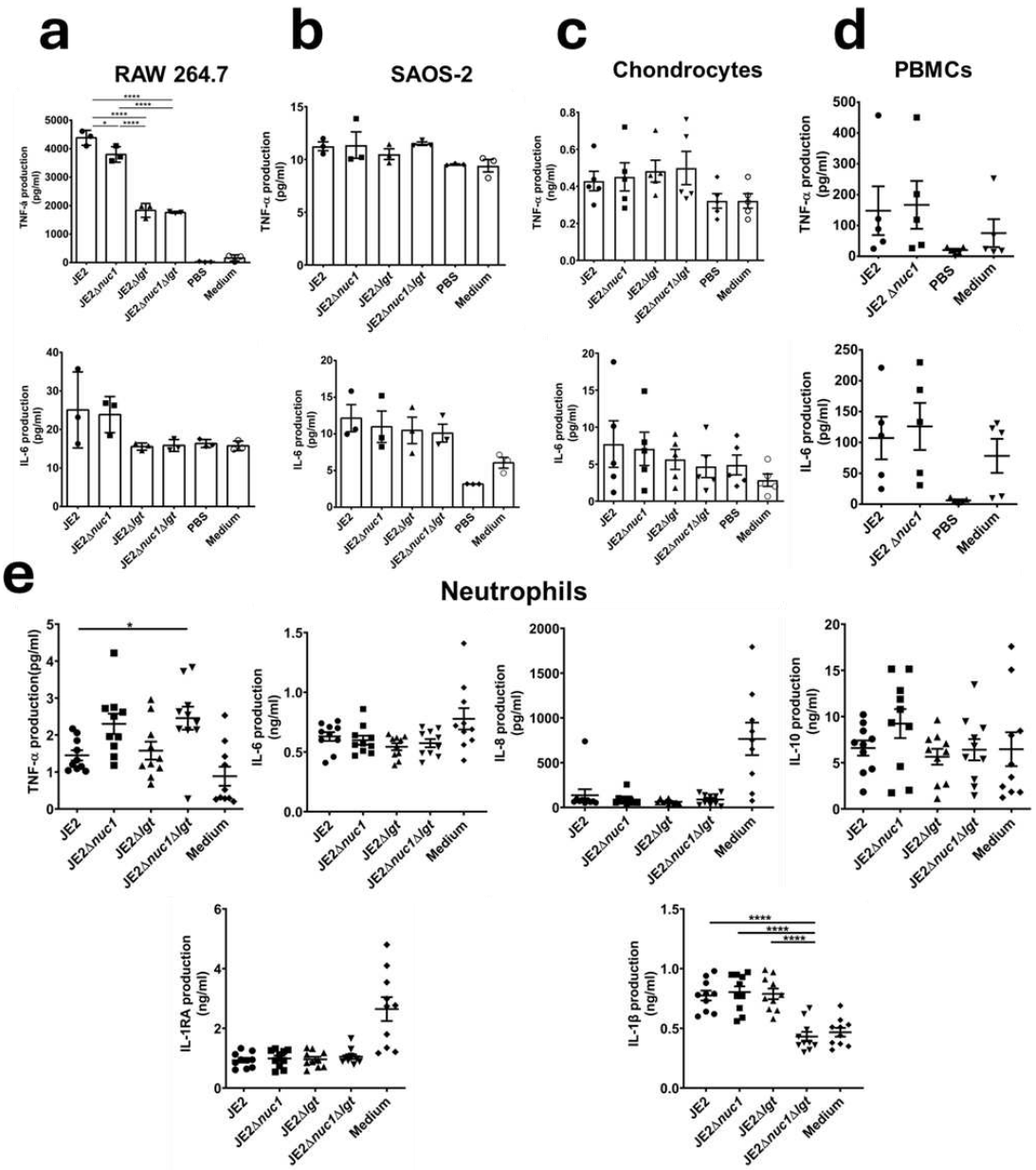

Fig. 2.6 Induction of cytokines by various host cells upon exposure to supernatant of JE2, JE2Δ*nuc1*, JE2Δ*lgt*, and JE2Δ*nuc1*Δ*lgt*. The PBS-washed bacteria were incubated with (**a**) RAW 264.7 at a MOI=30, (**b**) SAOS-2 cells at a MOI=3, (**c**) chondrocytes at a MOI=30 and (**d, e**) with PBMCs neutrophils at a MOI=50. Cellular supernatants were collected after 18 h for RAW 264.7, SAOS-2 cells and chondrocytes, and after 5 h for PBMC and neutrophils to measure various cytokines by ELISA assay. For PBMC and neutrophils, the experiments were displayed from n=5 and n = 10 donors, respectively. Triplet experiments were conducted; error bars indicate ± SEM; not significant, p>0.05; *p<0.05; and ****p<0.0001, one-way ANOVA with Dunnett's posttest.

The *nuc1* deletion mutant exhibits comparable pathogenicity to WT in larvae

Previous studies have shown that the USA300 and Newman strains exhibit distinct virulent properties; their pathogenicity differs depending on the infection model. To further determine the larvae's susceptibility to infection with JE2, NWT, and their mutants, an injection procedure was performed in *Galleria mellonella* larvae. The mortality of the larvae was checked daily. No death was detected in the control group; but 6.7 % of larvae injected with PBS died on the 1st day, potentially due to the injection injury. In contrast, all larvae injected with JE2 and JE2Δ*nuc1* died within 3 days, while those injected with NWT and Δ*nuc1* died within 2 days. However, the mortality rates were comparable within two groups (**Fig. 2.7a**).

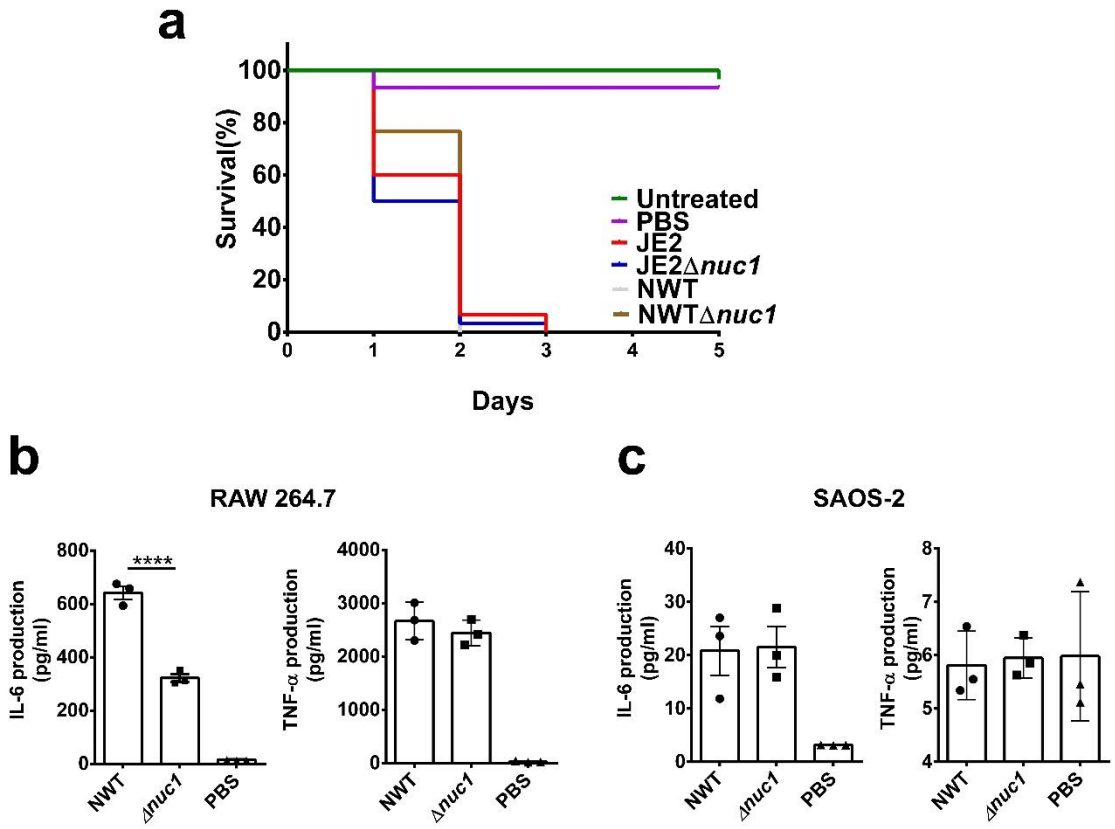

Fig. 2.7 Survival of the parental strains and their *nuc1* mutants' infection in *Galleria mellonella* larvae. (**a**)*G. mellonella* larvae were injected with JE2, JE2Δ*nuc1*, NWT and Δ*nuc1*. The larvae were checked for mortality every day over 5 days. The PBS-washed NWT and Δ*nuc1* were incubated with (**a**) RAW 264.7 at a MOI=30 and (**b**) SAOS-2 cells at a MOI=3 for 18 h. Cellular supernatants were collected after 18 h for ELISA assay. Triplet experiments were conducted; error bars indicate ± SEM; not significant p>0.05.

To further compare the similarity between Newman and USA300, NWT and its Δ*nuc1* strain were incubated with RAW 264.7 and SAOS-2 cells. There was less IL-6 production in RAW 264.7 and no significant difference in IL-6 and TNF-α expression in SAOS-2 when exposed to Δ*nuc1* strain (**Fig. 2.7b, c**)*, suggesting a similar immune response in the nuc1* deletion mutant *in Newman and JE2 strains.*

JE2Δ*nuc1* exhibit decreased survival in neutrophils

We determined bacterial survival and phagocytosis in neutrophils. With different conditions tested, we found that better results were obtained with an MOI=2 for the phagocytosis assay and an MOI=0.1 for the bacterial killing assay. Under these conditions, the survival of JE2Δ*nuc1* was decreased already at early time points in comparation to JE2 (**Fig. 2.8a**). This was consistent with a lower phagocytosis index in JE2Δ*nuc1* (**Fig. 2.8b**). Furthermore, the survival of JE2Δ*nuc1* was consistently lower at various time points within 1 hour (**Fig. 2.8c**). The extracellular killing was then examined via blocking the phagocytosis with cytochalasin D in neutrophils (**Fig. 2.8d**). The survival of JE2Δ*nuc1* was still impaired, suggesting the *nuc1*-deletion mutant was more sensitive to extracellular or intracellular killing.

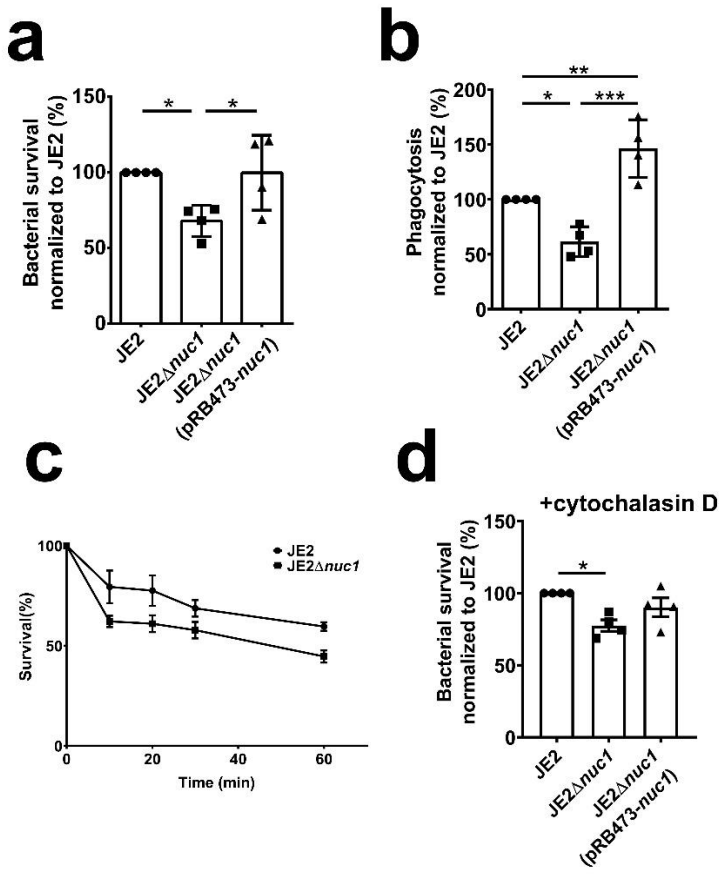

Fig. 2.8 Bacterial killing and phagocytosis studies in neutrophils. (**a, d**) For bacterial killing in neutrophils, JE2, JE2Δ*nuc1* and JE2Δ*nuc1* complemented with plasmid-expressed *nuc1* (JE2Δ*nuc1* pRB473-*nuc1*) were opsonized with 10% human pooled serum. (**b**)Fluorescence-labeled bacteria were incubated with neutrophils at a MOI of 1:2 and the phagocytosis index were calculated 1h after incubation via FACS. (**c**) Neutrophils were incubated with bacteria at a MOI=0.1 for 1h and bacterial survival was checked at 10min, 20min, 30min, and 60min after exposure to neutrophils. (**d**) neutrophils were incubated with cytochalasin D for 20 min then tested for bacterial killing with JE2 and its mutants. Neutrophils used in these experiments were obtained from 4 donors and the other experiments were performed at least three times; error bars indicate mean ± SEM. Statistical analyses were performed using one-way ANOVA with Dunnett's posttest. Statistical significance: not significant, $p>0.05$, *$p<0.05$; **$p<0.01$; and ***$p<0.001$.

JE2Δ*nuc1* exhibits decreased internalization in macrophages RAW 264.7

We continued to investigate whether live JE2 and its mutants differed in internalization by RAW 264.7 as their ability to bacterial phagocytosis. After 2 h incubation with *S. aureus* strains, membrane adherent and extracellular bacteria were killed, and then the CFU of internalized bacteria were determined. In RAW 264.7, we observed less CFUs upon incubation with the Δ*nuc1* mutants as compared to JE2 (**Fig. 2.9a**). In the complemented strain JE2Δ*nuc1* (pRB*nuc1*) JE2 phenotype was restored, suggesting

that internalization was affected by *nuc1* (**Fig. 2.9a**). However, no differences were detected in LDH release between JE2 and JE2Δ*nuc1* (**Fig. 2.9b**).

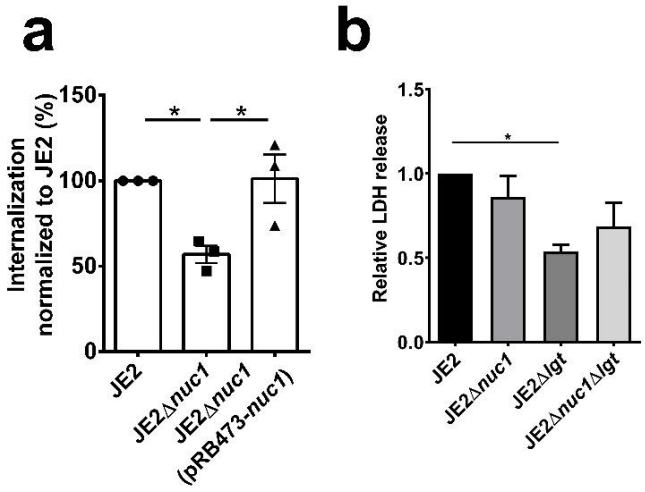

Fig. 2.9 Bacterial internalization in RAW 264.7. (**a**) To investigate bacterial survival in RAW 264.7, RAW 264.7 were incubated with JE2, JE2Δ*nuc1*, JE2Δ*nuc1*(pRB473-*nuc1*) at a MOI of 1:20 for 1.5 h. Extracellular and attached bacteria were removed by gentamicin and lysostaphin before lysing the cells. (**b**) The LDH release was measured before lysing the cell via commercial kit. The experiments were performed at least three times; error bars indicate mean ± SEM. Statistical analyses were performed using one-way ANOVA with Dunnett's posttest. Statistical significance: not significant, p>0.05, *p<0.05; **p<0.01; and ***p<0.001.

Effect of live bacteria and supernatant on NETs formation and clearing

Neutrophils act as the first defense line of the innate immune system and form NETs to clear pathogens. In *S. aureus*, NucA has been demonstrated to degrade extracellular DNA, thereby reducing NET formation and evading immune clearance. Here, the neutrophils were exposed to live bacteria (MOI=1:2) and bacterial supernatants (2%) for 2 h following eDNA-staining with SYTOX Green. Live bacteria caused a slow increase in NETosis, whereas the bacterial supernatant induced a stronger NET release in a shorter time (**Fig. 2.10a, b**). Additionally, neutrophils were still viable after 3 h incubation (**Fig. 2.10c**).

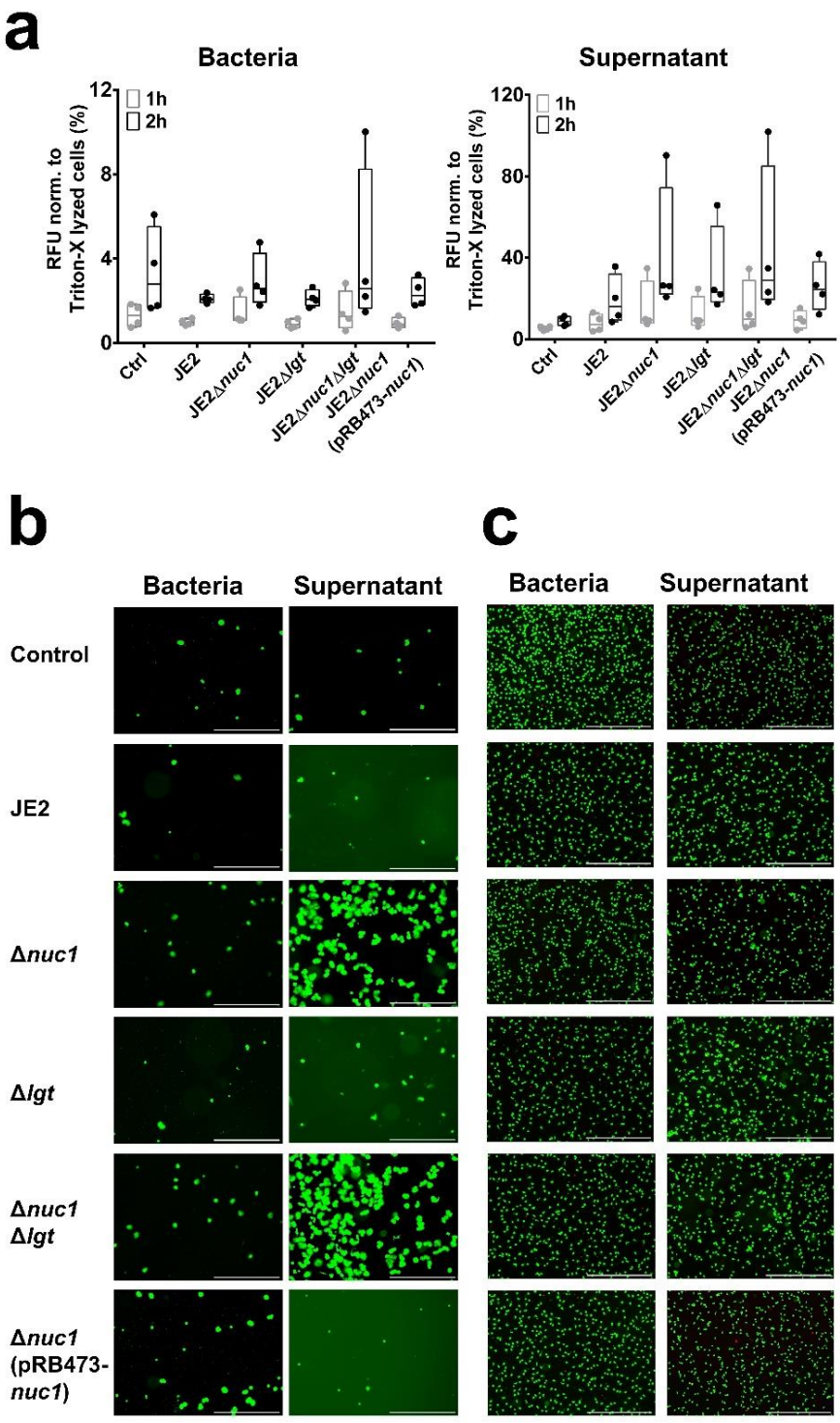

Fig. 2.10 NET formation screening upon exposure to live bacteria and supernatants of JE2 and its mutants. (**a**) Sytox Green assay of neutrophils exposed to JE2, JE2Δ*nuc1*, JE2Δ*lgt*, and JE2Δ*nuc1*Δ*lgt* with live bacteria (MOI=1:2) or overnight supernatant (2% volume) for 2 h. Relative fluorescence units (RFU) of Sytox Green normalized to Triton X-100-lysed neutrophils are shown. (**b**) Representative fluorescence images of Sytox Green staining after 3 h of incubation. Scale bar = 500 µm. (c) Exemplary pictures of viability staining for neutrophils exposed to JE2 and its mutants. Pictures were taken after 2 hours of incubation. Green: Calcein AM, Red: Ethidium Bromide, scale

bar: 500 µm. The graph displays the average values ±SEM obtained from n = 4 donors; not significant, p>0.05, one-way between-groups ANOVA with Dunnett's posttest.

Immunofluorescence staining of NET formation further confirmed NETosis occurred, as visible by positive staining for DNA (blue), MPO (green), and citrullinated histone H3 (CitH3, red) after 1 h incubation of neutrophils with bacterial cell-free supernatant but not with live bacteria. NET was higher in response to JE2Δ*nuc1* mutants and their supernatants than in the parental strain as can be observed in fluorescence microscopy images as well (**Fig. 2.11**). This suggests that the supernatant of Δ*nuc1* mutants is less effective in degrading DNA, resulting in increased levels of NETs.

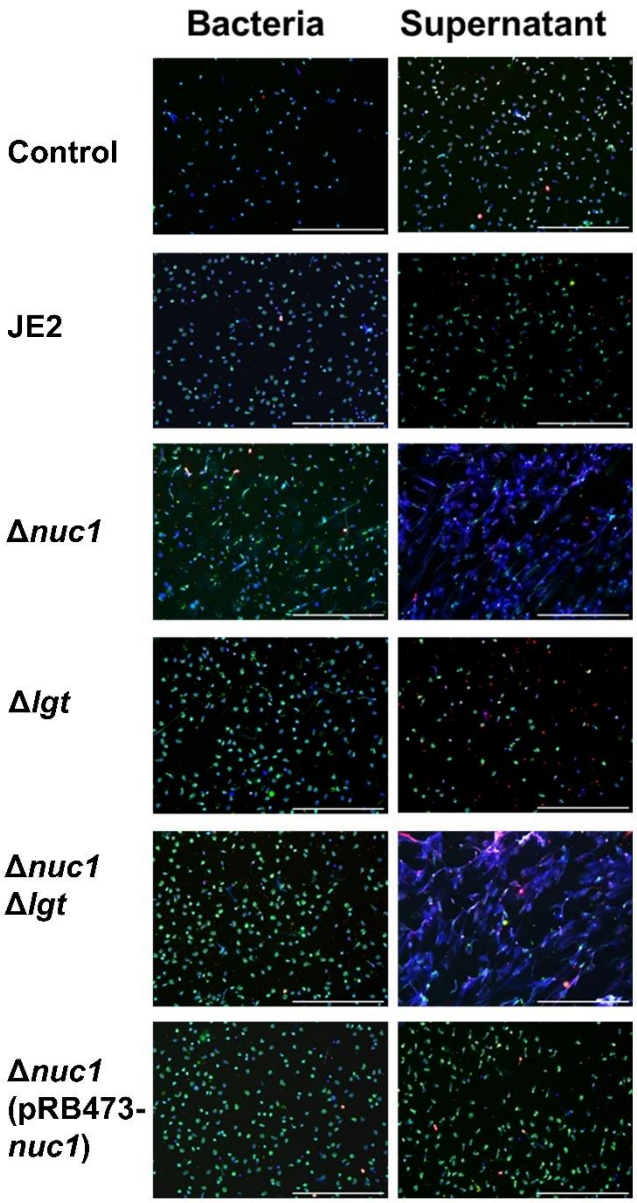

Fig. 2.11 NET formation upon exposure to live bacteria and supernatants of JE2 and its mutants. Representative images of immunofluorescent staining after 1 h of incubation. Blue: DNA (Hoechst 33342); Green: myeloperoxidase, MPO; Red: citrullinated histone H3, citH3, scale bar: 500 µm.

Concluding remarks

In *S. aureus*, thermonuclease is encoded by *nuc1* and secreted as mature NucA. It is a sugar nonspecific endonuclease that catalyzes the hydrolysis of both DNA and RNA at the 5' position of the phosphodiester bond with Ca^{2+} as a cofactor. While the role of NucA in the dispersal of eDNA based biofilms and NETs degradation has been well studied, relatively little is known about its role in septic arthritis.

In this study, we determined the *S. aureus* parental strain and its Δ*nuc1* mutant in a well-established mouse model of septic arthritis, which revealed that NucA is an important virulence factor in septic arthritis. *S. aureus* NWT-infected mice showed marked weight loss, much increased clinical arthritis frequency, a 3-fold higher abscess score, severe bone erosion and very high IL-6 levels in plasma. Furthermore, the Δ*nuc1*-infected mice showed hardly any signs of septic arthritis, almost no weight loss, their clinical arthritis and abscess scores were much lower, and the bacterial load in the kidneys was decreased (**Fig. 2.1**). Most notably, Δ*nuc1*-infected mice showed minimal bone erosion in the joints (**Fig. 2.2a-c**).

In order to understand the increased pathogenicity in septic arthritis with *nuc1*-expression strain, we further investigated *in vitro* assays to find the reasons. Here, we provide three potential lines of *in vitro* evidence to support our *in vivo* observations: 1) NucA efficiently degrades bacterial DNA, which can trigger the release of proinflammatory cytokines like TNF-α, known for their critical roles in septic arthritis development; 2) NucA production may increase the intracellular survival of *S. aureus*; 3) NucA produced by *S. aureus* effectively digests NETs formed by neutrophils, potentially aiding bacterial evasion from innate immune killing, and thereby promoting bacterial survival and exacerbating disease severity.

Previous studies have identified that bacterial DNA not only triggers an inflammatory response via the TLR9 receptor but also leads to arthritis. In the present study, we observed that gDNA from *S. aureus* induced TNF-α production in a dose-dependent manner in RAW 264.7 cells, which cells process a functional TLR9 pathway. In addition, the gDNA was progressively degraded by increasing concentrations of recombinant-NucA, which is associated with a decrease in TNF-α production (**Fig. 2.3e**). These observations promoted us to investigate Δ*nuc1* mutant, in which eDNA is not degraded, might elicit a stronger immune response than the parental strain in various cell types. However, we observed that the JE2Δ*nuc1* induced less IL-6 in SAOS-2 cells and less TNF-α in neutrophils (**Fig. 2.5b, e**), while the NWTΔ*nuc1* induced less IL-6 in RAW 264.7 cells (**Fig. 2.7b**). These results give a hint that NucA has an impact on immune stimulation though it is not the predominant impact factor.

Furthermore, we found that the JE2Δ*nuc1* mutant exhibited reduced survival, which could explain why we detected less bacteria inside neutrophils 1h after exposure to neutrophils (**Fig. 2.8a**). This encouraged us to investigate the internalization in other cell lines. Additionally, we also observed reduced numbers of JE2Δ*nuc1* in RAW 264.7 cells (**Fig. 2.9a**). These findings indicate that NucA increases *S. aureus* survival, likely both extracellularly and intracellularly, which may contribute to an increase in the severity of septic arthritis.

As NucA functions in NETs degradation, we also exposed neutrophils to live *S. aureus*. There was a time-dependent increase in stained eDNA, but there was no pronounced difference between stimulation with JE2 and its mutants until 2 h post-exposure (**Fig. 2.10**). When we incubated neutrophils with the corresponding supernatants, we observed a clear difference in the response to JE2Δ*nuc1* mutants as compared to other strains. Immunofluorescence analysis revealed a stronger DNA signal in response to JE2Δ*nuc1* supernatants, suggesting decreased NET degradation (**Fig. 2.11**).

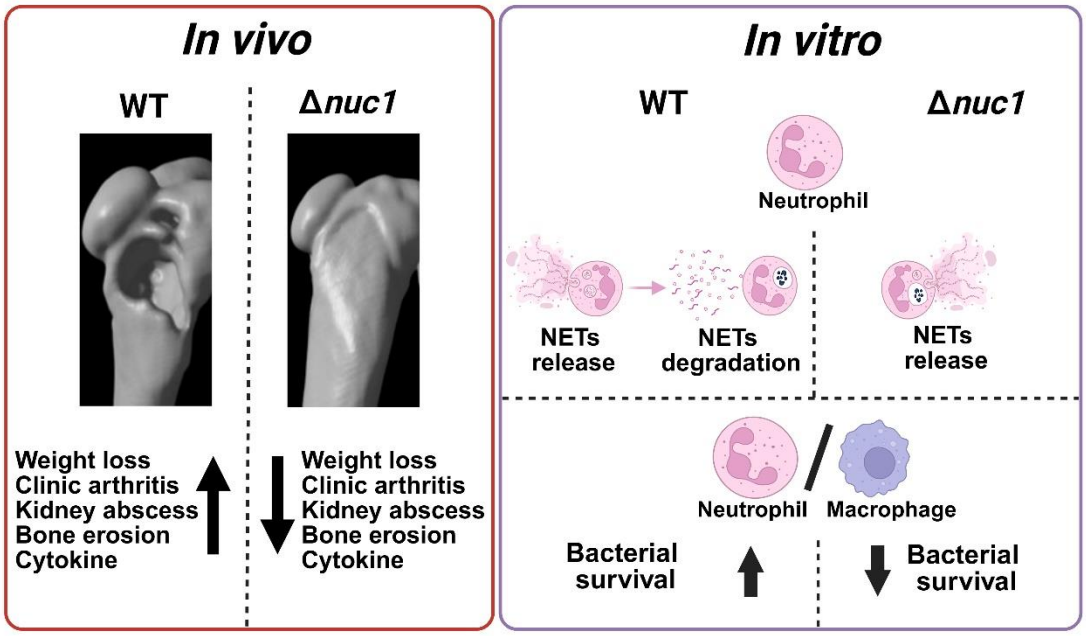

Fig. 2.12 Schematic representation of the differences in pathogenicity between the *S. aureus* wild-type strain (WT) and its Δ*nuc1* mutant in the mouse model for septic arthritis and under *in vitro* conditions. *In vivo*, WT-infected mice showed marked weight loss, increased clinical arthritis frequency, higher kidney abscess score, severe bone erosions, and higher cytokine levels than the Δ*nuc1*-infected mice. *In vitro*, the WT effectively digests NETs formed by neutrophils, which increases bacterial survival. This image is created in https://BioRender.com

Concluding remarks

Overall, our study suggests that NucA plays a crucial role in the pathogenesis of *S. aureus* septic arthritis, as evidenced by Δ*nuc1*-infected mice showing reduced arthritis severity, bone erosion, and kidney abscess formation, alongside lower bacterial loads. *In vitro* data further support these findings, demonstrating that NucA degrades bacterial DNA, shields *S. aureus* from killing, and digests neutrophil extracellular traps, ultimately promoting bacterial survival and worsening disease severity. In a summary image we illustrated the main differences between NucA-producing and -non-producing *S. aureus* strains (**Fig. 2.12**).

Chapter 2. Molecular Basis of Rhodomyrtone Resistance in *Staphylococcus aureus*

Aim of the study

Rom is an antibiotic against *S. aureus*, derived from *Rhodomyrtus tomentosa* leaves. Treatment with Rom induced decreased membrane potential in *S. aureus*. Additionally, the addition of limited saturated fatty acids has been found to rescue the growth of Rom-treated *S. aureus*. To better understand its antimicrobial mechanism, a Rom-resistance *S. aureus* (Rom^R) strain was developed in HGOO1, having a single point mutation in the regulatory *farR* gene.

Previous work in our group has demonstrated that the upregulation of *farE* in Rom^R causes high resistance phenotype. This was confirmed that *farE* deletion in either HGOO1 or Rom^R strain led to hypersensitivity to Rom. Furthermore, a comparative lipidome analysis of the supernatant and the pellet fraction revealed that the Rom^R strain excreted more PG and FAs than the parent strain or the Δ*farE* mutants. Combing these results, we aim to investigate the hypothesis that the overexpressed PG may interact with Rom, thereby abrogating its antimicrobial activity in Rom^R strain. Thus, static and dynamic light scattering (SLS and DLS) as well as isothermal titration calorimetry (ITC) analyses were employed to validate it. The results obtained from both analyses indicated that both PG and Rom were vesicular and reacted with each other to form a complex.

Concluding remarks

Rom is an antibiotic compound that has been shown to inhibit Gram-positive bacteria, such as *Bacillus* and *S. aureus*. It promotes bacterial membrane damage by inducing large invaginations and binding to phospholipid (P-lipid) head groups in Bacillus, while it decreases membrane potential in *S. aureus*. Additionally, the addition of limited saturated fatty acids has been demonstrated to eliminate the growth inhibition in *S. aureus*.

Previous work has constructed a Rom^R mutant derived from HG001, which exhibits resistance to Rom. Whole genomic sequence identified an amino acid mutation in *farR* in Rom^R mutant. The present work is focused on understanding the mechanism of high resistance in Rom^R mutant. Transcriptome analysis revealed that many genes are highly upregulated, especially *farE*, in Rom^R compared to the WT strain. Deletion of *farE* resensitized Rom^R mutant to Rom. These results provide evidence that upregulated expression of *farE* is associated with the Rom resistance. Consequently, Δ*farE* mutants were generated for further studies.

A comparative exolipidome analysis was performed on HG001, Rom^R, HG001Δ*farE*, and Rom^RΔ*farE* to analyze the FAs, lipids, PG, Lys-PG, DG, MGDG, and DGDG both analytically and quantitatively. It was monitored that Rom^R mutant secreted 2-fold greater FAs (C15:0, C17:0, C19:0, and C21:0) compared to the HG001 and Δ*farE* mutants. Furthermore, Rom^R mutant also exhibited markedly increase in the release of PG and Lys-PG. These findings indicate that a correlation between overexpression of *farE* and elevated levels of PG release in Rom^R. In addition, the supplementation of PG or FA led to suppression of Rom activity. Therefore, we hypothesized that Rom interacts with PG in Rom^R to eliminate the Rom activity.

To demonstrate the assumption, we used two methods to validate: SLS/DLS and ITC. For the SLS/DLS analysis, we selected PG (32:0) as the model and dissolved it as vesicles in a 10% DMSO/ PBS buffer. Rom was dissolved in the same buffer. The two samples were monitored separately in DLS. We found that PG maintains the vesicle size, while Rom forms nanoparticles and gradually aggregated. The combination of Rom and PG results in an augmentation of the vesicle size, which suggests that Rom indeed interacts with PG. Furthermore, the ITC analysis revealed that Rom rapidly binds to PG driven entropically. The interaction ratio was 1.49 and the K_D was 2.30 μM.

In summary, we identified that the Rom^R strain releases large amounts of PG into the supernatant and cell envelope via qualitative and quantitative lipidomic analyses,

indicating that FarE acts as a PG efflux pump. Rom resistance is mediated by the binding of PG to Rom, thereby neutralizing its antimicrobial activity.

References

Ahmed, S., S. Meghji, R. J. Williams, B. Henderson, J. H. Brock & S. P. Nair (2001) *Staphylococcus aureus* fibronectin binding proteins are essential for internalization by osteoblasts but do not account for differences in intracellular levels of bacteria. *Infect Immun,* 69**,** 2872-7.

Akira, S. & H. Hemmi (2003) Recognition of pathogen-associated molecular patterns by TLR family. *Immunol Lett,* 85**,** 85-95.

Ali, A., M. Na, M. N. Svensson, M. Magnusson, A. Welin, J. C. Schwarze, M. Mohammad, E. Josefsson, R. Pullerits & T. Jin (2015) IL-1 Receptor Antagonist Treatment Aggravates *Staphylococcal* Septic Arthritis and Sepsis in Mice. *PLoS One,* 10**,** e0131645.

Amagai, M., T. Yamaguchi, Y. Hanakawa, K. Nishifuji, M. Sugai & J. R. Stanley (2002) Staphylococcal exfoliative toxin B specifically cleaves desmoglein 1. *J Invest Dermatol,* 118**,** 845-50.

Anfinsen, C. B. (1968) Characterization of staphylococcal nuclease and the status of studies on its chemical synthesis. *Pure Appl Chem,* 17**,** 461-517.

Angelini, P. (2024) Plant-Derived Antimicrobials and Their Crucial Role in Combating Antimicrobial Resistance. *Antibiotics (Basel),* 13.

Arend, W. P. (2002) The balance between IL-1 and IL-1Ra in disease. *Cytokine Growth Factor Rev,* 13**,** 323-40.

Aulik, N. A., K. M. Hellenbrand & C. J. Czuprynski (2012) Mannheimia haemolytica and its leukotoxin cause macrophage extracellular trap formation by bovine macrophages. *Infect Immun,* 80**,** 1923-33.

Bekeredjian-Ding, I., C. Stein & J. Uebele (2017) The Innate Immune Response Against *Staphylococcus aureus*. *Curr Top Microbiol Immunol,* 409**,** 385-418.

Bell, J. K., G. E. Mullen, C. A. Leifer, A. Mazzoni, D. R. Davies & D. M. Segal (2003) Leucine-rich repeats and pathogen recognition in Toll-like receptors. *Trends Immunol,* 24**,** 528-33.

Berends, E. T., A. R. Horswill, N. M. Haste, M. Monestier, V. Nizet & M. von Kockritz-Blickwede (2010) Nuclease expression by S*taphylococcus aureus* facilitates escape from neutrophil extracellular traps. *J Innate Immun,* 2**,** 576-86.

Bergstrom, B., M. H. Aune, J. A. Awuh, J. F. Kojen, K. J. Blix, L. Ryan, T. H. Flo, T. E. Mollnes, T. Espevik & J. Stenvik (2015) TLR8 Senses *Staphylococcus aureus* RNA in Human Primary Monocytes and Macrophages and Induces IFN-beta Production via a TAK1-IKKbeta-IRF5 Signaling Pathway. *J Immunol,* 195**,** 1100-11.

Bhattacharya, M., E. T. M. Berends, X. Zheng, P. J. Hill, R. Chan, V. J. Torres & D. J. Wozniak (2020) Leukocidins and the Nuclease Nuc Prevent Neutrophil-Mediated Killing of *Staphylococcus aureus* Biofilms. *Infect Immun,* 88.

Bokarewa, M. I., T. Jin & A. Tarkowski (2006) *Staphylococcus aureus*: Staphylokinase. *Int J Biochem Cell Biol,* 38**,** 504-9.

Brinkmann, V., U. Reichard, C. Goosmann, B. Fauler, Y. Uhlemann, D. S. Weiss, Y. Weinrauch & A. Zychlinsky (2004) Neutrophil extracellular traps kill bacteria. *Science,* 303**,** 1532-5.

Bubeck Wardenburg, J., T. Bae, M. Otto, F. R. Deleo & O. Schneewind (2007) Poring over pores: alpha-hemolysin and Panton-Valentine leukocidin in *Staphylococcus aureus* pneumonia. *Nat Med,* 13**,** 1405-6.

References

Bubeck Wardenburg, J., W. A. Williams & D. Missiakas (2006) Host defenses against *Staphylococcus aureus* infection require recognition of bacterial lipoproteins. *Proc Natl Acad Sci U S A,* 103**,** 13831-6.

Buchanan, J. T., A. J. Simpson, R. K. Aziz, G. Y. Liu, S. A. Kristian, M. Kotb, J. Feramisco & V. Nizet (2006) DNase expression allows the pathogen group A *Streptococcus* to escape killing in neutrophil extracellular traps. *Curr Biol,* 16**,** 396-400.

Buddelmeijer, N. (2015) The molecular mechanism of bacterial lipoprotein modification--how, when and why? *FEMS Microbiol Rev,* 39**,** 246-61.

Bukowski, M., B. Wladyka & G. Dubin (2010) Exfoliative toxins of *Staphylococcus aureus*. *Toxins (Basel),* 2**,** 1148-65.

Burghardt, E. L., K. S. Flenker, K. C. Clark, J. Miguel, D. Ince, P. Winokur, B. Ford & J. O. McNamara, 2nd (2016) Rapid, Culture-Free Detection of *Staphylococcus aureus* Bacteremia. *PLoS One,* 11**,** e0157234.

Campbell, M. J., C. Bustamante-Gomez, Q. Fu, K. E. Beenken, H. Reyes-Pardo, M. S. Smeltzer & C. A. O'Brien (2024) RANKL-mediated osteoclast formation is required for bone loss in a murine model of Staphylococcus aureus osteomyelitis. *Bone,* 187**,** 117181.

Chan, M. P., M. Onji, R. Fukui, K. Kawane, T. Shibata, S. Saitoh, U. Ohto, T. Shimizu, G. N. Barber & K. Miyake (2015) DNase II-dependent DNA digestion is required for DNA sensing by TLR9. *Nat Commun,* 6**,** 5853.

Chase, J. W. & C. C. Richardson (1974) Exonuclease VII of *Escherichia coli*: mechanism of action. *Journal of Biological Chemistry,* 249**,** 4553-4561.

Chen, J., Z. Lu, J. Sakon & W. E. Stites (2000) Increasing the thermostability of staphylococcal nuclease: implications for the origin of protein thermostability. *J Mol Biol,* 303**,** 125-30.

Cho, S. C., M. Z. Sultan & S. S. Moon (2009) Anti-acne activities of pulsaquinone, hydropulsaquinone, and structurally related 1, 4-quinone derivatives. *Arch Pharm Res,* 32**,** 489-94.

Chorachoo, J., D. Saeloh, T. Srichana, T. Amnuaikit, K. S. Musthafa, S. Sretrirutchai & S. P. Voravuthikunchai (2016) Rhodomyrtone as a potential anti-proliferative and apoptosis inducing agent in HaCaT keratinocyte cells. *Eur J Pharmacol,* 772**,** 144-51.

Chow, O. A., M. von Kockritz-Blickwede, A. T. Bright, M. E. Hensler, A. S. Zinkernagel, A. L. Cogen, R. L. Gallo, M. Monestier, Y. Wang, C. K. Glass & V. Nizet (2010) Statins enhance formation of phagocyte extracellular traps. *Cell Host Microbe,* 8**,** 445-54.

Cotton, F. A., E. E. Hazen, Jr. & M. J. Legg (1979) *Staphylococcal* nuclease: proposed mechanism of action based on structure of enzyme-thymidine 3',5'-bisphosphate-calcium ion complex at 1.5-A resolution. *Proc Natl Acad Sci U S A,* 76**,** 2551-5.

Cuatrecasas, P., S. Fuchs & C. B. Anfinsen (1967) Catalytic properties and specificity of the extracellular nuclease of *Staphylococcus aureus*. *Journal of Biological Chemistry,* 242**,** 1541-1547.

Cunningham, L., B. W. Catlin & M. P. De Garilhe (1956) A deoxyribonuclease of micrococcus pyogenes1. *Journal of the American Chemical Society,* 78**,** 4642-4645.

Dalpke, A., J. Frank, M. Peter & K. Heeg (2006) Activation of toll-like receptor 9 by DNA from different bacterial species. *Infect Immun,* 74**,** 940-6.

References

Dang, P. M., C. Elbim, J. C. Marie, M. Chiandotto, M. A. Gougerot-Pocidalo & J. El-Benna (2006) Anti-inflammatory effect of interleukin-10 on human neutrophil respiratory burst involves inhibition of GM-CSF-induced p47PHOX phosphorylation through a decrease in ERK1/2 activity. *FASEB J,* 20**,** 1504-6.

Davies, L. C., S. J. Jenkins, J. E. Allen & P. R. Taylor (2013) Tissue-resident macrophages. *Nat Immunol,* 14**,** 986-95.

Davis, A., I. B. Moore, D. S. Parker & H. Taniuchi (1977) Nuclease B. A possible precursor of nuclease A, an extracellular nuclease of *Staphylococcus aureus*. *Journal of Biological Chemistry,* 252**,** 6544-6553.

Davis, A., G. R. Parr & H. Taniuchi (1979) A kinetic study of the folding of nuclease B, a possible precursor of staphylococcal nuclease A. *Biochim Biophys Acta,* 578**,** 505-10.

de Buhr, N., M. Stehr, A. Neumann, H. Y. Naim, P. Valentin-Weigand, M. von Kockritz-Blickwede & C. G. Baums (2015) Identification of a novel DNase of *Streptococcus suis* (EndAsuis) important for neutrophil extracellular trap degradation during exponential growth. *Microbiology (Reading),* 161**,** 838-50.

Deng, G. M., I. M. Nilsson, M. Verdrengh, L. V. Collins & A. Tarkowski (1999) Intra-articularly localized bacterial DNA containing CpG motifs induces arthritis. *Nat Med,* 5**,** 702-5.

Deng, G. M. & A. Tarkowski (2000) The features of arthritis induced by CpG motifs in bacterial DNA. *Arthritis Rheum,* 43**,** 356-64.

Deng, L., F. Costa, K. J. Blake, S. Choi, A. Chandrabalan, M. S. Yousuf, S. Shiers, D. Dubreuil, D. Vega-Mendoza, C. Rolland, C. Deraison, T. Voisin, M. D. Bagood, L. Wesemann, A. M. Frey, J. S. Palumbo, B. J. Wainger, R. L. Gallo, J. M. Leyva-Castillo, N. Vergnolle, T. J. Price, R. Ramachandran, A. R. Horswill & I. M. Chiu (2023) *S. aureus* drives itch and scratch-induced skin damage through a V8 protease-PAR1 axis. *Cell,* 186**,** 5375-5393 e25.

Deshpande, R. A. & V. Shankar (2002) Ribonucleases from T2 family. *Crit Rev Microbiol,* 28**,** 79-122.

Diep, B. A., S. R. Gill, R. F. Chang, T. H. Phan, J. H. Chen, M. G. Davidson, F. Lin, J. Lin, H. A. Carleton, E. F. Mongodin, G. F. Sensabaugh & F. Perdreau-Remington (2006) Complete genome sequence of USA300, an epidemic clone of community-acquired meticillin-resistant *Staphylococcus aureus*. *Lancet,* 367**,** 731-9.

Duan, T., Y. Du, C. Xing, H. Y. Wang & R. F. Wang (2022) Toll-Like Receptor Signaling and Its Role in Cell-Mediated Immunity. *Front Immunol,* 13**,** 812774.

DuMont, A. L., P. Yoong, C. J. Day, F. Alonzo, 3rd, W. H. McDonald, M. P. Jennings & V. J. Torres (2013) *Staphylococcus aureus* LukAB cytotoxin kills human neutrophils by targeting the CD11b subunit of the integrin Mac-1. *Proc Natl Acad Sci U S A,* 110**,** 10794-9.

Dziarski, R. & D. Gupta (2005) *Staphylococcus aureus* peptidoglycan is a toll-like receptor 2 activator: a reevaluation. *Infect Immun,* 73**,** 5212-6.

Ebner, P., A. Luqman, S. Reichert, K. Hauf, P. Popella, K. Forchhammer, M. Otto & F. Götz (2017) Non-classical Protein Excretion Is Boosted by PSMalpha-Induced Cell Leakage. *Cell Rep,* 20**,** 1278-1286.

El Kebir, D., L. Jozsef, W. Pan, L. Wang & J. G. Filep (2009) Bacterial DNA activates endothelial cells and promotes neutrophil adherence through TLR9 signaling. *J Immunol,* 182**,** 4386-94.

Erickson, A. & R. H. Deibel (1973) Production and heat stability of *staphylococcal* nuclease. *Appl Microbiol,* 25**,** 332-6.

References

Ewald, S. E. & G. M. Barton (2011) Nucleic acid sensing Toll-like receptors in autoimmunity. *Curr Opin Immunol,* 23**,** 3-9.

Ewald, S. E., A. Engel, J. Lee, M. Wang, M. Bogyo & G. M. Barton (2011) Nucleic acid recognition by Toll-like receptors is coupled to stepwise processing by cathepsins and asparagine endopeptidase. *J Exp Med,* 208**,** 643-51.

Ewald, S. E., B. L. Lee, L. Lau, K. E. Wickliffe, G. P. Shi, H. A. Chapman & G. M. Barton (2008) The ectodomain of Toll-like receptor 9 is cleaved to generate a functional receptor. *Nature,* 456**,** 658-62.

Falugi, F., H. K. Kim, D. M. Missiakas & O. Schneewind (2013) Role of protein A in the evasion of host adaptive immune responses by *Staphylococcus aureus*. *mBio,* 4**,** e00575-13.

Fischer, E., K. J. Van Zee, M. A. Marano, C. S. Rock, J. S. Kenney, D. D. Poutsiaka, C. A. Dinarello, S. F. Lowry & L. L. Moldawer (1992) Interleukin-1 receptor antagonist circulates in experimental inflammation and in human disease. *Blood,* 79**,** 2196-200.

Fischer, W., T. Mannsfeld & G. Hagen (1990) On the basic structure of poly(glycerophosphate) lipoteichoic acids. *Biochem Cell Biol,* 68**,** 33-43.

Fitzgerald, K. A. & J. C. Kagan (2020) Toll-like Receptors and the Control of Immunity. *Cell,* 180**,** 1044-1066.

Flannagan, R. S., B. Heit & D. E. Heinrichs (2015) Antimicrobial Mechanisms of Macrophages and the Immune Evasion Strategies of *Staphylococcus aureus*. *Pathogens,* 4**,** 826-68.

Forson, A. M., C. W. K. Rosman, T. G. van Kooten, H. C. van der Mei & J. Sjollema (2021) Micrococcal Nuclease stimulates *Staphylococcus aureus* Biofilm Formation in a Murine Implant Infection Model. *Front Cell Infect Microbiol,* 11**,** 799845.

Forson, A. M., H. C. van der Mei & J. Sjollema (2020) Impact of solid surface hydrophobicity and micrococcal nuclease production on *Staphylococcus aureus* Newman biofilms. *Sci Rep,* 10**,** 12093.

Foster, T. J., J. A. Geoghegan, V. K. Ganesh & M. Hook (2014) Adhesion, invasion and evasion: the many functions of the surface proteins of *Staphylococcus aureus*. *Nat Rev Microbiol,* 12**,** 49-62.

Friedrich, R., P. Panizzi, P. Fuentes-Prior, K. Richter, I. Verhamme, P. J. Anderson, S.-I. Kawabata, R. Huber, W. Bode & P. E. Bock (2003) Staphylocoagulase is a prototype for the mechanism of cofactor-induced zymogen activation. *Nature,* 425**,** 535-539.

Fuchs, T. A., U. Abed, C. Goosmann, R. Hurwitz, I. Schulze, V. Wahn, Y. Weinrauch, V. Brinkmann & A. Zychlinsky (2007) Novel cell death program leads to neutrophil extracellular traps. *J Cell Biol,* 176**,** 231-41.

Garcia-Arias, M., A. Balsa & E. M. Mola (2011) Septic arthritis. *Best Pract Res Clin Rheumatol,* 25**,** 407-21.

Gardiner, J. H. t., G. Komazin, M. Matsuo, K. Cole, F. Götz & T. C. Meredith (2020) Lipoprotein N-Acylation in *Staphylococcus aureus* Is Catalyzed by a Two-Component Acyl Transferase System. *mBio,* 11.

Geirsson, A. J., S. Statkevicius & A. Vikingsson (2008) Septic arthritis in Iceland 1990-2002: increasing incidence due to iatrogenic infections. *Ann Rheum Dis,* 67**,** 638-43.

Giai, C., C. D. Gonzalez, F. Sabbione, A. Garofalo, D. Ojeda, D. O. Sordelli, A. S. Trevani & M. I. Gomez (2016) *Staphylococcus aureus* Induces Shedding of IL-1RII in Monocytes and Neutrophils. *J Innate Immun,* 8**,** 284-98.

References

Gjertsson, I., O. H. Hultgren & A. Tarkowski (2002) Interleukin-10 ameliorates the outcome of *Staphylococcus aureus* arthritis by promoting bacterial clearance. *Clin Exp Immunol,* 130**,** 409-14.

Gomez, M. I., A. Lee, B. Reddy, A. Muir, G. Soong, A. Pitt, A. Cheung & A. Prince (2004) *Staphylococcus aureus* protein A induces airway epithelial inflammatory responses by activating TNFR1. *Nat Med,* 10**,** 842-8.

Gonzalez, J. J. I., M. F. Hossain, J. Neef, E. E. Zwack, C. M. Tsai, D. Raafat, K. Fechtner, L. Herzog, T. P. Kohler, R. Schluter, A. Reder, S. Holtfreter, G. Y. Liu, S. Hammerschmidt, U. Volker, V. J. Torres, J. M. van Dijl, C. H. Lillig, B. M. Broker & M. N. Darisipudi (2024) TLR4 sensing of IsdB of *Staphylococcus aureus* induces a proinflammatory cytokine response via the NLRP3-caspase-1 inflammasome cascade. *mBio,* 15**,** e0022523.

Graf, A., R. J. Lewis, S. Fuchs, M. Pagels, S. Engelmann, K. Riedel & J. Pane-Farre (2018) The hidden lipoproteome of *Staphylococcus aureus*. *Int J Med Microbiol,* 308**,** 569-581.

Gries, C. M., T. Biddle, J. L. Bose, T. Kielian & D. D. Lo (2020) *Staphylococcus aureus* Fibronectin Binding Protein A Mediates Biofilm Development and Infection. *Infect Immun,* 88.

Haas, T., J. Metzger, F. Schmitz, A. Heit, T. Muller, E. Latz & H. Wagner (2008) The DNA sugar backbone 2' deoxyribose determines toll-like receptor 9 activation. *Immunity,* 28**,** 315-23.

Hamilton, J. A. & P. P. Tak (2009) The dynamics of macrophage lineage populations in inflammatory and autoimmune diseases. *Arthritis Rheum,* 60**,** 1210-21.

Hashimoto, M., K. Tawaratsumida, H. Kariya, K. Aoyama, T. Tamura & Y. Suda (2006) Lipoprotein is a predominant Toll-like receptor 2 ligand in *Staphylococcus aureus* cell wall components. *Int Immunol,* 18**,** 355-62.

Hassoun, A., P. K. Linden & B. Friedman (2017) Incidence, prevalence, and management of MRSA bacteremia across patient populations-a review of recent developments in MRSA management and treatment. *Crit Care,* 21**,** 211.

Hattar, K., C. P. Reinert, U. Sibelius, M. Y. Gokyildirim, F. S. B. Subtil, J. Wilhelm, B. Eul, G. Dahlem, F. Grimminger, W. Seeger & U. Grandel (2017) Lipoteichoic acids from *Staphylococcus aureus* stimulate proliferation of human non-small-cell lung cancer cells in vitro. *Cancer Immunol Immunother,* 66**,** 799-809.

Hernandez, F. J., L. Huang, M. E. Olson, K. M. Powers, L. I. Hernandez, D. K. Meyerholz, D. R. Thedens, M. A. Behlke, A. R. Horswill & J. O. McNamara, 2nd (2014) Noninvasive imaging of *Staphylococcus aureus* infections with a nuclease-activated probe. *Nat Med,* 20**,** 301-6.

Herzog, S., F. Dach, N. de Buhr, S. Niemann, J. Schlagowski, D. Chaves-Moreno, C. Neumann, J. Goretzko, V. Schwierzeck, A. Mellmann, A. Dubbers, P. Kuster, H. Schultingkemper, U. Rescher, D. H. Pieper, M. von Kockritz-Blickwede & B. C. Kahl (2019) High Nuclease Activity of Long Persisting *Staphylococcus aureus* Isolates Within the Airways of Cystic Fibrosis Patients Protects Against NET-Mediated Killing. *Front Immunol,* 10**,** 2552.

Hirsch, J. G. & Z. A. Cohn (1960) Degranulation of polymorphonuclear leucocytes following phagocytosis of microorganisms. *J Exp Med,* 112**,** 1005-14.

Howden, B. P., S. G. Giulieri, T. Wong Fok Lung, S. L. Baines, L. K. Sharkey, J. Y. H. Lee, A. Hachani, I. R. Monk & T. P. Stinear (2023) *Staphylococcus aureus* host interactions and adaptation. *Nat Rev Microbiol,* 21**,** 380-395.

Hruz, P., A. S. Zinkernagel, G. Jenikova, G. J. Botwin, J. P. Hugot, M. Karin, V. Nizet & L. Eckmann (2009) NOD2 contributes to cutaneous defense against *Staphylococcus aureus* through alpha-toxin-dependent innate immune activation. *Proc Natl Acad Sci U S A,* 106**,** 12873-8.

Hu, Y., J. Meng, C. Shi, K. Hervin, P. M. Fratamico & X. Shi (2013) Characterization and comparative analysis of a second thermonuclease from *Staphylococcus aureus*. *Microbiol Res,* 168**,** 174-82.

Hu, Y., Y. Xie, J. Tang & X. Shi (2012) Comparative expression analysis of two thermostable nuclease genes in *Staphylococcus aureus*. *Foodborne Pathog Dis,* 9**,** 265-71.

Hu, Z., P. K. Kopparapu, P. Ebner, M. Mohammad, S. Lind, A. Jarneborn, C. Dahlgren, M. Schultz, M. Deshmukh, R. Pullerits, M. Nega, M. T. Nguyen, Y. Fei, H. Forsman, F. Götz & T. Jin (2022) Phenol-soluble modulin alpha and beta display divergent roles in mice with *staphylococcal* septic arthritis. *Commun Biol,* 5**,** 910.

Hynes, T. R. & R. O. Fox (1991) The crystal structure of staphylococcal nuclease refined at 1.7 Å resolution. *Proteins: Structure, Function, and Bioinformatics,* 10**,** 92-105.

Ibberson, C. B., C. L. Jones, S. Singh, M. C. Wise, M. E. Hart, D. V. Zurawski & A. R. Horswill (2014) *Staphylococcus aureus* hyaluronidase is a CodY-regulated virulence factor. *Infect Immun,* 82**,** 4253-64.

Imanishi, I., A. Nicolas, A. B. Caetano, T. L. P. Castro, N. R. Tartaglia, R. Mariutti, E. Guedon, S. Even, N. Berkova, R. K. Arni, N. Seyffert, V. Azevedo, K. Nishifuji & Y. Le Loir (2019) Exfoliative toxin E, a new *Staphylococcus aureus* virulence factor with host-specific activity. *Sci Rep,* 9**,** 16336.

Ivanov, I., J. A. Tainer & J. A. McCammon (2007) Unraveling the three-metal-ion catalytic mechanism of the DNA repair enzyme endonuclease IV. *Proc Natl Acad Sci U S A,* 104**,** 1465-70.

Janeway, C. A., Jr. (1989) Approaching the asymptote? Evolution and revolution in immunology. *Cold Spring Harb Symp Quant Biol,* 54 Pt 1**,** 1-13.

Jia, Y., Z. Guan, C. Liu, M. Huang, J. Li, J. Feng, B. Shen & G. Yang (2024) *Staphylococcus aureus* beta-hemolysin causes skin inflammation by acting as an agonist of epidermal growth factor receptor. *Microbiol Spectr,* 12**,** e0222723.

Jin, T., M. Mohammad, R. Pullerits & A. Ali (2021) Bacteria and Host Interplay in *Staphylococcus aureus* Septic Arthritis and Sepsis. *Pathogens,* 10.

Josse, J., F. Velard & S. C. Gangloff (2015) *Staphylococcus aureus* vs. Osteoblast: Relationship and Consequences in Osteomyelitis. *Front Cell Infect Microbiol,* 5**,** 85.

Kaesler, S., Y. Skabytska, K. M. Chen, W. E. Kempf, T. Volz, M. Koberle, F. Wolbing, U. Hein, T. Hartung, C. Kirschning, M. Rocken & T. Biedermann (2016) *Staphylococcus aureus*-derived lipoteichoic acid induces temporary T-cell paralysis independent of Toll-like receptor 2. *J Allergy Clin Immunol,* 138**,** 780-790 e6.

Kang, S. S., S. Y. Noh, O. J. Park, C. H. Yun & S. H. Han (2015) *Staphylococcus aureus* induces IL-8 expression through its lipoproteins in the human intestinal epithelial cell, Caco-2. *Cytokine,* 75**,** 174-80.

Kanneganti, T. D., M. Lamkanfi & G. Nunez (2007) Intracellular NOD-like receptors in host defense and disease. *Immunity,* 27**,** 549-59.

Kaplan, J. B. & A. R. Horswill (2024) Micrococcal nuclease regulates biofilm formation and dispersal in methicillin-resistant *Staphylococcus aureus* USA300. *mSphere,* 9**,** e0012624.

Katayama, Y., T. Baba, M. Sekine, M. Fukuda & K. Hiramatsu (2013) Beta-hemolysin promotes skin colonization by *Staphylococcus aureus*. *J Bacteriol,* 195**,** 1194-203.

Kawai, T. & S. Akira (2011) Toll-like receptors and their crosstalk with other innate receptors in infection and immunity. *Immunity,* 34**,** 637-50.

Kiedrowski, M. R., H. A. Crosby, F. J. Hernandez, C. L. Malone, J. O. McNamara, 2nd & A. R. Horswill (2014) Staphylococcus aureus Nuc2 is a functional, surface-attached extracellular nuclease. *PLoS One,* 9**,** e95574.

Kiedrowski, M. R., J. S. Kavanaugh, C. L. Malone, J. M. Mootz, J. M. Voyich, M. S. Smeltzer, K. W. Bayles & A. R. Horswill (2011) Nuclease modulates biofilm formation in community-associated methicillin-resistant *Staphylococcus aureus*. *PLoS One,* 6**,** e26714.

Kielian, T., E. D. Bearden, A. C. Baldwin & N. Esen (2004) IL-1 and TNF-alpha play a pivotal role in the host immune response in a mouse model of S*taphylococcus aureus*-induced experimental brain abscess. *J Neuropathol Exp Neurol,* 63**,** 381-96.

Kim, J., J. Yang, O. J. Park, S. S. Kang, W. S. Kim, K. Kurokawa, C. H. Yun, H. H. Kim, B. L. Lee & S. H. Han (2013) Lipoproteins are an important bacterial component responsible for bone destruction through the induction of osteoclast differentiation and activation. *J Bone Miner Res,* 28**,** 2381-91.

Krishna, S. & L. S. Miller (2012) Innate and adaptive immune responses against *Staphylococcus aureus* skin infections. *Semin Immunopathol,* 34**,** 261-80.

Kroh, H. K., P. Panizzi & P. E. Bock (2009) Von Willebrand factor-binding protein is a hysteretic conformational activator of prothrombin. *Proc Natl Acad Sci U S A,* 106**,** 7786-91.

Kurokawa, K., M. S. Kim, R. Ichikawa, K. H. Ryu, N. Dohmae, H. Nakayama & B. L. Lee (2012) Environment-mediated accumulation of diacyl lipoproteins over their triacyl counterparts in *Staphylococcus aureus*. *J Bacteriol,* 194**,** 3299-306.

Leejae, S., P. W. Taylor & S. P. Voravuthikunchai (2013) Antibacterial mechanisms of rhodomyrtone against important hospital-acquired antibiotic-resistant pathogenic bacteria. *J Med Microbiol,* 62**,** 78-85.

Lemaitre, B., E. Nicolas, L. Michaut, J.-M. Reichhart & J. A. Hoffmann (1996) The dorsoventral regulatory gene cassette spätzle/Toll/cactus controls the potent antifungal response in Drosophila adults. *Cell,* 86**,** 973-983.

Lenski, M. & M. A. Scherer (2014) The significance of interleukin-6 and lactate in the synovial fluid for diagnosing native septic arthritis. *Acta Orthop Belg,* 80**,** 18-25.

Ley, K., C. Laudanna, M. I. Cybulsky & S. Nourshargh (2007) Getting to the site of inflammation: the leukocyte adhesion cascade updated. *Nat Rev Immunol,* 7**,** 678-89.

Li, Y., I. C. Berke & Y. Modis (2012) DNA binding to proteolytically activated TLR9 is sequence-independent and enhanced by DNA curvature. *EMBO J,* 31**,** 919-31.

Limsuwan, S., E. N. Trip, T. R. Kouwen, S. Piersma, A. Hiranrat, W. Mahabusarakam, S. P. Voravuthikunchai, J. M. van Dijl & O. Kayser (2009)

Rhodomyrtone: a new candidate as natural antibacterial drug from Rhodomyrtus tomentosa. *Phytomedicine,* 16**,** 645-51.

Loffler, B., M. Hussain, M. Grundmeier, M. Bruck, D. Holzinger, G. Varga, J. Roth, B. C. Kahl, R. A. Proctor & G. Peters (2010) *Staphylococcus aureus* panton-valentine leukocidin is a very potent cytotoxic factor for human neutrophils. *PLoS Pathog,* 6**,** e1000715.

Lood, C., L. P. Blanco, M. M. Purmalek, C. Carmona-Rivera, S. S. De Ravin, C. K. Smith, H. L. Malech, J. A. Ledbetter, K. B. Elkon & M. J. Kaplan (2016) Neutrophil extracellular traps enriched in oxidized mitochondrial DNA are interferogenic and contribute to lupus-like disease. *Nat Med,* 22**,** 146-53.

Lowy, F. D. (2003) Antimicrobial resistance: the example of *Staphylococcus aureus*. *J Clin Invest,* 111**,** 1265-73.

Lu, Z., C. R. Dockery, M. Crosby, K. Chavarria, B. Patterson & M. Giedd (2016) Antibacterial Activities of Wasabi against *Escherichia coli* O157:H7 and *Staphylococcus aureus*. *Front Microbiol,* 7**,** 1403.

Ludwig, N., J. Thorner-van Almsick, S. Mersmann, B. Bardel, S. Niemann, A. I. Chasan, M. Schafers, A. Margraf, J. Rossaint, B. C. Kahl, A. Zarbock & H. Block (2023) Nuclease activity and protein A release of *Staphylococcus aureus* clinical isolates determine the virulence in a murine model of acute lung infection. *Front Immunol,* 14**,** 1259004.

Marriott, I., D. L. Gray, S. L. Tranguch, V. G. Fowler, Jr., M. Stryjewski, L. Scott Levin, M. C. Hudson & K. L. Bost (2004) Osteoblasts express the inflammatory cytokine interleukin-6 in a murine model of *Staphylococcus aureus* osteomyelitis and infected human bone tissue. *Am J Pathol,* 164**,** 1399-406.

Mathews, C. J., V. C. Weston, A. Jones, M. Field & G. Coakley (2010) Bacterial septic arthritis in adults. *Lancet,* 375**,** 846-55.

McGavin, M. J., C. Zahradka, K. Rice & J. E. Scott (1997) Modification of the *Staphylococcus aureus* fibronectin binding phenotype by V8 protease. *Infection and immunity,* 65**,** 2621-2628.

McGuinness, W. A., S. D. Kobayashi & F. R. DeLeo (2016) Evasion of Neutrophil Killing by *Staphylococcus aureus*. *Pathogens,* 5.

Menezes, G. B., W. Y. Lee, H. Zhou, C. C. Waterhouse, D. C. Cara & P. Kubes (2009) Selective down-regulation of neutrophil Mac-1 in endotoxemic hepatic microcirculation via IL-10. *J Immunol,* 183**,** 7557-68.

Metzler, K. D., T. A. Fuchs, W. M. Nauseef, D. Reumaux, J. Roesler, I. Schulze, V. Wahn, V. Papayannopoulos & A. Zychlinsky (2011) Myeloperoxidase is required for neutrophil extracellular trap formation: implications for innate immunity. *Blood,* 117**,** 953-9.

Miller, J. R., S. Kovacevic & L. E. Veal (1987) Secretion and processing of staphylococcal nuclease by *Bacillus subtilis*. *J Bacteriol,* 169**,** 3508-14.

Mills, K. B., J. J. Maciag, C. Wang, J. A. Crawford, T. J. Enroth, K. C. Keim, Y. F. Dufrene, D. A. Robinson, P. D. Fey, A. B. Herr & A. R. Horswill (2024) *Staphylococcus aureus* skin colonization is mediated by SasG lectin variation. *Cell Rep,* 43**,** 114022.

Miyata, M., H. Kobayashi, T. Sasajima, Y. Sato & R. Kasukawa (2000) Unmethylated oligo-DNA containing CpG motifs aggravates collagen-induced arthritis in mice. *Arthritis Rheum,* 43**,** 2578-82.

Mohamed, W., E. Domann, T. Chakraborty, G. Mannala, K. S. Lips, C. Heiss, R. Schnettler & V. Alt (2016) TLR9 mediates *S. aureus* killing inside osteoblasts via induction of oxidative stress. *BMC Microbiol,* 16**,** 230.

References

Mohammad, M., M. Na, Z. Hu, M. T. Nguyen, P. K. Kopparapu, A. Jarneborn, A. Karlsson, A. Ali, R. Pullerits, F. Götz & T. Jin (2021) *Staphylococcus aureus* lipoproteins promote abscess formation in mice, shielding bacteria from immune killing. *Commun Biol,* 4**,** 432.

Mohammad, M., M. T. Nguyen, C. Engdahl, M. Na, A. Jarneborn, Z. Hu, A. Karlsson, R. Pullerits, A. Ali, F. Götz & T. Jin (2019) The YIN and YANG of lipoproteins in developing and preventing infectious arthritis by *Staphylococcus aureus*. *PLoS Pathog,* 15**,** e1007877.

Moormeier, D. E., J. L. Bose, A. R. Horswill & K. W. Bayles (2014) Temporal and stochastic control of *Staphylococcus aureus* biofilm development. *mBio,* 5**,** e01341-14.

Na, M., Z. Hu, M. Mohammad, M. D. N. Stroparo, A. Ali, Y. Fei, A. Jarneborn, P. Verhamme, O. Schneewind, D. Missiakas & T. Jin (2020) The Expression of von Willebrand Factor-Binding Protein Determines Joint-Invading Capacity of *Staphylococcus aureus*, a Core Mechanism of Septic Arthritis. *mBio,* 11.

Nair, S. P., M. Bischoff, M. M. Senn & B. Berger-Bachi (2003) The sigma B regulon influences internalization of *Staphylococcus aureus* by osteoblasts. *Infect Immun,* 71**,** 4167-70.

Nguyen, M. T., B. Kraft, W. Yu, D. D. Demircioglu, T. Hertlein, M. Burian, M. Schmaler, K. Boller, I. Bekeredjian-Ding, K. Ohlsen, B. Schittek & F. Götz (2015) The vSaα Specific Lipoprotein Like Cluster (lpl) of *S. aureus* USA300 Contributes to Immune Stimulation and Invasion in Human Cells. *PLoS Pathog,* 11**,** e1004984.

Nguyen, M. T., A. Luqman, K. Bitschar, T. Hertlein, J. Dick, K. Ohlsen, B. Broker, B. Schittek & F. Götz (2018a) Staphylococcal (phospho)lipases promote biofilm formation and host cell invasion. *Int J Med Microbiol,* 308**,** 653-663.

Nguyen, M. T., L. Peisl, F. Barletta, A. Luqman & F. Götz (2018b) Toll-Like Receptor 2 and Lipoprotein-Like Lipoproteins Enhance *Staphylococcus aureus* Invasion in Epithelial Cells. *Infect Immun,* 86.

Nguyen, M. T., J. Saising, P. M. Tribelli, M. Nega, S. M. Diene, P. Francois, J. Schrenzel, C. Sproer, B. Bunk, P. Ebner, T. Hertlein, N. Kumari, T. Hartner, D. Wistuba, S. P. Voravuthikunchai, U. Mader, K. Ohlsen & F. Götz (2019) Inactivation of farR Causes High Rhodomyrtone Resistance and Increased Pathogenicity in Staphylococcus aureus. *Front Microbiol,* 10**,** 1157.

Nickerson, N. N., V. Joag & M. J. McGavin (2008) Rapid autocatalytic activation of the M4 metalloprotease aureolysin is controlled by a conserved N-terminal fungalysin-thermolysin-propeptide domain. *Mol Microbiol,* 69**,** 1530-43.

Ning, R., X. Zhang, X. Guo & Q. Li (2011) *Staphylococcus aureus* regulates secretion of interleukin-6 and monocyte chemoattractant protein-1 through activation of nuclear factor kappaB signaling pathway in human osteoblasts. *Brazilian Journal of Infectious Diseases,* 15**,** 189-194.

O'Brien, G. J., G. Riddell, J. S. Elborn, M. Ennis & G. Skibinski (2006) *Staphylococcus aureus* enterotoxins induce IL-8 secretion by human nasal epithelial cells. *Respir Res,* 7**,** 115.

Ogston, A. (1881) Report upon micro-organisms in surgical diseases. *British medical journal,* 1**,** 369. b2.

Ohto, U., T. Shibata, H. Tanji, H. Ishida, E. Krayukhina, S. Uchiyama, K. Miyake & T. Shimizu (2015) Structural basis of CpG and inhibitory DNA recognition by Toll-like receptor 9. *Nature,* 520**,** 702-5.

Olson, M. E., T. K. Nygaard, L. Ackermann, R. L. Watkins, O. W. Zurek, K. B. Pallister, S. Griffith, M. R. Kiedrowski, C. E. Flack, J. S. Kavanaugh, B. N. Kreiswirth, A. R. Horswill & J. M. Voyich (2013) *Staphylococcus aureus* nuclease is an SaeRS-dependent virulence factor. *Infect Immun,* 81**,** 1316-24.

Opal, S. M. & V. A. DePalo (2000) Anti-inflammatory cytokines. *Chest,* 117**,** 1162-72.

Osiri, M., K. Ruxrungtham, S. Nookhai, Y. Ohmoto & U. Deesomchok (1998) IL-1beta, IL-6 and TNF-alpha in synovial fluid of patients with non-gonococcal septic arthritis. *Asian Pac J Allergy Immunol,* 16**,** 155-60.

Osuchowski, M. F., K. Welch, J. Siddiqui & D. G. Remick (2006) Circulating cytokine/inhibitor profiles reshape the understanding of the SIRS/CARS continuum in sepsis and predict mortality. *J Immunol,* 177**,** 1967-74.

Paharik, A. E., W. Salgado-Pabon, D. K. Meyerholz, M. J. White, P. M. Schlievert & A. R. Horswill (2016) The Spl Serine Proteases Modulate *Staphylococcus aureus* Protein Production and Virulence in a Rabbit Model of Pneumonia. *mSphere,* 1.

Papayannopoulos, V. (2018) Neutrophil extracellular traps in immunity and disease. *Nat Rev Immunol,* 18**,** 134-147.

Papayannopoulos, V., K. D. Metzler, A. Hakkim & A. Zychlinsky (2010) Neutrophil elastase and myeloperoxidase regulate the formation of neutrophil extracellular traps. *J Cell Biol,* 191**,** 677-91.

Parker, D. & A. Prince (2012) *Staphylococcus aureus* induces type I IFN signaling in dendritic cells via TLR9. *J Immunol,* 189**,** 4040-6.

Peschel, A. & M. Otto (2013) Phenol-soluble modulins and staphylococcal infection. *Nat Rev Microbiol,* 11**,** 667-73.

Petri, B., M. Phillipson & P. Kubes (2008) The physiology of leukocyte recruitment: an in vivo perspective. *J Immunol,* 180**,** 6439-46.

Pilsczek, F. H., D. Salina, K. K. Poon, C. Fahey, B. G. Yipp, C. D. Sibley, S. M. Robbins, F. H. Green, M. G. Surette, M. Sugai, M. G. Bowden, M. Hussain, K. Zhang & P. Kubes (2010) A novel mechanism of rapid nuclear neutrophil extracellular trap formation in response to Staphylococcus aureus. *J Immunol,* 185**,** 7413-25.

Pohar, J., D. Lainscek, R. Fukui, C. Yamamoto, K. Miyake, R. Jerala & M. Bencina (2015) Species-Specific Minimal Sequence Motif for Oligodeoxyribonucleotides Activating Mouse TLR9. *J Immunol,* 195**,** 4396-405.

Pohar, J., D. Lainscek, K. Ivicak-Kocjan, M. M. Cajnko, R. Jerala & M. Bencina (2017) Short single-stranded DNA degradation products augment the activation of Toll-like receptor 9. *Nat Commun,* 8**,** 15363.

Rautenberg, M., H. S. Joo, M. Otto & A. Peschel (2011) Neutrophil responses to staphylococcal pathogens and commensals via the formyl peptide receptor 2 relates to phenol-soluble modulin release and virulence. *FASEB J,* 25**,** 1254-63.

Remick, D. G. (2005) Interleukin-8. *Crit Care Med,* 33**,** S466-7.

Rigby, K. M. & F. R. DeLeo (2012) Neutrophils in innate host defense against *Staphylococcus aureus* infections. *Semin Immunopathol,* 34**,** 237-59.

Roberts, T. L., J. A. Dunn, T. D. Terry, M. P. Jennings, D. A. Hume, M. J. Sweet & K. J. Stacey (2005) Differences in macrophage activation by bacterial DNA and CpG-containing oligonucleotides. *J Immunol,* 175**,** 3569-76.

Rosenbach, F. J. & A. J. F. Rosenbach. 1884. *Mikro-organismen bei den Wund-infections-krankheiten des Menschen*. JF Bergmann.

Sadik, C. D., N. D. Kim & A. D. Luster (2011) Neutrophils cascading their way to inflammation. *Trends Immunol,* 32**,** 452-60.

Saeloh, D., V. Tipmanee, K. K. Jim, M. P. Dekker, W. Bitter, S. P. Voravuthikunchai, M. Wenzel & L. W. Hamoen (2018) The novel antibiotic rhodomyrtone traps membrane proteins in vesicles with increased fluidity. *PLoS Pathog,* 14**,** e1006876.

Saising, J., M.-T. Nguyen, T. Härtner, P. Ebner, A. A. M. Bhuyan, A. Berscheid, M. Muehlenkamp, S. Schäkermann, N. Kumari & M. E. Maier (2018) Rhodomyrtone (Rom) is a membrane-active compound. *Biochimica Et Biophysica Acta (BBA)-Biomembranes,* 1860**,** 1114-1124.

Saising, J. & S. P. Voravuthikunchai (2012) Anti Propionibacterium acnes activity of rhodomyrtone, an effective compound from *Rhodomyrtus tomentosa* (Aiton) *Hassk.* leaves. *Anaerobe,* 18**,** 400-4.

Salni, D., M. Sargent, B. Skelton, I. Soediro, M. Sutisna, A. White & E. Yulinah (2002) Rhodomyrtone, an antibotic from Rhodomyrtus tomentosa. *Australian Journal of Chemistry,* 55**,** 229-232.

Samani, S. S., A. Khojastehnezhad, M. Ramezani, M. Alibolandi, F. T. Yazdi, S. A. Mortazavi, Z. Khoshbin, K. Abnous & S. M. Taghdisi (2021) Ultrasensitive detection of micrococcal nuclease activity and *Staphylococcus aureus* contamination using optical biosensor technology-A review. *Talanta,* 226**,** 122168.

Sankaran, K. & H. C. Wu (1994) Lipid modification of bacterial prolipoprotein. Transfer of diacylglyceryl moiety from phosphatidylglycerol. *J Biol Chem,* 269**,** 19701-6.

Schett, G. & E. Gravallese (2012) Bone erosion in rheumatoid arthritis: mechanisms, diagnosis and treatment. *Nat Rev Rheumatol,* 8**,** 656-64.

Schilcher, K., F. Andreoni, S. Uchiyama, T. Ogawa, R. A. Schuepbach & A. S. Zinkernagel (2014) Increased neutrophil extracellular trap-mediated *Staphylococcus aureus* clearance through inhibition of nuclease activity by clindamycin and immunoglobulin. *J Infect Dis,* 210**,** 473-82.

Schroder, J. M. (1989) The monocyte-derived neutrophil activating peptide (NAP/interleukin 8) stimulates human neutrophil arachidonate-5-lipoxygenase, but not the release of cellular arachidonate. *J Exp Med,* 170**,** 847-63.

Schroder, N. W., S. Morath, C. Alexander, L. Hamann, T. Hartung, U. Zahringer, U. B. Gobel, J. R. Weber & R. R. Schumann (2003) Lipoteichoic acid (LTA) of *Streptococcus pneumoniae* and *Staphylococcus aureus* activates immune cells via Toll-like receptor (TLR)-2, lipopolysaccharide-binding protein (LBP), and CD14, whereas TLR-4 and MD-2 are not involved. *J Biol Chem,* 278**,** 15587-94.

Segal, A. W. (2005) How neutrophils kill microbes. *Annu Rev Immunol,* 23**,** 197-223.

Shaghayegh, G., C. Cooksley, M. Ramezanpour, P. J. Wormald, A. J. Psaltis & S. Vreugde (2022) Chronic Rhinosinusitis, *S. aureus* Biofilm and Secreted Products, Inflammatory Responses, and Disease Severity. *Biomedicines,* 10.

Shen, B., P. Singh, R. Liu, J. Qiu, L. Zheng, L. D. Finger & S. Alas (2005) Multiple but dissectible functions of FEN-1 nucleases in nucleic acid processing, genome stability and diseases. *Bioessays,* 27**,** 717-29.

Sieprawska-Lupa, M., P. Mydel, K. Krawczyk, K. Wojcik, M. Puklo, B. Lupa, P. Suder, J. Silberring, M. Reed, J. Pohl, W. Shafer, F. McAleese, T. Foster, J. Travis & J. Potempa (2004) Degradation of human antimicrobial peptide LL-37 by

Staphylococcus aureus-derived proteinases. *Antimicrob Agents Chemother,* 48**,** 4673-9.

Silver, L. L. (2011) Challenges of antibacterial discovery. *Clin Microbiol Rev,* 24**,** 71-109.

Sinha, B., P. P. Francois, O. Nusse, M. Foti, O. M. Hartford, P. Vaudaux, T. J. Foster, D. P. Lew, M. Herrmann & K. H. Krause (1999) Fibronectin-binding protein acts as *Staphylococcus aureus* invasin via fibronectin bridging to integrin alpha5beta1. *Cell Microbiol,* 1**,** 101-17.

Siriyong, T., J. C. Ontong, S. Leejae, S. Suwalak, P. J. Coote & S. P. Voravuthikunchai (2020) In vivo safety assessment of rhodomyrtone, a potent compound, from Rhodomyrtus tomentosa leaf extract. *Toxicol Rep,* 7**,** 919-924.

Smagur, J., K. Guzik, L. Magiera, M. Bzowska, M. Gruca, I. B. Thogersen, J. J. Enghild & J. Potempa (2009) A new pathway of staphylococcal pathogenesis: apoptosis-like death induced by Staphopain B in human neutrophils and monocytes. *J Innate Immun,* 1**,** 98-108.

Sofrata, A., E. M. Santangelo, M. Azeem, A. K. Borg-Karlson, A. Gustafsson & K. Putsep (2011) Benzyl isothiocyanate, a major component from the roots of *Salvadora persica* is highly active against Gram-negative bacteria. *PLoS One,* 6**,** e23045.

Son, E. D., H. J. Kim, T. Park, K. Shin, I. H. Bae, K. M. Lim, E. G. Cho & T. R. Lee (2014) *Staphylococcus aureus* inhibits terminal differentiation of normal human keratinocytes by stimulating interleukin-6 secretion. *J Dermatol Sci,* 74**,** 64-71.

Sparwasser, T., T. Miethke, G. Lipford, K. Borschert, H. Hacker, K. Heeg & H. Wagner (1997) Bacterial DNA causes septic shock. *Nature,* 386**,** 336-7.

Stelzner, K., A. Boyny, T. Hertlein, A. Sroka, A. Moldovan, K. Paprotka, D. Kessie, H. Mehling, J. Potempa, K. Ohlsen, M. J. Fraunholz & T. Rudel (2021) Intracellular *Staphylococcus aureus* employs the cysteine protease staphopain A to induce host cell death in epithelial cells. *PLoS Pathog,* 17**,** e1009874.

Stoll, H., J. Dengjel, C. Nerz & F. Götz (2005) *Staphylococcus aureus* deficient in lipidation of prelipoproteins is attenuated in growth and immune activation. *Infect Immun,* 73**,** 2411-23.

Suciu, D. & M. Inouye (1996) The 19-residue pro-peptide of staphylococcal nuclease has a profound secretion-enhancing ability in *Escherichia coli*. *Mol Microbiol,* 21**,** 181-95.

Sumby, P., K. D. Barbian, D. J. Gardner, A. R. Whitney, D. M. Welty, R. D. Long, J. R. Bailey, M. J. Parnell, N. P. Hoe, G. G. Adams, F. R. Deleo & J. M. Musser (2005) Extracellular deoxyribonuclease made by group A *Streptococcus* assists pathogenesis by enhancing evasion of the innate immune response. *Proc Natl Acad Sci U S A,* 102**,** 1679-84.

Swanson, J. A. (2008) Shaping cups into phagosomes and macropinosomes. *Nature reviews Molecular cell biology,* 9**,** 639-649.

Takano, S., K. Uchida, M. Miyagi, G. Inoue, J. Aikawa, H. Fujimaki, A. Minatani, M. Sato, K. Iwabuchi & M. Takaso (2016) Synovial macrophage-derived IL-1beta regulates the calcitonin receptor in osteoarthritic mice. *Clin Exp Immunol,* 183**,** 143-9.

Takeuchi, O. & S. Akira (2010) Pattern recognition receptors and inflammation. *Cell,* 140**,** 805-20.

Tam, K. & V. J. Torres (2019) *Staphylococcus aureus* Secreted Toxins and Extracellular Enzymes. *Microbiol Spectr,* 7.

Tanaka, M., P. Mroz, T. Dai, L. Huang, Y. Morimoto, M. Kinoshita, Y. Yoshihara, K. Nemoto, N. Shinomiya, S. Seki & M. R. Hamblin (2012) Photodynamic therapy can induce a protective innate immune response against murine bacterial arthritis via neutrophil accumulation. *PLoS One,* 7**,** e39823.

Tantawy, E., N. Schwermann, T. Ostermeier, A. Garbe, H. Bahre, M. Vital & V. Winstel (2022) *Staphylococcus aureus* Multiplexes Death-Effector Deoxyribonucleosides to Neutralize Phagocytes. *Front Immunol,* 13**,** 847171.

Thammavongsa, V., J. W. Kern, D. M. Missiakas & O. Schneewind (2009) *Staphylococcus aureus* synthesizes adenosine to escape host immune responses. *J Exp Med,* 206**,** 2417-27.

Thammavongsa, V., D. M. Missiakas & O. Schneewind (2013) *Staphylococcus aureus* degrades neutrophil extracellular traps to promote immune cell death. *Science,* 342**,** 863-6.

Tong, S. Y., J. S. Davis, E. Eichenberger, T. L. Holland & V. G. Fowler, Jr. (2015) *Staphylococcus aureus* infections: epidemiology, pathophysiology, clinical manifestations, and management. *Clin Microbiol Rev,* 28**,** 603-61.

Tsai TsungHsien, T. T., T. T. Tsai TzungHsun, W. W. Wu WenHuey, T. TePeng & T. P. Tsai PoJung (2010) In vitro antimicrobial and anti-inflammatory effects of herbs against *Propionibacterium acnes*.

Tucker, P. W., E. E. Hazen, Jr. & F. A. Cotton (1978) *Staphylococcal* nuclease reviewed: a prototypic study in contemporary enzymology. I. Isolation; physical and enzymatic properties. *Mol Cell Biochem,* 22**,** 67-77.

Tuffs, S. W., M. I. Goncheva, S. X. Xu, H. C. Craig, K. J. Kasper, J. Choi, R. S. Flannagan, S. M. Kerfoot, D. E. Heinrichs & J. K. McCormick (2022) Superantigens promote *Staphylococcus aureus* bloodstream infection by eliciting pathogenic interferon-gamma production. *Proc Natl Acad Sci U S A,* 119.

Uchiyama, S., F. Andreoni, R. A. Schuepbach, V. Nizet & A. S. Zinkernagel (2012) DNase Sda1 allows invasive M1T1 Group A *Streptococcus* to prevent TLR9-dependent recognition. *PLoS Pathog,* 8**,** e1002736.

Urban, C. F., D. Ermert, M. Schmid, U. Abu-Abed, C. Goosmann, W. Nacken, V. Brinkmann, P. R. Jungblut & A. Zychlinsky (2009) Neutrophil extracellular traps contain calprotectin, a cytosolic protein complex involved in host defense against Candida albicans. *PLoS Pathog,* 5**,** e1000639.

van der Meer, A. J., A. Achouiti, A. van der Ende, A. A. Soussan, S. Florquin, A. de Vos, S. S. Zeerleder & T. van der Poll (2016) Toll-like receptor 9 enhances bacterial clearance and limits lung consolidation in murine pneumonia caused by methicillin resistant *Staphylococcus aureus*. *Mol Med,* 22**,** 292-299.

Verdrengh, M. & A. Tarkowski (1997) Role of neutrophils in experimental septicemia and septic arthritis induced by *Staphylococcus aureus*. *Infect Immun,* 65**,** 2517-21.

Voyich, J. M., C. Vuong, M. DeWald, T. K. Nygaard, S. Kocianova, S. Griffith, J. Jones, C. Iverson, D. E. Sturdevant, K. R. Braughton, A. R. Whitney, M. Otto & F. R. DeLeo (2009) The SaeR/S gene regulatory system is essential for innate immune evasion by *Staphylococcus aureus*. *J Infect Dis,* 199**,** 1698-706.

Wang, J. E., P. F. Jorgensen, M. Almlof, C. Thiemermann, S. J. Foster, A. O. Aasen & R. Solberg (2000) Peptidoglycan and lipoteichoic acid from *Staphylococcus*

aureus induce tumor necrosis factor alpha, interleukin 6 (IL-6), and IL-10 production in both T cells and monocytes in a human whole blood model. *Infect Immun,* 68**,** 3965-70.

Wang, T. & C. He (2018) Pro-inflammatory cytokines: The link between obesity and osteoarthritis. *Cytokine & growth factor reviews,* 44**,** 38-50.

Wang, Y., J. Wysocka, J. Sayegh, Y. H. Lee, J. R. Perlin, L. Leonelli, L. S. Sonbuchner, C. H. McDonald, R. G. Cook, Y. Dou, R. G. Roeder, S. Clarke, M. R. Stallcup, C. D. Allis & S. A. Coonrod (2004) Human PAD4 regulates histone arginine methylation levels via demethylimination. *Science,* 306**,** 279-83.

Wertheim, H. F., D. C. Melles, M. C. Vos, W. van Leeuwen, A. van Belkum, H. A. Verbrugh & J. L. Nouwen (2005) The role of nasal carriage in *Staphylococcus aureus* infections. *Lancet Infect Dis,* 5**,** 751-62.

West, A. P., A. A. Koblansky & S. Ghosh (2006) Recognition and signaling by toll-like receptors. *Annu Rev Cell Dev Biol,* 22**,** 409-37.

White, M. J., J. M. Boyd, A. R. Horswill & W. M. Nauseef (2014) Phosphatidylinositol-specific phospholipase C contributes to survival of *Staphylococcus aureus* USA300 in human blood and neutrophils. *Infect Immun,* 82**,** 1559-71.

Widaa, A., T. Claro, T. J. Foster, F. J. O'Brien & S. W. Kerrigan (2012) *Staphylococcus aureus* protein A plays a critical role in mediating bone destruction and bone loss in osteomyelitis. *PLoS One,* 7**,** e40586.

Winstel, V., D. Missiakas & O. Schneewind (2018) *Staphylococcus aureus* targets the purine salvage pathway to kill phagocytes. *Proc Natl Acad Sci U S A,* 115**,** 6846-6851.

Winterbourn, C. C. & A. J. Kettle (2013) Redox reactions and microbial killing in the neutrophil phagosome. *Antioxid Redox Signal,* 18**,** 642-60.

Wu, H. M., J. Wang, B. Zhang, L. Fang, K. Xu & R. Y. Liu (2016) CpG-ODN promotes phagocytosis and autophagy through JNK/P38 signal pathway in *Staphylococcus aureus*-stimulated macrophage. *Life Sci,* 161**,** 51-9.

Yang, W. (2011) Nucleases: diversity of structure, function and mechanism. *Q Rev Biophys,* 44**,** 1-93.

Yarovinsky, F., D. Zhang, J. F. Andersen, G. L. Bannenberg, C. N. Serhan, M. S. Hayden, S. Hieny, F. S. Sutterwala, R. A. Flavell, S. Ghosh & A. Sher (2005) TLR11 activation of dendritic cells by a protozoan profilin-like protein. *Science,* 308**,** 1626-9.

Yeo, L., N. Adlard, M. Biehl, M. Juarez, T. Smallie, M. Snow, C. D. Buckley, K. Raza, A. Filer & D. Scheel-Toellner (2016) Expression of chemokines CXCL4 and CXCL7 by synovial macrophages defines an early stage of rheumatoid arthritis. *Ann Rheum Dis,* 75**,** 763-71.

Yipp, B. G., B. Petri, D. Salina, C. N. Jenne, B. N. Scott, L. D. Zbytnuik, K. Pittman, M. Asaduzzaman, K. Wu, H. C. Meijndert, S. E. Malawista, A. de Boisfleury Chevance, K. Zhang, J. Conly & P. Kubes (2012) Infection-induced NETosis is a dynamic process involving neutrophil multitasking in vivo. *Nat Med,* 18**,** 1386-93.

Yokota, K., K. Sato, T. Miyazaki, H. Kitaura, H. Kayama, F. Miyoshi, Y. Araki, Y. Akiyama, K. Takeda & T. Mimura (2014) Combination of tumor necrosis factor alpha and interleukin-6 induces mouse osteoclast-like cells with bone resorption activity both in vitro and in vivo. *Arthritis Rheumatol,* 66**,** 121-9.

References

Yoshitake, F., S. Itoh, H. Narita, K. Ishihara & S. Ebisu (2008) Interleukin-6 directly inhibits osteoclast differentiation by suppressing receptor activator of NF-kappaB signaling pathways. *J Biol Chem,* 283**,** 11535-40.

Yu, J., F. Jiang, F. Zhang, M. Hamushan, J. Du, Y. Mao, Q. Wang, P. Han, J. Tang & H. Shen (2021) Thermonucleases Contribute to *Staphylococcus aureus* Biofilm Formation in Implant-Associated Infections-A Redundant and Complementary Story. *Front Microbiol,* 12**,** 687888.

Zhao, C. C., Q. M. Xie, J. Xu, X. B. Yan, X. Y. Fan & H. M. Wu (2020) TLR9 mediates the activation of NLRP3 inflammasome and oxidative stress in murine allergic airway inflammation. *Mol Immunol,* 125**,** 24-31.

Acknowledgements

Firstly, I would like to express my profound gratitude to my supervisor, Prof. Dr. Friedrich Götz, for his patient guidance and support throughout my whole work. He offered me the opportunity to explore the host-staphylococcal infection project, built valuable collaborations, and assisted in addressing challenges. I would also like to thank Prof. Dr. Andreas Peschel, who was my second supervisor, for his helpful suggestions about my research project.

I would appreciate the help from my cooperators. I extend my appreciation to the group from University of Gothenburg, Prof. Tao Jin and Meghshree Vinod Deshmukh, for their invaluable help in developing mice model and paper submission. A sincere acknowledgement goes to the group from BG Unfallklinik Tübingen, Prof. Andreas Nüssler, Sabrina Ehnert, and Filiz Sahin, who assisted in the neutrophil experiments. I also indebted to Prof. Alexander N.R. Weber from University of Tübingen for his thoughtful comments and for providing specialized cell lines. I also extend my thanks to the members of my Thesis Advisory Committee, Prof. Christiane Wolz and Dr. Bernhard Krismer, for their constructive suggestions about my work.

My deep gratitude goes to China Council Scholarship, which provided financial support for my doctoral studies and gave me the chance to study in a foreign country. My sincere appreciation to the IGIM, Graduate Academy, and Welcome Centre for all the helpful trainings and activities.

I would also express my gratitude to all my colleagues in the Microbial Genetics group for their support and help. I am immensely grateful for all the memories we have made. I want to thank people from AG Peschel for their friendly support with equipment, experimental suggestions and seminar discussions.

Finally, I would express deepest gratitude to my family for their constant understanding, encouragement and love throughout my journey. I would also thank for all my friends. Thank you for all your sincere support when I felt depressed and doubted myself, which keep me going and face challenges.

Appendix: Publications from the current thesis

communications biology

A Nature Portfolio journal

Article

https://doi.org/10.1038/s42003-025-07920-4

Staphylococcus aureus thermonuclease NucA is a key virulence factor in septic arthritis

Ningna Li[1], Meghshree Vinod Deshmukh[2], Filiz Sahin[3], Nourhane Hafza[1], Aparna Viswanathan Ammanath[1], Sabrina Ehnert[3], Andreas Nüssler[3], Alexander N. R. Weber[4], Tao Jin[2] & Friedrich Götz[1]

Septic arthritis, primarily caused by *Staphylococcus aureus*, poses a significant risk of both mortality and morbidity due to its aggressive nature. The *nuc1*-encoded thermonuclease NucA of *S. aureus* degrades extracellular DNA/RNA, allowing the pathogen to escape neutrophil extracellular traps (NETs) and maintain the infection unabated. Here we show that in the mouse model for hematogenous septic arthritis, the Δ*nuc1* mutant is much less pathogenic and the severity of clinical septic arthritis is markedly reduced, including decreased weight loss, lower kidney bacterial load, reduced bone erosion, and much less IL-6 production. In vitro, *S. aureus* genomic DNA induces a robust TNF-α response in macrophage-like RAW 264.7 cells abrogated when the DNA is degraded by NucA. Moreover, the wild type induces high levels of TNF-α, IL-10, and IL-6 in neutrophils and osteoblast-like SAOS-2 cells, respectively. NucA exacerbates septic arthritis by increasing extracellular and intracellular survival of bacteria.

Septic arthritis, the most aggressive joint disease carrying high mortality and morbidity risk, is predominantly caused by *Staphylococcus aureus*[1]. In half of the patients, even when they receive immediate treatment, the joint damage caused by septic arthritis is often irreversible, leading to permanent joint dysfunction[2]. It is known that innate immunity, including neutrophils and the complement system, protects from the development of septic arthritis[3,4].

S. aureus is one of the most successful bacterial pathogens because it expresses many colonization and pathogenicity factors, such as envelope-bound adhesins, or many secreted exoenzymes, including exotoxins, proteases, coagulase, collagenase, hyaluronidase, lipases, and nucleases. *S. aureus* encodes two nucleases: NucA, which is secreted and encoded by *nuc1*, and Nuc2, which is membrane-anchored with the C-terminus facing the extracellular environment and encoded by *nuc2*[5]. Of the two nucleases, it is the NucA that plays the crucial role in degrading extracellular DNA and RNA (eDNA and eRNA, respectively)[6,7].

The *nuc1* gene encodes a pre-pro-protein that is composed of a signal peptide, which is cleaved off by the signal peptidase, and a short pro-region which is processed by a protease releasing the mature and fully active NucA. NucA, also referred to as thermonuclease, is a Ca^{2+}-dependent, nonspecific endonuclease that catalyzes the hydrolysis of both DNA and RNA at the 5' position of the phosphodiester bond-producing nucleoside 3'-phosphates and 3'-phosphooligonucleotide as end-products[8].

NucA functions to degrade extracellular DNA (eDNA), thus promoting the dispersal and destabilization of biofilm. Consequently, in the *S. aureus* Δ*nuc1* mutant biofilm formation was shown to be much more pronounced than in the parent strain. Additionally, neutrophils displayed higher NET formation when exposed to biofilms from the *nuc1* null mutant, and killed more bacterial cells, suggesting NucA is essential for the survival of *S. aureus* biofilms irrespective of whether the bacterium is phagocytosed or not[9,10]. Survival analysis in a hematogenous implant-associated infection mouse model indicated that *nuc1* expression is associated with higher mortality[11]. NucA also plays an important role in bacterial escape from NETs. NETs are released at sites of infection by activated neutrophils and consist of nuclear or mitochondrial DNA as a backbone with embedded antimicrobial peptides, histones, and cell-specific proteases, thereby providing an extracellular matrix to entrap and kill various microbes[12]. NucA delayed bacterial clearance in the lung and increased mortality after intranasal infection, thus promoting resistance against NET-mediated antimicrobial activity of neutrophils; consequently, the *nuc1* deficient mutant was significantly more susceptible to extracellular killing by activated

[1]Interfaculty Institute of Microbiology and Infection Medicine, University of Tübingen, Tübingen, Germany. [2]Department of Rheumatology and Inflammation Research, Institute of Medicine, Sahlgrenska Academy, University of Gothenburg, Gothenburg, Sweden. [3]Siegfried Weller Institute for trauma research, BG Unfallklinik Tübingen, University of Tübingen, Tübingen, Germany. [4]Interfaculty Institute for Cell Biology, Department of Immunology, Section Innate Immunity, University of Tübingen, Tübingen, Germany. e-mail: friedrich.goetz@uni-tuebingen.de

neutrophils[13]. However, it is not only the degradation of DNA by NucA that is important for the escape from NETs but also the concomitant production of nucleoside 3'-phosphates and 3'-phosphooligonucleotides, which act as substrates for the adenosine synthase also secreted by *S. aureus*. The adenosine synthase converts the NucA products to deoxyadenosine, which triggers caspase-3-mediated apoptosis in immune cells[14].

Here we have investigated the role of NucA in a well-established mouse model of septic arthritis[15]. Our data show that in the hematogenous septic arthritis mouse model, NucA causes severe bone destruction, rapid weight loss, and high proinflammatory cytokine production. In vitro analysis suggests that reduced killing by neutrophils as well as the NET degrading activity of NucA and its induction of proinflammatory cytokines in certain host cells could be responsible for the high in vivo pathogenicity of a NucA-expressing strain.

Results

The *S. aureus* Newman Δ*nuc1* mutant is much less pathogenic in the mouse model of septic arthritis

To assess the role of NucA, *S. aureus* Newman wild-type (NWT) and its Δ*nuc1* mutant were evaluated in a mouse model of *S. aureus* septic arthritis. Naval Medical Research Institute (NMRI) mice were employed in this study. Mice received intravenous inoculations with either NWT or Δ*nuc1* and were observed for 7 days to monitor the infection process and immune response. Remarkably, Δ*nuc1*-infected mice exhibited minimal weight loss until day 7, whereas NWT-infected mice continued to lose weight up to 20% by the experiment's termination on day 7 (Fig. 1a). The severity of septic arthritis was assessed by clinical arthritis frequency and clinical arthritis score (see "Materials and Methods" for details). Here, Δ*nuc1*-infected mice displayed significantly lower clinical arthritis symptoms than NWT-infected mice. Twenty percent of Δ*nuc1*-infected mice developed mild clinical arthritis symptoms up to day 7. In contrast, 40% of NWT-infected mice exhibited clinical arthritis symptoms as early as day 3, and by day 5, all animals had developed severe septic arthritis (Fig. 1b). Not only was the frequency of arthritis higher, but the clinical arthritis score was also elevated in mice infected with the NWT strain compared to the mutant strain (Fig. 1c). Importantly, both the kidney bacterial load (Fig. 1d) and kidney abscess scores (Fig. 1e) were significantly lower in the mice infected with the Δ*nuc1* mutant compared to those infected with its parental strain. Figure 1f illustrates the clear differences in kidney abscess formation between NWT- and Δ*nuc1*-infected mice.

To further confirm our clinical observations, we conducted micro-computed tomography (μCT) scans on all joints from mice inoculated with *S. aureus* (see Materials and Methods for details). Intravenous injection of *S. aureus* NWT into NMRI mice resulted in severe bone destruction in 12% of joints after 7 days post-infection, whereas mice infected with the Δ*nuc1* mutant showed almost no sign of bone erosion (Fig. 2a and b). Figure 2c shows representative 3D images of a wrist, a knee, and a shoulder from mice infected either with the Δ*nuc1* mutant or the NWT strain.

Infection with wild-type *S. aureus* results in a significant increase in the levels of IL-6 and S100A8/A9

IL-6 and TNF-α are essential for septic arthritis development[16,17]. S100A8/A9 serves as a predictor of septic arthritis in bacteremic mice, and KC (CXCL1)

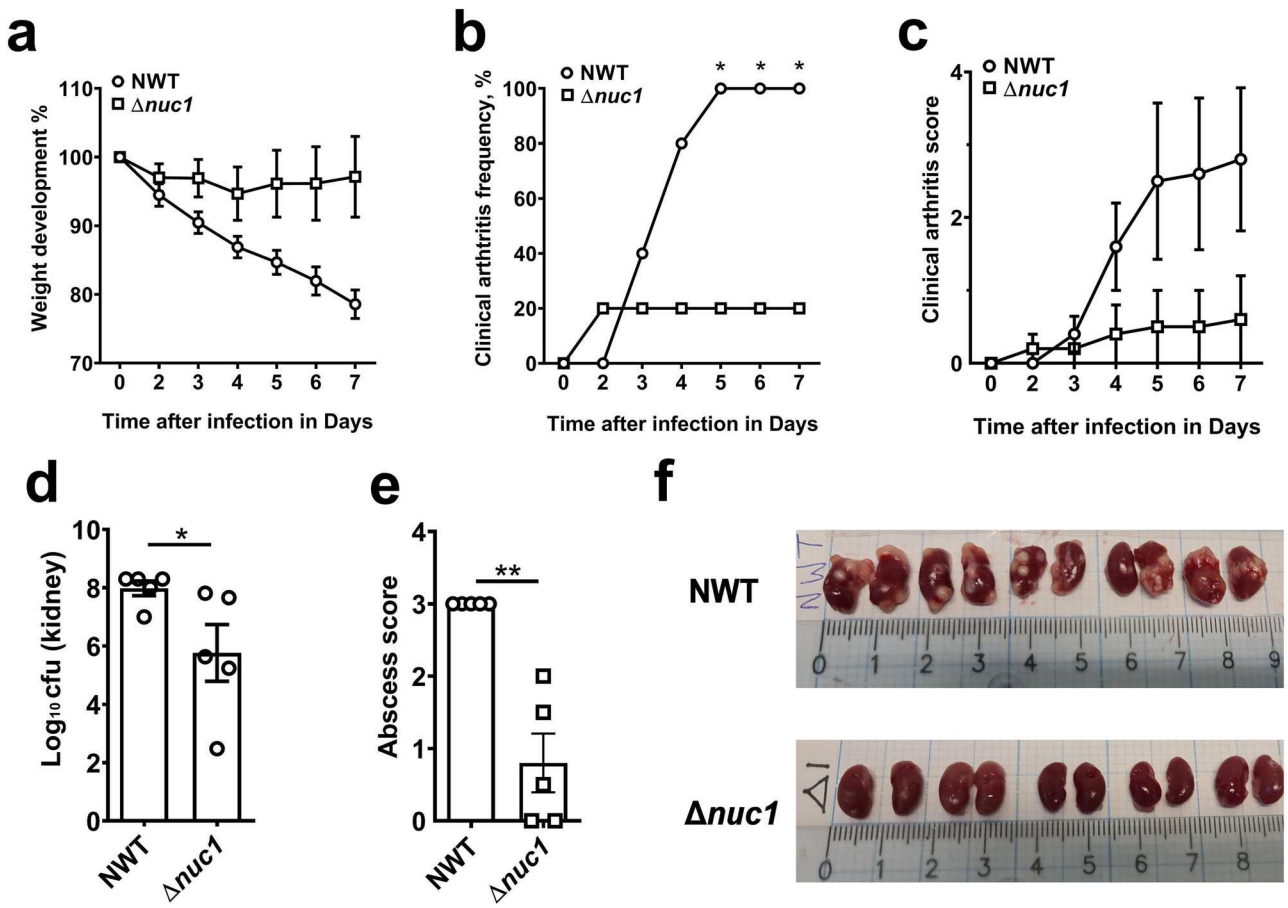

Fig. 1 | *S. aureus* Newman wild-type strain (NWT) imparts more severe arthritis and virulence than its Δ*nuc1* mutant during infection in NMRI mice. a Weight development, (**b**) clinical arthritis frequency, and (**c**) score were measured from mice infected with either NWT or Δ*nuc1* mutant for 7 days. **d** Bacterial counts in the kidney, (**e**) kidney abscess score, and (**f**) representative kidney abscess images from mice were investigated on day 7 post-infection. Statistical analyses were performed using the Mann-Whitney U test (**a**, **c**), where the data were presented as the mean ± SEM (standard error of the mean). Statistical significance: not significant, $p > 0.05$; $^{*}p < 0.05$; $^{**}p < 0.01$.

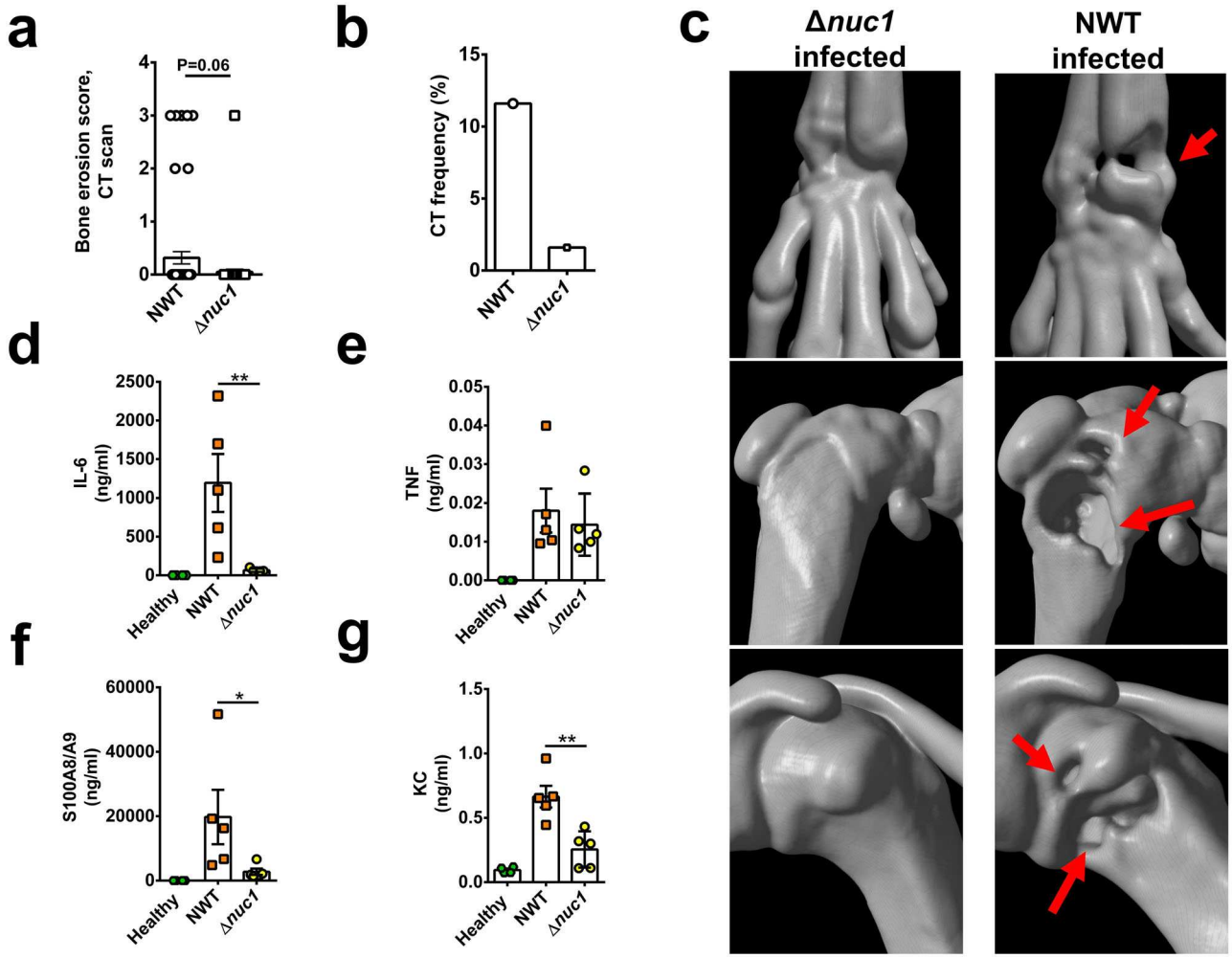

Fig. 2 | Monitoring bone erosion by microcomputed tomography (μCT) and cytokine levels in mice infected with NWT or Δ*nuc1*. **a** Bone erosion score and (**b**) CT frequency of the joints in NMRI mice intravenously injected with *S. aureus* NWT or its Δ*nuc1* mutant on day 7 post-infection. **c** Representative 3D images of micro-computed tomography (μCT) scanning of the mice joints (hand, knee, shoulder) created with μCT scanner after infection. Right panel: NWT; left panel: Δ*nuc1*; red arrow indicates bone erosion. **d–g** Levels of IL-6, TNF-α, KC, and S100A8/A9 were measured in plasma derived from NMRI mice intravenously injected with NWT or Δ*nuc1*. Statistical analyses were performed using the Fisher exact test (**a**) and Mann-Whitney U test (**b**, **d–g**), where the data were represented in mean ± SEM (**b**, **d–g**)., where the data were represented in mean ± SEM. Statistical significance: not significant, $p > 0.05$; $^{*}p < 0.05$; $^{**}p < 0.01$.

recruits neutrophils, key innate immune cells essential for disease control[4,18]. Accordingly, on day 7 post-infection we collected blood samples from the infected mice and measured the levels of these immune mediators: IL-6, TNF-α, KC (CXCL1), and S100A8/A9. As shown in Fig. 2d-g, the levels of IL-6, KC (CXCL1), and S100A8/A9 were markedly reduced in Δ*nuc1*-infected mice as compared to NWT-infected mice. While the TNF-α levels tended to be lower in Δ*nuc1*-infected mice, the difference did not reach statistical significance. Collectively, our results indicate that NucA is a crucial virulence factor for *S. aureus* pathogenicity in an infection model of septic arthritis. We further investigated possible reasons for the reduced pathogenicity of the Δ*nuc1* mutant in the septic mouse model using different host cells.

NucA digestion of gDNA decreases TNF-α production in mouse macrophages

S. aureus produces various virulence factors and triggers inflammation. Previous research found that the DNA from *S. aureus*, containing unmethylated CpG motifs, acts as a factor that triggers arthritis and septic shock[19,20]. Unmethylated bacterial DNA and CpG motifs are recognized by the toll-like receptor 9 (TLR9), which is expressed in immune cells such as macrophages and dendritic cells[21,22]. Recognition via the TLR9 pathway initiates the host response to *S. aureus* infection.

As staphylococcal macromolecules are frequently contaminated with lipoproteins/lipopeptides that are sensitively detected by Toll-like receptor 2 (TLR2) at picomolar levels, cytokine induction could be due to these constituents. Therefore, the mutant *S. aureus* USA300 LAC JE2Δ*lgt* was tested here as a control to recognize a possible interference of TLR2 and TLR9 ligands on cytokine production. JE2 is a plasmid-cured derivative of USA300 LAC strain, which is still methicillin-resistant and an important model strain to study *S. aureus* virulence[23]. JE2Δ*lgt* lacks the phosphatidylglycerol: prolipoprotein diacylglyceryl transferase Lgt, and therefore no lipidation of lipoproteins takes place and no TLR2 response can be triggered by this mutant[24,25]. By including this mutant and the double mutant JE2Δ*nuc1*Δ*lgt* together with JE2 and JE2Δ*nuc1* in the comparative immunostimulation studies, it is possible to specifically detect NucA-induced cytokine induction.

The mouse macrophage-like RAW 264.7 cells were treated with increasing concentrations of gDNA from JE2Δ*lgt* and RAW 264.7 (negative control). The standard CpG oligonucleotides ODN2006 and the non-CpG oligonucleotides ODN2137 were used as positive and negative controls, respectively (Fig. 3a). gDNA from *S. aureus* JE2Δ*lgt* increased the production of the proinflammatory cytokine TNF-α in mouse macrophage-like RAW 264.7 cells in a concentration-dependent manner, while gDNA from RAW 264.7 cells did not (Fig. 3a). At a dose of 10 ng/ml, *S. aureus* gDNA

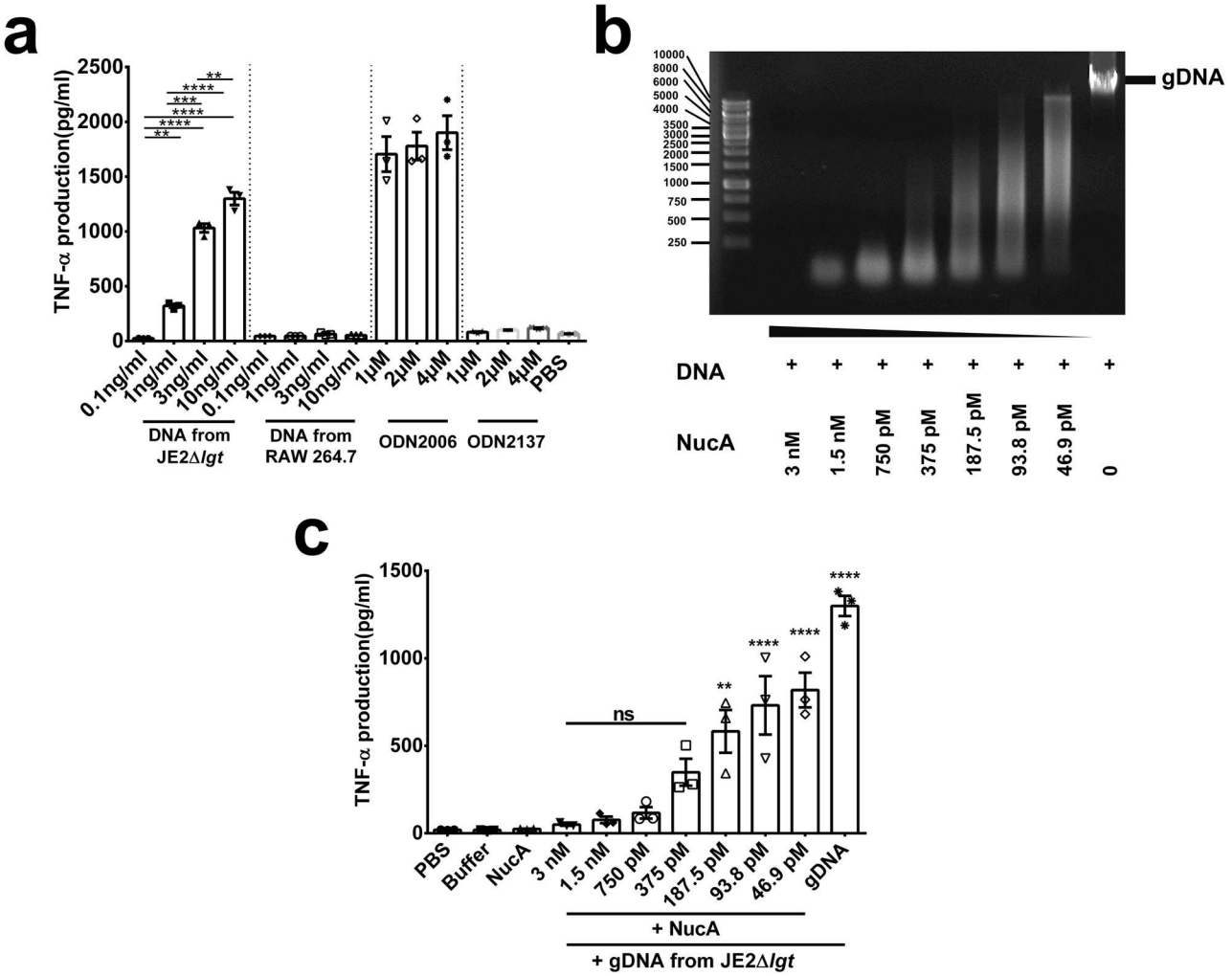

Fig. 3 | Induction of TNF-α by macrophages upon exposure to diverse DNA. **a** Stimulation of mouse macrophage RAW 264.7 cells with JE2Δ*lgt* gDNA, mammalian gDNA, ODN2006 (CpG oligonucleotide), and ODN2137 (GpC dinucleotides) at varying concentrations for 18 h, followed by TNF-α measurements. **b** Agarose gel analysis showed the degradation of JE2Δ*lgt* gDNA by gradually decreasing NucA concentration. **c** Undigested and digested JE2Δ*lgt* gDNA were incubated with RAW 264.7 cells for 18 h. Released TNF-α in cellular supernatants was quantified by ELISA. Data represent the mean ± SEM from three independent experiments; ns(not significant), $p > 0.05$; $^{*}p < 0.05$; $^{****}p < 0.0001$, one-way ANOVA with Dunnett's posttest.

induced the release of high TNF-α levels, as did exposure to 1 μM ODN2006, indicating a high immunostimulatory activity of the staphylococcal DNA.

Comparative virulence studies in different *S. aureus* model strains have shown that the USA300 and Newman strain not only have comparable lethality in a mouse sepsis model but are also similar in their hemolytic activity and biofilm formation[26]. However, in other studies have shown that the two strains exhibit distinct virulence properties; their pathogenicity differs depending on the infection model[27–29]. Both strains also express NucA and the corresponding Δ*nuc1* mutants could be complemented by pRB473-*nuc1* (Supplementary Fig. 1a). Therefore we used both for the whole study. In *S. aureus*, NucA is secreted into the supernatant and degrades extracellular DNA and RNA[5]. This was demonstrated when we incubated the supernatant of JE2 and its mutants JE2Δ*nuc1*, JE2Δ*lgt*, and JE2Δ*nuc1*Δ*lgt* with *S. aureus* gDNA for 1 h to evaluate the nuclease activity. In all mutants in which *nuc1* was deleted, the gDNA remained intact, whereas in JE2 and the JE2Δ*lgt* mutant, the gDNA was completely degraded, indicating that NucA is responsible for gDNA degradation (Supplementary Fig. 1b, 7b). Furthermore, the degradation of eDNA by recombinant NucA, which was expressed and purified from *Escherichia coli* (Supplementary Figs. 2, 7c), suggested that NucA plays a role in controlling DNA/RNA-dependent immune stimulation. Indeed, the stepwise degradation of *S. aureus* gDNA by increasing amounts of NucA (from 46 pM to 3 nM) correlated with a stepwise decrease in TNF-α production (Fig. 3b, c and Supplementary Fig. 7a).

The *S. aureus nuc1* deletion mutants have an impact on cytokine production in various cell lines

S. aureus activates different host cells, including macrophages, neutrophils, and osteoblasts[30–32]. We further investigated whether the immune stimulation of JE2 and its mutants differed in RAW 264.7, neutrophils, and osteoblast-like SAOS-2 cells. We incubated live *S. aureus* JE2 and its JE2Δ*nuc1*, JE2Δ*lgt*, and JE2Δ*nuc1*Δ*lgt* mutants for 18 h with RAW 264.7, SAOS-2 cells, and 5 h with neutrophils, respectively. To assess the immune responses elicited by different bacterial strains, we measured cytokine production, including classically pro-inflammatory mediators such as TNF-α and IL-6, as well as anti-inflammatory cytokines such as IL-10 and IL-1Ra. IL-10 was also very high in sepsis patients, and IL-1Ra and IL-10 also influenced the inflammatory response[33–35]. There was no difference in IL-6 and TNF-α production in RAW 264.7 upon exposure to either JE2 or JE2Δ*nuc1* (Fig. 4a). In SAOS-2 cells, IL-6 production was decreased in response to all mutants, but there was no difference in TNF-α production. In neutrophils, the production of TNF-α, IL-10, and IL-1Ra was markedly decreased in response to all the mutants (Fig. 4b, c), particularly those lacking *lgt* (JE2Δ*lgt* and JE2Δ*nuc1*Δ*lgt*). It is not unexpected that the Δ*lgt*

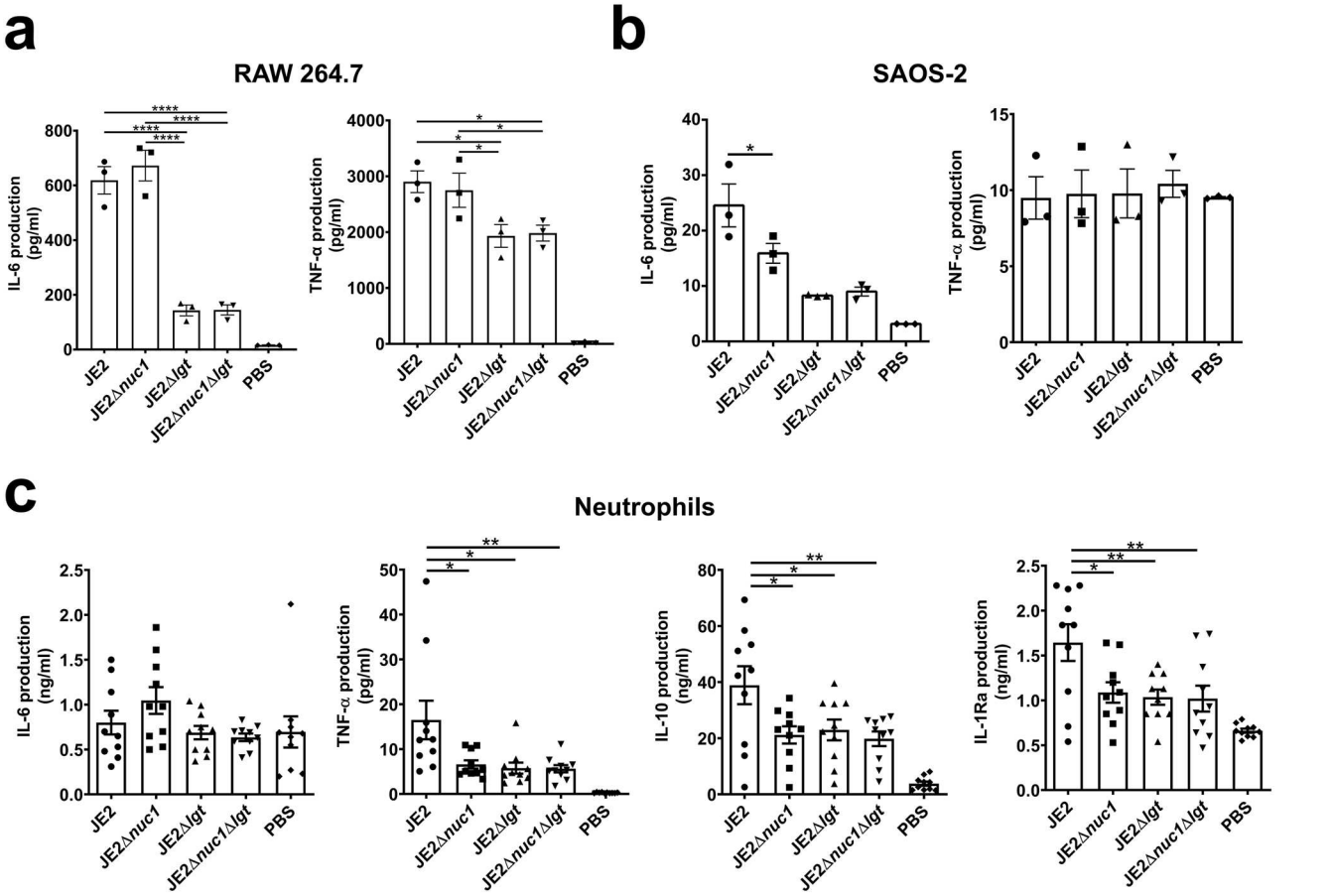

Fig. 4 | Induction of cytokines by various host cells upon exposure to live JE2, JE2Δ*nuc1*, JE2Δ*lgt*, and JE2Δ*nuc1*Δ*lgt*. The PBS-washed bacteria were incubated with (**a**) RAW 264.7 cells at an MOI = 30, (**b**) SAOS-2 cells at an MOI = 3, and (**c**) with neutrophils at an MOI = 50. Cellular supernatants were collected after 18 h for RAW 264.7 and SAOS-2 cells, and after 5 h for neutrophils to measure various cytokines by ELISA assay. For neutrophils, the experiments were displayed from $n = 10$ donors. Triplet experiments were conducted; error bars indicate ± SEM; not significant, $p > 0.05$; *$p < 0.05$; **$p < 0.01$; and ****$p < 0.0001$, one-way ANOVA with Dunnett's posttest.

mutants induce less cytokines since lipoproteins/lipopeptides trigger a very strong innate immune response. As compared with NWT, there was less IL-6 production in RAW 264.7 and no significant difference in IL-6 and TNF-α in SAOS-2 when exposed to the Δ*nuc1* strain (Supplementary Fig. 3). As the generated mutants showed hardly any difference in growth and hemolytic activity as compared to the parental strain (Supplementary Fig. 1a, c and d), we assume that all the effects seen are mainly due to the deletion of *nuc1* or *lgt* genes.

JE2Δ*nuc1* exhibits decreased internalization or survival in various host cells

S. aureus can be engulfed by multiple cells[36,37]. We determined bacterial survival and phagocytosis in neutrophils, following a previously used protocol[38,39]. With different conditions tested, we found that better results were obtained with an MOI (multiplicity of infection)=2 for the phagocytosis assay and an MOI = 0.1 for the bacterial killing assay. Under these conditions, the survival of JE2Δ*nuc1* was decreased already at early time points as compared to JE2 (Fig. 5a). This was consistent with a lower phagocytosis index in JE2Δ*nuc1* (Fig. 5a). This led us to investigate whether live JE2 and its mutants differ in internalization by other host cells such as RAW 264.7. To assess only intracellular survival, membrane adherent and extracellular bacteria were killed after 1.5 h incubation, and then the CFU of internalized bacteria per host cell was determined. In RAW 264.7 we observed lower intracellular numbers of JE2Δ*nuc1* cells as compared to JE2 and the complementation strain JE2Δ*nuc1*(pRB473-*nuc1*), suggesting that survival was affected by *nuc1* (Fig. 5b).

Effect of live bacteria and supernatant on NETs formation and clearing

Neutrophils act as the first defense line of the innate immune system and form NETs to clear pathogens[38]. NETs consist of a DNA backbone coated with various proteins, such as myeloperoxidase (MPO), nuclear proteins (histones), neutrophil elastase (NE), and calprotectin[40,41]. In *S. aureus*, NucA can degrade extracellular DNA, thereby reducing NET formation and evading immune clearance. Here, the neutrophils were exposed to live bacteria (MOI = 1:2) and bacterial supernatants (2%) for 2 h following eDNA-staining with SYTOX Green. Live bacteria caused a slow increase in NETosis, whereas the bacterial supernatant induced a stronger NET release in a shorter time (Fig. 6a, b). Additionally, neutrophils were still viable after 3 h incubation (Supplementary Fig. 4).

Immunofluorescence staining of NET formation (Fig. 6c and Supplementary Figs. 5, 6) further confirmed NETosis occurred, as visible by positive staining for DNA (blue), MPO (green), and citrullinated histone H3 (CitH3, red) after 1 h incubation of neutrophils with bacterial cell-free supernatant but not with live bacteria. NET was higher in response to JE2Δ*nuc1* mutants and their supernatants than in the parental strain, as also can be observed in fluorescence microscopy images (Fig. 6c and Supplementary Fig. 6). This suggests that the supernatant of Δ*nuc1* mutants is less effective in degrading DNA, resulting in increased levels of NETs.

Discussion

The comparative studies between *S. aureus* parental strain and the Δ*nuc1* mutant revealed that NucA is an important virulence factor in septic

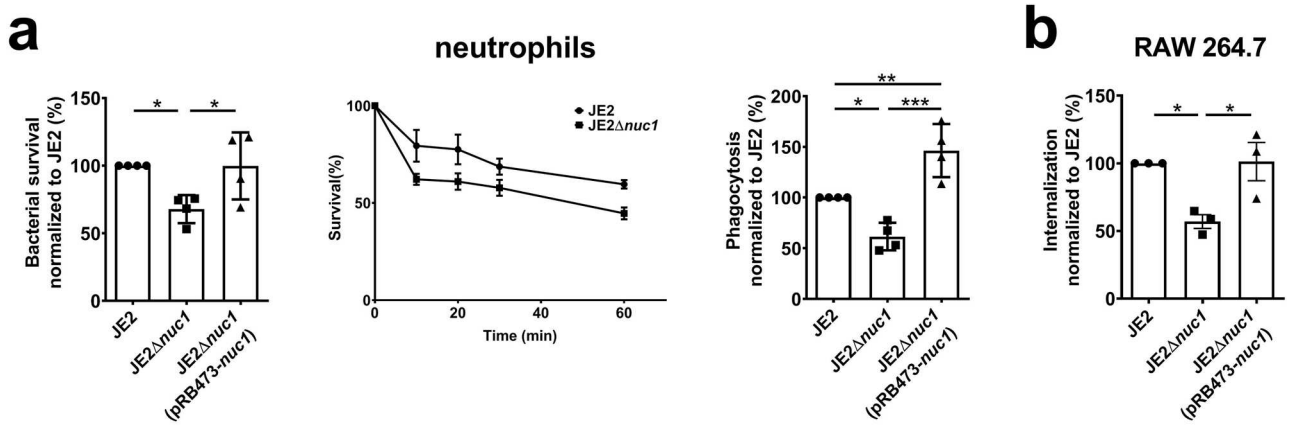

Fig. 5 | Bacterial killing and phagocytosis studies in various cells. a For bacterial killing in neutrophils, JE2, JE2Δ*nuc1* and JE2Δ*nuc1* complemented with plasmid-expressed *nuc1* (JE2Δ*nuc1* pRB473-*nuc1*) were opsonized with 10% human pooled serum. Neutrophils were incubated with bacteria at an MOI = 0.1 for 1 h and bacterial survival was checked at 10 min, 20 min, 30 min, and 1 h after exposure to neutrophils. Fluorescence-labeled bacteria were incubated with neutrophils at an MOI of 1:2 and the phagocytosis index was calculated 1 h after incubation via FACS. **b** To investigate bacterial survival in RAW 264.7, RAW 264.7 was incubated with JE2, JE2Δ*nuc1,* and JE2Δ*nuc1*(pRB473-*nuc1*) at an MOI of 1:20 for 1.5 h. Extracellular and attached bacteria were removed by gentamicin and lysostaphin before lysing the cells. Neutrophils used in these experiments were obtained from 4 donors and the other experiments were performed at least three times; error bars indicate mean ± SEM. Statistical analyses were performed using one-way ANOVA with Dunnett's posttest. Statistical significance: not significant, $p > 0.05$, $^{*}p < 0.05$; $^{**}p < 0.01$; and $^{***}p < 0.001$.

arthritis. *S. aureus* NWT-infected mice showed marked weight loss, much increased clinical arthritis frequency, a 3-fold higher abscess score, severe bone erosion, and very high IL-6 content in the plasma. In contrast, the Δ*nuc1*-infected mice showed hardly any signs of septic arthritis, almost no weight loss, their clinical arthritis and abscess scores were much lower, and the bacterial load in kidneys was decreased (Fig. 1). Most remarkable, however, was that Δ*nuc1*-infected mice showed almost no bone erosion in the joints (Fig. 2a, b, c). Here, we provide three lines of in vitro evidence to support our in vivo observations: 1) NucA efficiently degrades bacterial DNA, which can trigger the release of proinflammatory cytokines like TNF-α, known for their critical roles in septic arthritis development; 2) NucA production may increase the intracellular survival of *S. aureus*; 3) NucA produced by *S. aureus* effectively digests NETs formed by neutrophils, potentially aiding bacterial evasion from innate immune killing, and thereby promoting bacterial survival and exacerbating disease severity.

Most bacteria release DNA and RNA during proliferation. In *S. aureus* DNA is released during cell lysis resulting from induction of prophages or activation of proteins with holin-like properties such as CidA and LrgA[42]. The secreted NucA degrades eDNA/RNA very efficiently to allow the reuse of the degradation products. How powerful NucA is in degrading eDNA is illustrated in Supplementary Fig. 1b and 7b. When the supernatants of JE2 and its mutants were incubated with gDNA, it was completely degraded within 1 h by the supernatant of JE2 but not by the Δ*nuc1* mutants. This efficient degradation of eDNA not only ensures the reuse of nucleic acid building blocks but also the escape of staphylococci from a biofilm community or NETs, providing NucA-expressing bacteria a clear advantage during infection[43].

It is known that bacterial DNA triggers an inflammatory response and induces cytokine production via the TLR9 receptor[21,22]. Further studies in mice have proven that DNA from *S. aureus* results in arthritis[20,44]. To check the potential involvement of bacterial DNA and the role of NucA in inflammation, gDNA was isolated from the JE2Δ*lgt* mutant to avoid lipoprotein contamination. The NucA-digested DNA and intact DNA were then incubated with RAW 264.7 cells. In these cells, staphylococcal DNA induced TNF-α production in a dose-dependent manner (Fig. 3a); as the gDNA was progressively degraded by increasing concentrations of NucA, TNF-α production decreased with progressing degradation (Fig. 3b, c and Supplementary Fig. 7a). Similar results were also obtained with Group A *Streptococcus* (GAS), which produces the DNase Sda1 to prevent IFN-α and TNF-α secretion by murine macrophages[45]. TNF-α is recognized as pathogenic in the initiation and progression of septic arthritis[16]. Moreover, combining antibiotics with a TNF-α inhibitor yielded superior results as compared to antibiotics alone, effectively reducing synovitis and joint destruction in a mouse model of septic arthritis[46]. Simultaneously, TNF-α plays a crucial role in the Th1 response and primes phagocytes for effective elimination of pathogens[47]. Anti-TNF-α treatment has been shown to compromise immune killing efficacy, leading to increased kidney bacterial load in a mouse model of *S. aureus* septic arthritis[48]. Hence, NucA disrupts the immune-stimulating effect of bacterial DNA, potentially leading to an elevated kidney bacterial load.

As we showed that NucA-digested bacterial eDNA has no immune-stimulating activity in murine macrophages, we expected that the Δ*nuc1* mutant, in which eDNA is not degraded (Supplementary Fig. 1b, 7b), would elicit a stronger immune response than the parental strain in various cell types. *S. aureus* stimulates the immune response in various cells, including macrophages and neutrophils, as well as non-immune cells, such as osteoblast cells[30–32]. In addition, osteoblasts and osteoclasts are responsible for bone remodeling and construction[49,50]. Accordingly, macrophages RAW 264.7, osteoblast cells SAOS-2 and neutrophils were employed in this study. JE2Δ*nuc1* mutant triggered no IL-6 or TNF-α production in RAW 264.7 (Fig. 4a, b). What we see is that lipoproteins play a decisive role in immune stimulation in RAW 264.7 cells, which is in agreement with earlier results[25,51,52]. However, JE2Δ*nuc1* mutant induced less IL-6 in SAOS-2 cells and less TNF-α in neutrophils, while NWTΔ*nuc1* induced less IL-6 in RAW264.7 cells (Fig. 4 and Supplementary Fig. 3). In addition to measuring pro-inflammatory cytokines, we also measured the production of anti-inflammatory cytokines, IL-10 and IL-1Ra, in neutrophils to assess the balance between pro- and anti-inflammatory responses during infection. IL-10 is critical for regulating and balancing the infection and immune response, which typically increases during inflammation[53,54]. IL-1Ra, as a natural antagonist of IL-1 signaling and related to extensive IL-10 production, could influence the inflammatory response and is used to treat inflammation[55,56]. IL-1R knock-out mice developed more severe septic arthritis, but IL-1R treatment for inflammation-related diseases could also increase the infections in sepsis[35,48,57]. When neutrophils were exposed to the parental strain and its mutants, JE2Δ*nuc1* showed less IL-10 and IL-1Ra production. Those results give a hint that NucA has an impact on immune stimulation.

The next key question that arises in this context is the molecular causes of NucA-induced septic arthritis and bone erosion. To investigate this, we

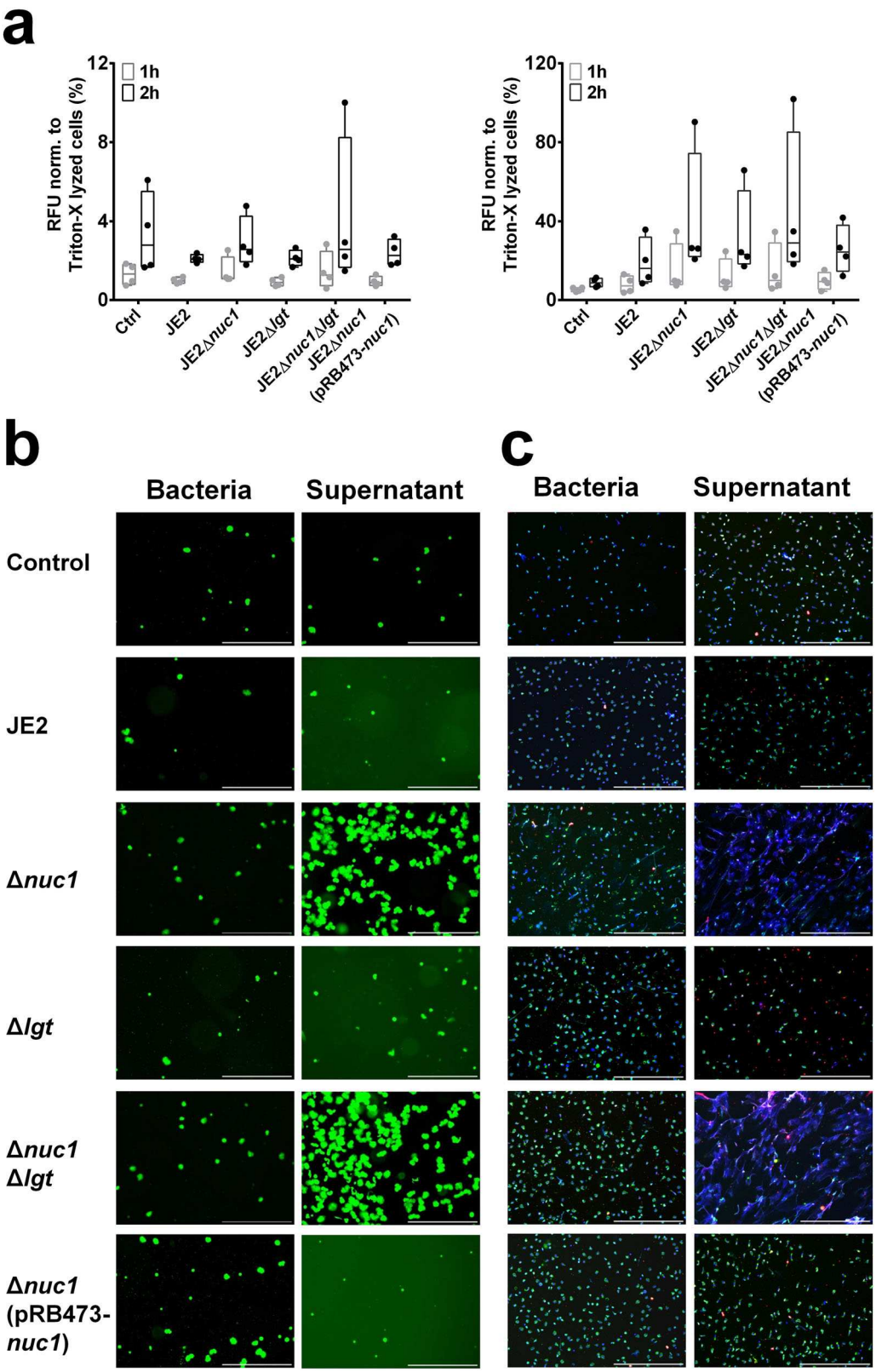

Fig. 6 | NET formation upon exposure to live bacteria and supernatants of JE2 and its mutants. a Sytox Green assay of neutrophils exposed to JE2, JE2Δ*nuc1*, JE2Δ*lgt*, and JE2Δ*nuc1*Δ*lgt* with live bacteria (MOI = 1:2) or overnight supernatant (2% volume) for 2 h. Relative fluorescence units (RFU) of Sytox Green normalized to Triton X-100-lysed neutrophils are shown. **b** Representative fluorescence images of Sytox Green staining after 3 h of incubation. Scale bar = 500 µm. **c** Representative images of immunofluorescent staining after 1 h of incubation. Blue: DNA (Hoechst 33342); Green: myeloperoxidase, MPO; Red: citrullinated histone H3, citH3, scale bar: 500 µm. The graph displays the average values ± SEM obtained from 4 donors; not significant, $p > 0.05$, one-way between-groups ANOVA with Dunnett's posttest.

measured the levels of several cytokines in the blood of mice on 7 days post-infection. Previous studies have shown that IL-6 and TNF-α are critical for septic arthritis development[16,17]. Patients who have septic arthritis exhibit high concentrations of TNF[58,59]. Lack of TNF-α has been associated with an inefficient ability to clear bacteria[16]. In addition, KC attracts neutrophils that control septic arthritis, and S100A8/A9 has been identified as an early predictor of septic arthritis during *S. aureus* bacteremia[4,18]. Since in vivo experiments showed minimal differences in TNF-α induction after infection with WT or *nuc1* mutant, we further investigated this phenotype in vitro. However, in macrophage-like and osteoblast-like cells, JE2 and JE2Δ*nuc1* did not cause any significant difference in TNF-α production (Fig. 4a, b and Supplementary Fig. 3). In neutrophils, more TNF-α production was induced by the parental strain than by the *nuc1* mutant. In the septic arthritis mouse model, NWT induced an almost 100-fold higher IL-6 production in plasma than its Δ*nuc1* mutant. The very high IL-6 content in the blood reflects the severity of septic arthritis by infection with the NucA-expressing strain. In fact, sepsis or acute respiratory distress syndrome is correlated with an increased IL-6 content. However, there is no significant difference in IL-6 production between JE2 and its Δ*nuc1* mutant in the different cell cultures, showing once again that the in vitro situation does not always reflect the in vivo situation. IL-6, which is mainly produced by macrophages and T lymphocytes in response to pathogens, is not only a key player in rheumatoid arthritis, but it also promotes megakaryocyte maturation and the release of platelets when reaching the bone marrow. IL-6 has emerged alongside IL-1 and TNF as a master regulator of inflammation: it is essential for innate and adaptive immunity, is required for efficient pathogen clearance, and has important physiological roles in humans regulating the acute-phase response, hematopoiesis, metabolic rate, lipid homeostasis, and neural development.

The pronounced upregulation of S100A8/A9 in NWT-infected mice compared to the Δ*nuc1*-infected mice could be induced by IL-6-triggered inflammation and leukocyte recruitment[60,61]. The high levels of IL-6 and S100A8/A9 at the end of the mouse experiment reflect the severity of infection. Inflammatory cytokines play a role in the bone remodeling process. For example, in IL-6 deficient mice, bone erosion was reduced[62]. Therefore, the NucA-expressing strain could cause high IL-6 production, which may lead to uncontrolled progression of bone destruction by osteoclasts.

Furthermore, we also found that the JE2Δ*nuc1* mutant exhibited reduced survival, which could explain why we detected less bacteria inside neutrophils 1 h after exposure to neutrophils (Fig. 5a). This encouraged us to investigate the internalization in other cell lines. As shown in Fig. 5b, we also observed reduced numbers of JE2Δ*nuc1* in RAW 264.7 cells. These findings indicate that NucA increases *S. aureus* survival, likely both extracellularly and intracellularly, which may contribute to an increase in the severity of septic arthritis.

In hematogenous septic arthritis, compromised innate immune defenses increase the likelihood that bacteria in the bloodstream invade joints, ultimately leading to the development of septic arthritis[15]. Neutrophils are recognized as vital immune cells guarding against *S. aureus* septic arthritis. Neutrophil-depleted mice exhibited heightened and more frequent septic arthritis, coupled with compromised bacterial clearance as evidenced by elevated CFU counts in both blood and kidneys[4]. We also compared the effects of live bacteria and the corresponding culture supernatant on degradation of neutrophil extracellular traps (NETs). NETs represent a form of innate immune response that prevents microorganisms from spreading, while the high local concentration of antimicrobial agents may kill bacteria[63,64]. The *S. aureus* thermonuclease NucA is known to degrade the DNA within NETs to escape scavenging and killing[38]. It has been shown that the combined activity of *S. aureus* nuclease and adenosine synthase converts extracellular DNA to deoxyadenosine (dAdo) in staphylococcal abscesses. Human equilibrative nucleoside transporter 1 (hENT1) mediates dAdo transportation in macrophages, leading to caspase-3-induced apoptosis[14,65,66]. This could be happening in our model as well, but we did not analyze the viability of macrophages isolated from abscesses.

When we exposed neutrophils to live *S. aureus*, we observed a time-dependent increase in stained eDNA, but there was no pronounced difference between stimulation with JE2 and its mutants (Fig. 6a, b) until 2 h after exposure. When we incubated neutrophils with the corresponding supernatants, we observed a clear difference in the response to JE2Δ*nuc1* mutants as compared to other strains (Fig. 6c and Supplementary Fig. 6). Immunofluorescence revealed a stronger DNA signal in response to JE2Δ*nuc1* supernatants, suggesting decreased NET degradation. The question remains as to why we did not see a major difference between the wild-type and the Δ*nuc1* live bacteria. We assume that by washing the bacterial cells with PBS, NucA is washed out and the bacteria are rapidly phagocytosed and killed when incubated with neutrophils.

Overall, our study suggests that NucA plays a crucial role in the pathogenesis of *S. aureus* septic arthritis, as evidenced by Δ*nuc1*-infected mice showing reduced arthritis severity, bone erosion, and kidney abscess formation, alongside lower bacterial loads. In vitro data further support these findings, demonstrating that NucA degrades bacterial DNA, shields *S. aureus* from killing, and digests neutrophil extracellular traps, ultimately promoting bacterial survival and worsening disease severity. How NucA triggers severe bone erosion is the subject of further research. In a summary image, we illustrated the main differences between NucA-producing and -non-producing *S. aureus* strains (Supplementary Fig. 8).

Materials and methods

Bacterial strains, plasmids, primers, and culture conditions

Bacterial strains and plasmids used in this study are described in Supplementary Table 1. All the primers are listed in Supplementary Table 2. *Escherichia coli* BL21 (DE3) was grown in Luria-broth medium (LB), and *Staphylococcus aureus* strains were cultured in tryptic soy broth (TSB, Millipore, Merck) or basic medium (BM) broth (Luria broth supplemented with 0.1% K_2HPO_4 and 0.1% glucose) or stored as previously mentioned[67]. To keep the plasmids in the bacteria, *E. coli* was supplied with ampicillin or kanamycin and *S. aureus* was supplied with 10 μg/ml chloramphenicol. For comparison of growth kinetics, the *S. aureus* JE2, Newman, and their mutants were grown in TSB medium, and measured with Varioskan LUX Multimode Microplate Reader (Thermo Fisher) for 24 h.

Deletion of *nuc1* and *lgt* in *S. aureus*

nuc1 is the nuclease1-encoding gene and *lgt* is the lipoprotein diacylglyceryl transferase enzyme-encoding gene[7,25]. For deleting *nuc1* and *lgt* genes, the knockout plasmid pBASE6 was employed. The disruption primers were designed to contain upstream and downstream of the target gene regions. Fragments were generated by PCR and subcloned into EcoRV-digested pBASE6 vector, resulting in pBASE6Δ*nuc1* and pBASE6Δ*lgt*. The resulting plasmids were transformed into *E. coli* DC10B for amplification. Then, plasmids were isolated and verified by DNA sequencing. The correct plasmids pBASE6Δ*nuc1* and pBASE6Δ*lgt* were transformed into an intermediate host, *S. aureus* RN4220, by electroporation to restrict foreign DNA and then into *S. aureus* JE2 or *S. aureus* Newman (NWT). The process for deletion of *lgt* and *nuc1* from *S. aureus* was followed as previously described[68]. Positive colonies were incubated in TSB with 10 μg/ml chloramphenicol (Cm) at 43 °C overnight and then transferred to TSB supplemented 7.5 μg/ml Cm at 43 °C for another overnight incubation. The culture was plated and a single colony was picked for inoculation at 30 °C. The overnight culture was diluted and plated onto TSA plates containing 1 μg/ml anhydrotetracycline (ATc) for two days. Colonies from the plate were streaked on TSA with or without Cm. The colonies that could grow on TSA plate but not on TSA with Cm were selected for PCR verification, resulting in JE2Δ*nuc1*, NewmanΔ*nuc1*, JE2Δ*lgt,* and JE2Δ*nuc1*Δ*lgt*.

Construction of complementation strain

For complementation, the plasmid pRB473-*nuc1* was introduced. The *nuc1* fragment was amplified, ligated to pRB473 plasmids, and transformed into *E. coli* DC10B. Positive colonies were selected and verified via DNA sequencing. The correct plasmid was purified and transformed

into JE2Δ*nuc1* and Δ*nuc1*, yielding JE2Δ*nuc1*(pRB473-*nuc1*) and Δ*nuc1*(pRB473-*nuc1*).

Hemolytic activity and nuclease activity assays

Bacteria were grown in TSB medium overnight. The OD578 of overnight culture was adjusted and spotted on the Blood Agar (TSA with Sheep Blood) plates (Thermo Fisher) at 37 °C, and then the hemolysis zone was measured. The supernatants of overnight culture were checked for nuclease activity using DNase Test Agar with Toluidine Blue (Merck, Millipore). The DNase Test Agar plates were incubated at 37°C.

Mouse model for *S. aureus* septic arthritis

To compare the pathogenicity of *S. aureus* Newman wild-type strain (NWT) and its Δ*nuc1* mutant, a septic arthritis mouse model was used. NMRI female mice, aged 8 weeks, were purchased from Envigo (Venray, Netherlands). All mice were housed at the animal facility at the University of Gothenburg. Mice were kept under standard temperature and light conditions and were fed laboratory chow and water ad libitum. Mice ($n = 5$/group) housed in the same cage were randomly assigned to receive an intravenous injection of 200 µl of an arthritic dose of either *S. aureus* Newman strain (2.8×10^6 CFU/mouse) or Δ*nuc1* mutant (2.8×10^6 CFU/mouse). Mice were monitored for weight loss and clinical signs of arthritis from day 0 to day 7 in a manner blinded to the bacterial strains. Morphine (Abcur AB, 10 mg/kg) was administered subcutaneously (s.c.) daily to all mice starting three days after infection to alleviate pain associated with septic arthritis. On day 7, mice were sacrificed to collect samples, including blood, kidneys, and joints. Kidneys were collected aseptically and scored on a scale of 0 (no abscess), 1 (mild abscess), 2 (moderate abscess) to 3 (severe abscess). The kidneys were then minced and diluted with sterile PBS. Dilutions were plated on horse blood agar plates, incubated at 37 °C for 24 h, and the colonies obtained were counted using a colony counter (Stuart Scientific, Made in the UK).

Clinical evaluation of arthritis

Observers (M.D. and T.J.) blinded to the treatment groups visually inspected all 4 limbs of each mouse. Arthritis was defined as erythema and/or swelling of the joints. A clinical scoring system ranging from 0 to 3 was used for each paw (0, no inflammation; 1, mild visible swelling and/or erythema; 2, moderate swelling and/or erythema; and 3, marked swelling and/or erythema).

Microcomputed Tomography (µCT)

On 7 day post-infection, the mice were sacrificed and all paws were scanned by SkyScan 1176 µCT (Bruker, Antwerp, Belgium). The scanning was conducted at 55 kV/ 455 µA, with a 0.2-mm aluminum filter. The exposure time was 47 ms. The X-ray projections were obtained at 0.7° intervals with a scanning angular rotation of 180°. The NRecon software (version 1.6.9.8; Bruker) was used to reconstruct 3D images which were further evaluated by using CT-Analyzer (version 2.7.0; Bruker). Each joint was evaluated by two researchers (M.D. and T.J.), in a blinded manner, using a scoring system from 0 to 3 (0: healthy joint; 1: mild bone destruction; 2: moderate bone destruction; and 3: marked bone destruction) as previously described[17].

NucA expression and purification

NucA is an extracellular enzyme, which is secreted as mature Nuc1. The *nucA* gene was cloned into the vector pET28a with C-terminal His-tag and this construct was transformed into *E. coli* BL21(DE3). The transformant carrying pET28a-NucA-6xHis was grown in LB at 37 °C supplemented with 50 µg/ml ampicillin. When OD600 reached 0.6–0.8, the bacteria were induced with 1 mM IPTG at 18 °C overnight for overexpressing NucA. The overnight culture was collected, resuspended in buffer A (50 mM Tris-HCl pH 8.0, 300 mM NaCl), and lysed by an ultrasonic sonicator with a pulse every 4 s for 4 min. The lysate was centrifuged at $14{,}000 \times g$ for 1 h. The supernatant of lysate was collected and then loaded onto an Ni-NTA column. Fractions containing NucA were collected with Buffer B (20 mM Tris-HCl pH 8.0, 200 mM NaCl, 250 mM imidazole) and analyzed by SDS-PAGE. NucA enzyme was dialyzed with PBS, concentrated, flash-frozen in liquid nitrogen, and stored at -80°C until use.

Genomic bacterial DNA (gDNA) degradation assay with NucA

S. aureus JE2Δ*lgt* was cultured in TSB medium overnight. The bacterial pellet was collected and resuspended in TE buffer supplemented with lysostaphin and RNase at 37 °C for 30 min. Bacterial gDNA was then purified via phenol-chloroform-isoamyl alcohol, precipitated with isopropanol, washed with ethanol, and then dissolved in H_2O[69]. gDNA was incubated with varying concentrations of recombinant NucA for 1 h at 37 °C. Samples were then added to RAW 264.7 cells for stimulation and loaded on the agarose gel for visualization.

Preparation of bacteria and bacterial supernatant

BM medium was used for inoculating *S. aureus* at 37 °C with shaking from fresh BM agar plates. Cultures were harvested after 16 h by centrifuging and washed with PBS. To get bacterial dosage (MOI, multiplicity of infection), bacteria were calculated to OD/CFU. Bacterial supernatants were collected and filtered with a 0.2 µm pyrogen-free round column. The supernatants were kept on ice until use and adjusted to equal concentrations according to bacterial number. The supernatant was tested for its ability to degrade gDNA and its activity on neutrophils.

Neutrophil isolation

Venous blood was freshly collected by EDTA-tubes (Sarstedt, Germany) from several healthy individuals. 6 mL blood was layered on 6 mL of Lymphocyte poly-cell separation medium (Cedarlane, Burlington, Canada). Centrifugation was done without pause, at $500 \times g$ for 40 min at room temperature. The PMN layer was collected and washed twice with 12 mL PBS, and centrifuged at $400 \times g$ for 10 min at room temperature with settings of acceleration 5 and deceleration 4. Cells were resuspended in RPMI medium without phenol red (Sigma-Aldrich, Darmstadt, Germany). Cell counts were obtained by the Trypan Blue exclusion method, utilizing a Neubauer counting chamber.

Cell culture and immune stimulation assay

The murine macrophage cell line RAW 264.7 was cultured in Dulbecco's modified Eagle's medium (gibco) supplemented with 10% fetal bovine serum (FBS) and 1% penicillin-streptomycin at 37 °C with 5% CO_2. The human osteoblast-like cell line SAOS-2 was grown in McCoy's 5 A Medium (Sigma) supplemented with 15% FBS, 1% glucose, and 1% penicillin-streptomycin. Prior to stimulation, RAW 264.7 and SAOS-2 cells were seeded in 96-well plates and incubated overnight until reaching confluency, while neutrophils were directly seeded into the plates before adding all stimulants. Immune stimulation was performed for 18 h at 37 °C and 5% CO_2, except for neutrophils which were stimulated for 5 h. The cellular supernatants were then collected and stored at −20 °C until determining the cytokines production.

Detection of cytokines by ELISA

Cytokines collected from the cellular supernatants of different cell lines were measured with the uncoated ELISA kit (Invitrogen) according to instructions. The plasma levels of IL-6, TNF-α, keratinocyte chemoattractant (KC), and S100A8/A9 in blood collected from NMRI mice intravenously infected with Newman WT (NWT) and Δ*nuc1* were quantified using DuoSet ELISA kits (R&D Systems Europe) according to the manufacturer's instructions.

Neutrophil bacterial killing assay

JE2 and JE2Δ*nuc1* were grown overnight. Bacteria were collected, regrown to the log phase, washed with PBS, and opsonized with 10% human pooled serum in RPMI for 1 h at 37 °C. Neutrophils were seeded in 24-well plates, incubated with bacteria (100%) at an MOI = 0.1. After 10 min, 20 min, 30 min, and 1 h, the neutrophils were lysed with ice-cold ddH_2O and centrifuged for 15 min at 4 °C. The lysates were plated on agar plates with serial

dilutions and CFUs were counted the next day. The *S. aureus* survival (killing) was calculated by comparing the counted CFU to the original added CFU and normalized to JE2.

Phagocytosis assay

Bacteria were grown overnight, collected, regrown until the log phase, and washed with PBS. Bacteria were opsonized with 10% human pooled serum in RPMI without phenol red for 1 h at 37 °C and then were labeled with Alexa Flour 633 conjugate (Invitrogen, W21404) for 20 min at 37 °C. The unlabeled fluorochrome was washed twice by PBS. Neutrophils were seeded into 24-well plates and incubated with bacteria at an MOI = 2. After 1 h incubation, the neutrophils were fixed with 3.7% formaldehyde for 20 min on ice. The fluorescence intensity of fixed neutrophils was determined with a BD FACSCalibur (BD Biosciences). The phagocytotic index was calculated as number of fluorescent-positive neutrophils multiplied by the fluorescence mean and normalized to JE2 parent strain to minimize the individual error. This index shows how many bacteria were phagocytosed per cell.

Internalization assay

RAW 264.7 cells were seeded in 24-well plates with 500 µl of culture medium until reaching confluency. Cells were washed with PBS, and the pre-warmed culture medium without antibiotics was added to each well. Bacteria were grown to the log phase before infection. The cells were then incubated with bacteria for 1.5 h to yield an MOI of 20:1. After incubation, gentamycin, and lysostaphin were added to kill the extracellular bacteria for 1 h. The cells were lysed with 0.1% Triton X-100 supplemented with 0.05% Trypsin and lysates were plated to determine internalized bacteria[70]. Internalization was calculated as CFU of internalized bacteria/host cell-seeded and normalized to JE2.

Sytox green assay

Isolated neutrophils were prepared to be 2×10^5 cells/mL, and then 1 µM Sytox Green (Thermo Fisher, Waltham, USA) was added. 1% Triton X-100 solution was used for extracellular DNA normalization. Cells were stimulated for 5 h with MOI = 1:2 live bacteria and 2% overnight bacterial supernatant. Fluorescent intensity was measured every 30 min at Ex 485 nm/Em 520 nm, and the cells were incubated at 37 °C with 5% CO_2 by the microplate reader (FluoStar Omega, BMG Labtech, Ortenberg, Germany). Microscopic images were taken with EVOS Fl (Thermo Fisher) fluorescence microscope at 3 h of incubation.

Live-dead staining

Isolated neutrophils were incubated with an MOI of 1:2 live bacteria and 2% overnight bacterial supernatant. To visualize live cells, neutrophils were stained with 2 µM Calcein AM and Ethidium Bromide for 10 min at 37 °C in RPMI medium without phenol red. Images were taken with the EVOS Fl (Thermo Fisher) fluorescence microscope.

Immunofluorescence

Neutrophils were diluted to 3×10^5 cells/mL and seeded onto self-prepared poly-L-lysine coated chamber slides. The cells were incubated with live bacteria at an MOI of 2 and 2% overnight bacterial supernatant at 37 °C in a 5% CO_2 for 1 h. Following incubation, the cells were fixed with 4% formaldehyde and permeabilized using 0.5% Triton X-100. After blocking with 5% bovine serum albumin (BSA) in PBS, the cells were incubated overnight with myeloperoxidase (1:200 in PBS, sc-52707, Santa Cruz Biotechnology, Heidelberg, Germany) and citH3 (1:1000 in PBS, ab5103, Abcam). After washing with PBS, the staining was continued with an Alexa Fluor-488 conjugated secondary antibody (1:1000 in PBS, A10667, Invitrogen, Carlsbad, CA, USA) and Hoechst 33342 (2 µg/mL) for 2 h. The chambers were then removed, and the slides were mounted using Fluoromount G mounting medium (Thermo Fisher) and covered with coverslip. Microscopy was conducted using an EVOS Fl fluorescence microscope (Thermo Fisher).

Ethical statement

The Ethics Committee of Animal Research of Gothenburg approved all experiments conducted on mice. The mouse experiments were performed in accordance with the Swedish Board of Agriculture's regulations and recommendations on animal experiments. We have complied with all relevant ethical regulations for animal use. Blood was collected from healthy adult volunteers and written informed consent was given. The institutional review board of the University of Tübingen approved the study and all adult subjects provided informed consent. This study was done in accordance with the ethics committee of the medical faculty of the University of Tübingen that approved the study (Approval number 015/2014 BO2). All ethical regulations relevant to human research participants were followed.

Statistics and reproducibility

All the data were analyzed using GraphPad Prism (version 6.0; GraphPad Software). The data are presented in mean ± standard error of the mean (SEM). Statistical significance: ns (not significant) $p > 0.05$; $^{*}p < 0.05$; $^{**}p < 0.01$; $^{***}p < 0.001$; $^{****}p < 0.0001$. Details of statistical analyses for each experiment are provided in "Materials and Methods".

Reporting summary

Further information on research design is available in the Nature Portfolio Reporting Summary linked to this article.

Data availability

Primary source data are provided in Supplementary Data 1. Additional requests for the data and materials in this study are available from the corresponding author upon reasonable request.

Received: 2 August 2024; Accepted: 11 March 2025;
Published online: 10 April 2025

References

1. Mathews, C. J., Weston, V. C., Jones, A., Field, M. & Coakley, G. Bacterial septic arthritis in adults. *Lancet* **375**, 846–855 (2010).
2. Kaandorp, C. J., Krijnen, P., Moens, H. J., Habbema, J. D. & van Schaardenburg, D. The outcome of bacterial arthritis: a prospective community-based study. *Arthritis Rheum.* **40**, 884–892 (1997).
3. Na, M. et al. Deficiency of the complement component 3 but not factor b aggravates *Staphylococcus aureus* septic arthritis in mice. *Infect. Immun.* **84**, 930–939 (2016).
4. Verdrengh, M. & Tarkowski, A. Role of neutrophils in experimental septicemia and septic arthritis induced by *Staphylococcus aureus*. *Infect. Immun.* **65**, 2517–2521 (1997).
5. Tang, J. et al. Two thermostable nucleases coexisted in *Staphylococcus aureus*: evidence from mutagenesis and in vitro expression. *FEMS Microbiol. Lett.* **284**, 176–183 (2008).
6. Kiedrowski, M. R. et al. *Staphylococcus aureus* Nuc2 is a functional, surface-attached extracellular nuclease. *PLoS One* **9**, e95574 (2014).
7. Hu, Y., Xie, Y., Tang, J. & Shi, X. Comparative expression analysis of two thermostable nuclease genes in *Staphylococcus aureus*. *Foodborne Pathog. Dis.* **9**, 265–271 (2012).
8. Cuatrecasas, P., Fuchs, S. & Anfinsen, C. B. The interaction of nucleotides with the active site of staphylococcal nuclease. Spectrophotometric studies. *J. Biol. Chem.* **242**, 4759–4767 (1967).
9. Bhattacharya, M. et al. Leukocidins and the nuclease Nuc prevent neutrophil-mediated killing of *Staphylococcus aureus* biofilms. *Infect. Immun.* **88** (2020).
10. Bhattacharya, M. et al. *Staphylococcus aureus biofilms* release leukocidins to elicit extracellular trap formation and evade neutrophil-mediated killing. *Proc. Natl. Acad. Sci. USA* **115**, 7416–7421 (2018).
11. Yu, J. et al. Thermonucleases contribute to *Staphylococcus aureus* biofilm formation in implant-associated infections-A redundant and complementary story. *Front. Microbiol.* **12**, 687888 (2021).

12. von Kockritz-Blickwede, M. & Nizet, V. Innate immunity turned inside-out: antimicrobial defense by phagocyte extracellular traps. *J. Mol. Med.***87**, 775–783 (2009).
13. Berends, E. T. et al. Nuclease expression by *Staphylococcus aureus* facilitates escape from neutrophil extracellular traps. *J. Innate Immun.* **2**, 576–586 (2010).
14. Thammavongsa, V., Missiakas, D. M. & Schneewind, O. *Staphylococcus aureus* degrades neutrophil extracellular traps to promote immune cell death. *Science* **342**, 863–866 (2013).
15. Jin, T. Exploring the role of bacterial virulence factors and host elements in septic arthritis: insights from animal models for innovative therapies. *Front. Microbiol.* **15**, 1356982 (2024).
16. Hultgren, O., Eugster, H. P., Sedgwick, J. D., Korner, H. & Tarkowski, A. TNF/lymphotoxin-alpha double-mutant mice resist septic arthritis but display increased mortality in response to *Staphylococcus aureus*. *J. Immunol.* **161**, 5937–5942 (1998).
17. Fatima, F. et al. Radiological features of experimental staphylococcal septic arthritis by micro computed tomography scan. *PLoS One* **12**, e0171222 (2017).
18. Deshmukh, M. et al. Gene expression of S100a8/a9 predicts *Staphylococcus aureus*-induced septic arthritis in mice. *Front. Microbiol.* **14**, 1146694 (2023).
19. Sparwasser, T. et al. Bacterial DNA causes septic shock. *Nature* **386**, 336–337 (1997).
20. Deng, G. M., Nilsson, I. M., Verdrengh, M., Collins, L. V. & Tarkowski, A. Intra-articularly localized bacterial DNA containing CpG motifs induces arthritis. *Nat. Med.* **5**, 702–705 (1999).
21. Krieg, A. M. et al. CpG motifs in bacterial DNA trigger direct B-cell activation. *Nature* **374**, 546–549 (1995).
22. Hemmi, H. et al. A Toll-like receptor recognizes bacterial DNA. *Nature* **408**, 740–745 (2000).
23. Fey, P. D. et al. A genetic resource for rapid and comprehensive phenotype screening of nonessential *Staphylococcus aureus* genes. *mBio* **4**, e00537–00512 (2013).
24. Hashimoto, M. et al. Not lipoteichoic acid but lipoproteins appear to be the dominant immunobiologically active compounds in *Staphylococcus aureus*. *J. Immunol.* **177**, 3162–3169 (2006).
25. Stoll, H., Dengjel, J., Nerz, C. & Götz, F. *Staphylococcus aureus* deficient in lipidation of prelipoproteins is attenuated in growth and immune activation. *Infect. Immun.* **73**, 2411–2423 (2005).
26. Herbert, S. et al. Repair of global regulators in *Staphylococcus aureus* 8325 and comparative analysis with other clinical isolates. *Infect. Immun.* **78**, 2877–2889 (2010).
27. Dos Santos, D. C. et al. *Staphylococcus chromogenes*, a coagulase-negative *Staphylococcus* species that can clot plasma. *J. Clin. Microbiol.* **54**, 1372–1375 (2016).
28. Baba, T., Bae, T., Schneewind, O., Takeuchi, F. & Hiramatsu, K. Genome sequence of *Staphylococcus aureus* strain Newman and comparative analysis of staphylococcal genomes: polymorphism and evolution of two major pathogenicity islands. *J. Bacteriol.* **190**, 300–310 (2008).
29. Kennedy, A. D. et al. Targeting of alpha-hemolysin by active or passive immunization decreases severity of USA300 skin infection in a mouse model. *J. Infect. Dis.* **202**, 1050–1058 (2010).
30. Bost, K. L. et al. *Staphylococcus aureus* infection of mouse or human osteoblasts induces high levels of interleukin-6 and interleukin-12 production. *J. Infect. Dis.* **180**, 1912–1920 (1999).
31. Marriott, I. et al. Osteoblasts produce monocyte chemoattractant protein-1 in a murine model of *Staphylococcus aureus* osteomyelitis and infected human bone tissue. *Bone* **37**, 504–512 (2005).
32. Gunn, N. J. et al. A human osteocyte cell line model for studying *Staphylococcus aureus* persistence in osteomyelitis. *Front. Cell Infect. Microbiol.* **11**, 781022 (2021).
33. Alanara, T., Karstila, K., Moilanen, T., Silvennoinen, O. & Isomaki, P. Expression of IL-10 family cytokines in rheumatoid arthritis: elevated levels of IL-19 in the joints. *Scand. J. Rheumatol.* **39**, 118–126 (2010).
34. Osuchowski, M. F., Welch, K., Siddiqui, J. & Remick, D. G. Circulating cytokine/inhibitor profiles reshape the understanding of the SIRS/CARS continuum in sepsis and predict mortality. *J. Immunol.* **177**, 1967–1974 (2006).
35. Hultgren, O. H., Svensson, L. & Tarkowski, A. Critical role of signaling through IL-1 receptor for development of arthritis and sepsis during *Staphylococcus aureus* infection. *J. Immunol.* **168**, 5207–5212 (2002).
36. Nair, S. P., Bischoff, M., Senn, M. M. & Berger-Bachi, B. The sigma B regulon influences internalization of *Staphylococcus aureus* by osteoblasts. *Infect. Immun.* **71**, 4167–4170 (2003).
37. Almeida, R. A., Matthews, K. R., Cifrian, E., Guidry, A. J. & Oliver, S. P. *Staphylococcus aureus* invasion of bovine mammary epithelial cells. *J. Dairy Sci.* **79**, 1021–1026 (1996).
38. Lu, T., Porter, A. R., Kennedy, A. D., Kobayashi, S. D. & DeLeo, F. R. Phagocytosis and killing of *Staphylococcus aureus* by human neutrophils. *J. Innate Immun.* **6**, 639–649 (2014).
39. Weiss, E., Schlatterer, K., Beck, C., Peschel, A. & Kretschmer, D. Formyl-Peptide receptor activation enhances phagocytosis of community-acquired methicillin-resistant *Staphylococcus aureus*. *J. Infect. Dis.* **221**, 668–678 (2020).
40. Halverson, T. W., Wilton, M., Poon, K. K., Petri, B. & Lewenza, S. DNA is an antimicrobial component of neutrophil extracellular traps. *PLoS Pathog.* **11**, e1004593 (2015).
41. Papayannopoulos, V., Metzler, K. D., Hakkim, A. & Zychlinsky, A. Neutrophil elastase and myeloperoxidase regulate the formation of neutrophil extracellular traps. *J. Cell Biol.* **191**, 677–691 (2010).
42. Ranjit, D. K., Endres, J. L. & Bayles, K. W. CidA and LrgA proteins exhibit holin-like properties. *J. Bacteriol.* **193**, 2468–2476 (2011).
43. Sultan, A. R. et al. During the early stages of *Staphylococcus aureus* biofilm formation, induced neutrophil extracellular traps are degraded by autologous thermonuclease. *Infect. Immun.* **87** (2019).
44. Deng, G. M. & Tarkowski, A. The role of bacterial DNA in septic arthritis. *Int J. Mol. Med.* **6**, 29–33 (2000).
45. Uchiyama, S., Andreoni, F., Schuepbach, R. A., Nizet, V. & Zinkernagel, A. S. DNase Sda1 allows invasive M1T1 Group A *Streptococcus* to prevent TLR9-dependent recognition. *PLoS Pathog.* **8**, e1002736 (2012).
46. Fei, Y. et al. The combination of a tumor necrosis factor inhibitor and antibiotic alleviates staphylococcal arthritis and sepsis in mice. *J. Infect. Dis.* **204**, 348–357 (2011).
47. Onnheim, K., Bylund, J., Boulay, F., Dahlgren, C. & Forsman, H. Tumour necrosis factor (TNF)-alpha primes murine neutrophils when triggered via formyl peptide receptor-related sequence 2, the murine orthologue of human formyl peptide receptor-like 1, through a process involving the type I TNF receptor and subcellular granule mobilization. *Immunology* **125**, 591–600 (2008).
48. Ali, A. et al. CTLA4 immunoglobulin but not anti-tumor necrosis factor therapy promotes staphylococcal septic arthritis in mice. *J. Infect. Dis.* **212**, 1308–1316 (2015).
49. Nakashima, K. & de Crombrugghe, B. Transcriptional mechanisms in osteoblast differentiation and bone formation. *Trends Genet.* **19**, 458–466 (2003).
50. Köllisch, G. et al. Various members of the Toll-like receptor family contribute to the innate immune response of human epidermal keratinocytes. *Immunology* **114**, 531–541 (2005).
51. Nguyen, M. T. & Götz, F. Lipoproteins of Gram-positive bacteria: key players in the immune response and virulence. *Microbiol. Mol. Biol. Rev.* **80**, 891–903 (2016).
52. Nguyen, M. T. et al. Lipid moieties on lipoproteins of commensal and non-commensal staphylococci induce differential immune responses. *Nat. Commun.* **8**, 2246 (2017).
53. Leech, J. M., Lacey, K. A., Mulcahy, M. E., Medina, E. & McLoughlin, R. M. IL-10 Plays Opposing Roles during *Staphylococcus aureus* Systemic and Localized Infections. *J. Immunol.* **198**, 2352–2365 (2017).

54. Kasten, K. R., Muenzer, J. T. & Caldwell, C. C. Neutrophils are significant producers of IL-10 during sepsis. *Biochem. Biophys. Res. Commun.* **393**, 28–31 (2010).
55. Fischer, E. et al. Interleukin-1 receptor antagonist circulates in experimental inflammation and in human disease. *Blood* **79**, 2196–2200 (1992).
56. Dinarello, C. A. Interleukin-1 and interleukin-1 antagonism. *Blood* **77**, 1627–1652 (1991).
57. Ali, A. et al. IL-1 receptor antagonist treatment aggravates staphylococcal septic arthritis and sepsis in mice. *PLoS One* **10**, e0131645 (2015).
58. Talebi-Taher, M., Shirani, F., Nikanjam, N. & Shekarabi, M. Septic versus inflammatory arthritis: discriminating the ability of serum inflammatory markers. *Rheumatol. Int.* **33**, 319–324 (2013).
59. Saez-Llorens, X. et al. Tumor necrosis factor alpha and interleukin 1 beta in synovial fluid of infants and children with suppurative arthritis. *Am. J. Dis. Child* **144**, 353–356 (1990).
60. Ma, L., Sun, P., Zhang, J. C., Zhang, Q. & Yao, S. L. Proinflammatory effects of S100A8/A9 via TLR4 and RAGE signaling pathways in BV-2 microglial cells. *Int J. Mol. Med.* **40**, 31–38 (2017).
61. Gopal, R. et al. S100A8/A9 proteins mediate neutrophilic inflammation and lung pathology during tuberculosis. *Am. J. Respir. Crit. Care Med.* **188**, 1137–1146 (2013).
62. Wong, P. K. et al. Interleukin-6 modulates production of T lymphocyte-derived cytokines in antigen-induced arthritis and drives inflammation-induced osteoclastogenesis. *Arthritis Rheum.* **54**, 158–168 (2006).
63. Brinkmann, V. et al. Neutrophil extracellular traps kill bacteria. *Science* **303**, 1532–1535 (2004).
64. Fuchs, T. A. et al. Novel cell death program leads to neutrophil extracellular traps. *J. Cell Biol.* **176**, 231–241 (2007).
65. Winstel, V., Missiakas, D. & Schneewind, O. *Staphylococcus aureus* targets the purine salvage pathway to kill phagocytes. *Proc. Natl. Acad. Sci. USA* **115**, 6846–6851 (2018).
66. von Kockritz-Blickwede, M. & Winstel, V. Molecular prerequisites for neutrophil extracellular trap formation and evasion mechanisms of *Staphylococcus aureus*. *Front. Immunol.* **13**, 836278 (2022).
67. Mohammad, M. et al. The role of *Staphylococcus aureus* lipoproteins in hematogenous septic arthritis. *Sci. Rep.* **10**, 7936 (2020).
68. Geiger, T. et al. The stringent response of *Staphylococcus aureus* and its impact on survival after phagocytosis through the induction of intracellular PSMs expression. *PLoS Pathog.* **8**, e1003016 (2012).
69. Dalpke, A., Frank, J., Peter, M. & Heeg, K. Activation of toll-like receptor 9 by DNA from different bacterial species. *Infect. Immun.* **74**, 940–946 (2006).
70. Nguyen, M. T. et al. The vSaα specific lipoprotein like cluster (*lpl*) of *S. aureus* USA300 contributes to immune stimulation and invasion in human cells. *PLoS Pathog.* **11**, e1004984 (2015).

Acknowledgements

This work was supported by funding from the Deutsche Forschungsgemeinschaft the Germany's Excellence Strategy—EXC 2124—390838134 "Controlling Microbes to Fight Infections" to F.G., grants from the Swedish state under the agreement between the Swedish Government and the county councils, the ALF-agreement grant number ALFGBG-823941 to T.J., N.L. was supported by the Chinese Scholarship Council. We are grateful to Stefanie Krajewski, Clinical Research Laboratory, Department of Thoracic, Cardiac and Vascular Surgery, University Hospital Tübingen, 72076 Tübingen, Germany, for providing us with SAOS-2 cells. S.E. received funding from the German Research Council (EH471/5-1). The funders had no role in design, analysis, and reporting of the study. A.W. received funding from the DFG Collaborative Research Center (CRC) 156 "The skin as a sensor and effector organ orchestrating local and systemic immune responses" (project B05) and DFG Priority Programs SPP 2225 "EXIT Strategies of Intracellular Pathogens" (projects 446404928 and We-4195/25-1). We acknowledge support by Open Access Publishing Fund of University of Tübingen.

Author contributions

F.G., N.L. designed the study and the experiments; T.J., M.V.D. designed and carried out the septic arthritis model; F.S., S.E., A.N., and N.L. carried out neutrophil experiments; N.L., N.H. constructed deletion mutants; N.L., A.V.A., and A.W. carried out cell lines experiments; F.G., N.L. wrote the manuscript. All authors read and approved the final manuscript.

Funding

Open Access funding enabled and organized by Projekt DEAL.

Competing interests

The authors declare no competing interests.

Additional information

Supplementary information The online version contains supplementary material available at https://doi.org/10.1038/s42003-025-07920-4.

Correspondence and requests for materials should be addressed to Friedrich Götz.

Peer review information *Communications Biology* thanks Mohini Bhattacharya and the other, anonymous, reviewers for their contribution to the peer review of this work. Primary Handling Editors: Christopher LaRock and Mengtan Xing. A peer review file is available.

Supplementary Information

Supplementary Table 1. Bacterial strains and plasmids used in this study.

Bacterial strains or Plasmids	Descriptions	Reference
E. coli BL21	Laboratory strain	[1]
E. coli DC10B	*E. coli* K12, Δ*dcm* mutant	[2]
S. aureus USA300 JE2	CA-MRSA strain USA300 LAC cured of plasmids	[3]
JE2Δ*nuc1*	*nuc1* gene deleted in JE2	This study
JE2Δ*lgt*	*lgt* gene deleted (phosphatidylglycerol:prolipoprotein diacylglyceryl transferase)	This study
JE2Δ*nuc1*Δ*lgt*	*nuc1*-*lgt* double deletion	This study
JE2Δ*nuc1*(pRB473-*nuc1*)	pRB473 carrying *nuc1*	This study
S. aureus Newman (NWT)	*S. aureus* Newman wildtype, clinical isolate	[4]
Δ*nuc1*	*nuc1* gene deleted in NWT	This study
Δ*nuc1*(pRB473-*nuc1*)	pRB473 carrying *nuc1*	This study
S. aureus RN4220	Restriction-deficient derivative of NCTC8325-4	[5]
pET28a	Expression plasmid	
pBASE6	Shuttle plasmid	[6]
pRB473	Shuttle plasmid	[7]

Supplementary Table 2. Oligonucleotides used in this study.

Oligonucleotide	Seq
lgtupF	CGCGCAGATCTGTCGACGATGATATGATAAGAAGAGATGTAAGAGTAG
lgtupR	CACTACTTCACTTTTTTTGTGTTAAATACAATACCCATTCAACCTA
lgtdownF	GAATGGGTATTGTATTTAACACAAAAAAAGTGAAGTAGTGATAGTT
lgtdownR	TGCAGGCATGCAAGCTTGATACACGATGATCTTGAACTTCTT
nuc1upF	CGCGCAGATCTGTCGACGATCCATCAACAAATTATACCGTTTTTC
nuc1upR	TGTCTTCGCTCCAAATATTTCATACATATGCCAGCACTTAATA
nuc1downF	TAAGTGCTGGCATATGTATGAAATATTTGGAGCGAAGACAAC
nuc1downR	TGCAGGCATGCAAGCTTGATAACAAGATTACTGAATTATTATGAGATT
nucapET28F	TAAGAAGGAGATATACCATGGCAACTTCAACTAAAAAATTACATAA
nucapET28R	TTCGGGCTTTGTTAGCAGCCTTA TTGACCTGAATCAGCGT
pET28F	GGCTGCTAACAAAGCCCGAAAG
pET28R	CATGGTATATCTCCTTCTTAAAGTTAAACAA
pRB473nuc1F	CGACTCTAGAGGATCAATTTTACAAATAAGGCTAAATA
pRB473nuc1R	GTGCGAATTCGAGCTCTTTTGATACTATTTACTTTTTTAATTCTGAAT

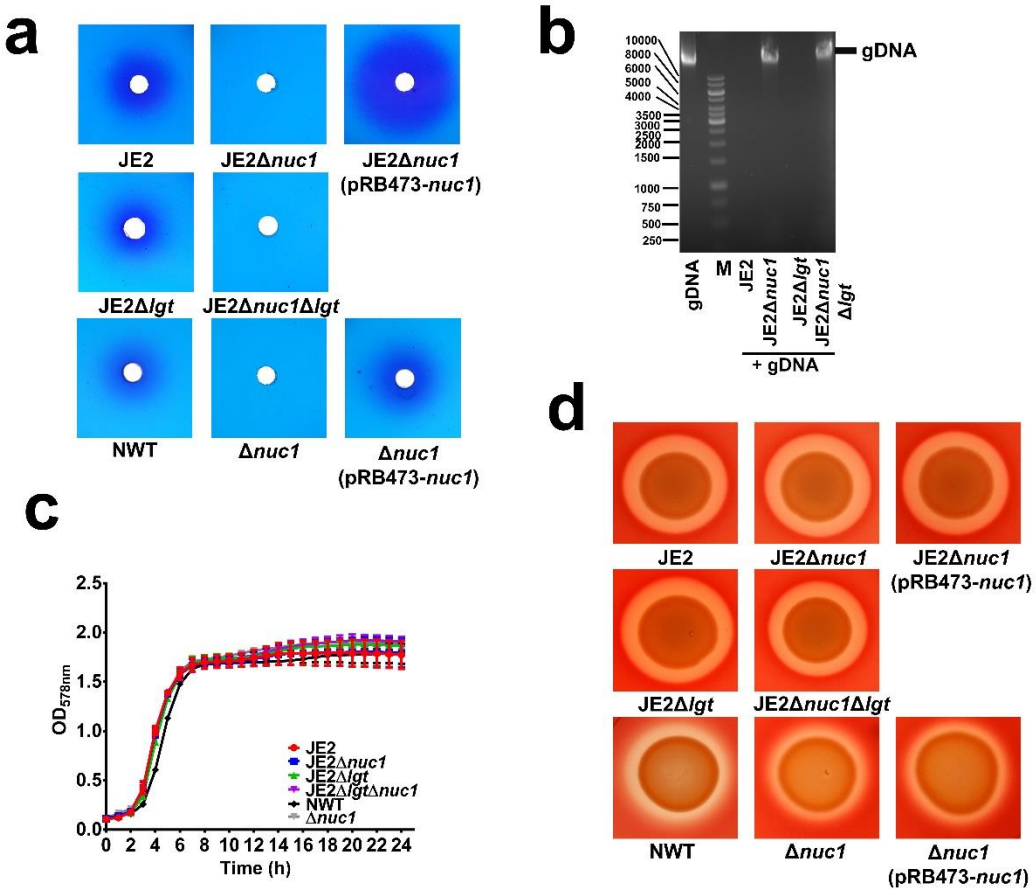

Supplementary Figure 1. Characteristics of JE2, Newman and their mutants. a Nuclease activity, **c** growth in TSB medium, and **d** hemolytic activity of JE2 JE2Δ*nuc1*, JE2Δ*lgt*, JE2Δ*nuc1*Δ*lgt,* JE2Δ*nuc1*(pRB473-*nuc1*), Newman (NWT), Δ*nuc1* and Δ*nuc1*(pRB473-*nuc1*). **b** JE2Δ*lgt* gDNA was incubated with overnight cultural supernatant from JE2, JE2Δ*nuc1*, JE2Δ*lgt*, and JE2Δ*nuc1*Δ*lgt* for 1 h at 37 ºC. The degradation of DNA was visualized through agarose gel electrophoresis.

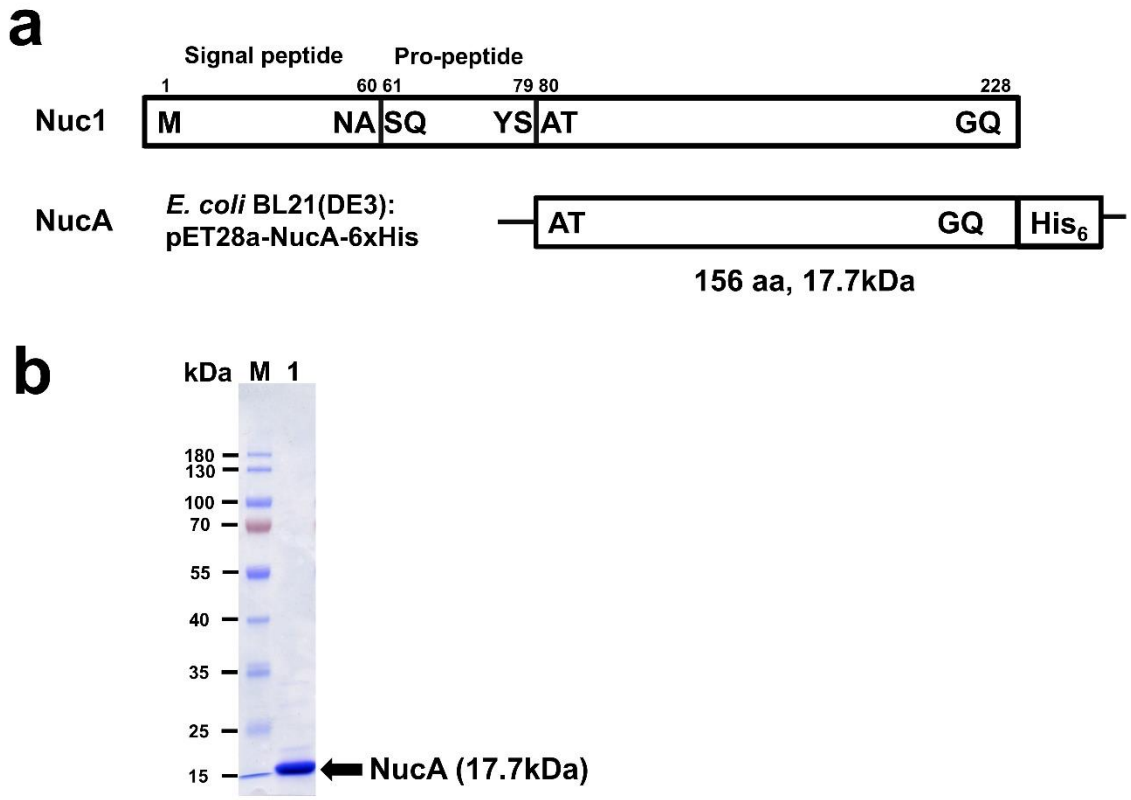

Supplementary Figure 2. Organization of the Nuc1, NucA protein sequence and production of NucA. a Nuc1 is organized as a pre-pro-enzyme. The pre-pro-enzyme is processed to the mature nuclease NucA. Sequence of the mature NucA that was expressed in *E. coli* BL21(DE3) (pET28a-NucA-6x-His) as a C-terminal His-tag fusion protein. **b** Demonstration of Ni-NTA purified NucA in SDS-PAGE. NucA was used in gDNA hydrolysis assays.

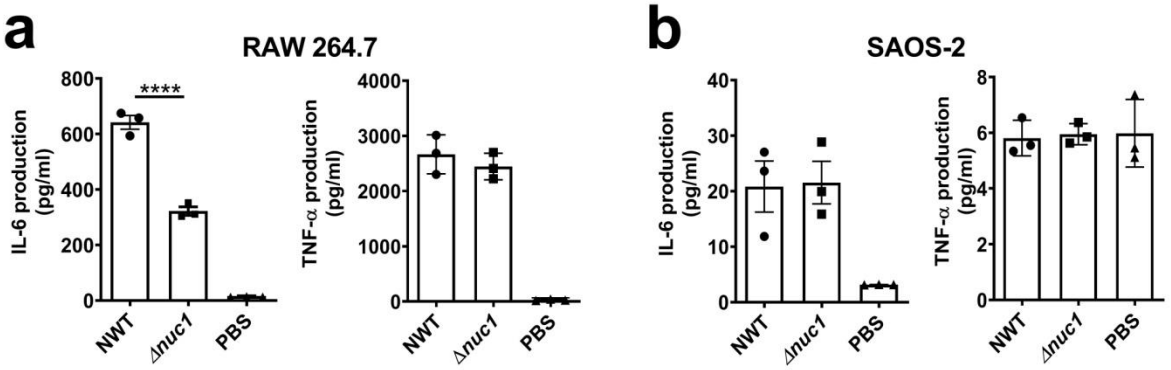

Supplementary Figure 3. Induction of cytokines by host cells upon exposure to live Newman (NWT) and its mutant Δ*nuc1*. The PBS-washed bacteria were incubated with **a** RAW 264.7 at an MOI=30 and **b** SAOS-2 cells at an MOI=3. Cellular supernatants were collected after 18 h for ELISA assay. Triplet experiments were conducted; error bars indicate ± SEM; not significant $p>0.05$; ****$p<0.0001$, one-way ANOVA with Dunnett's posttest.

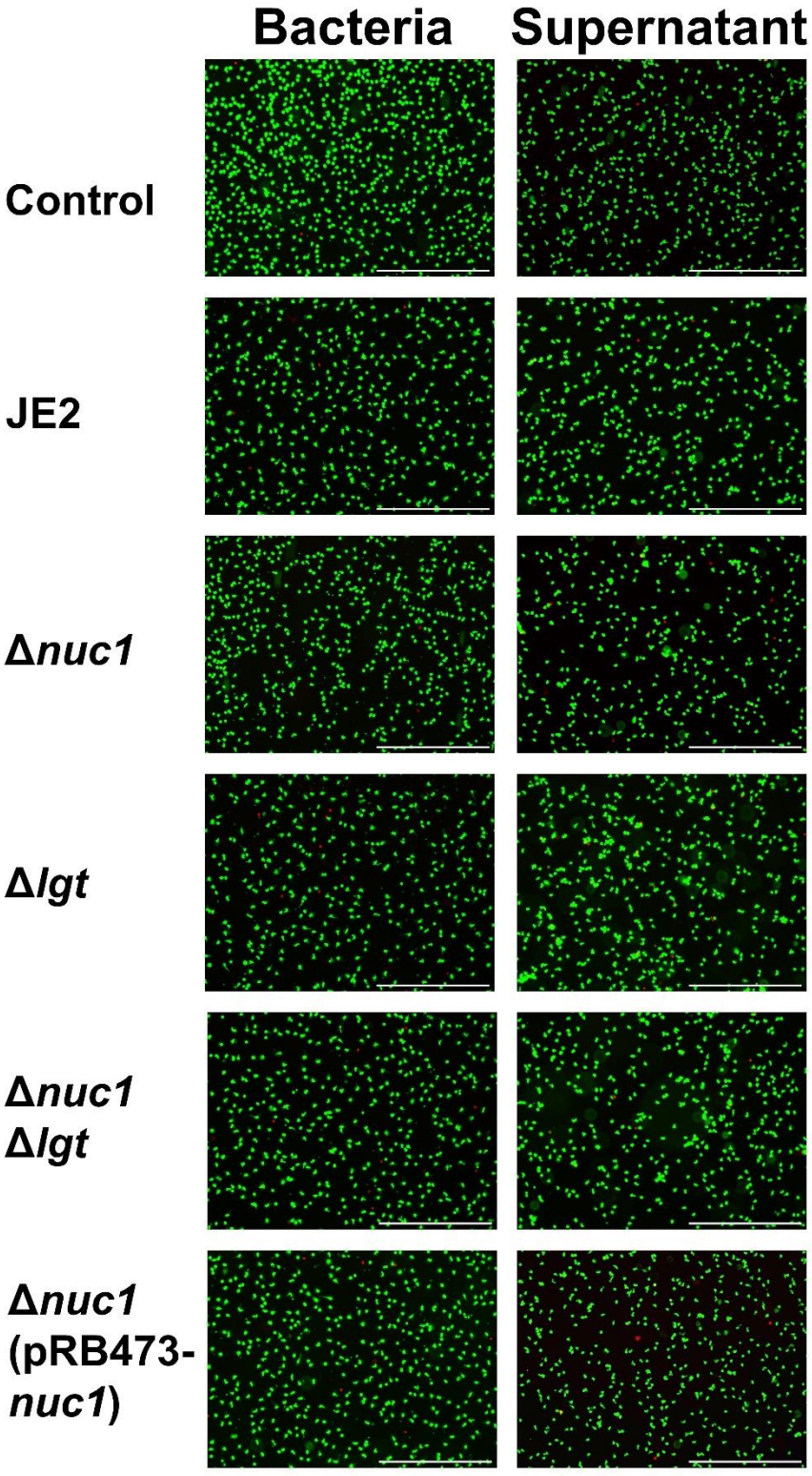

Supplementary Figure 4. Exemplary pictures of viability staining for neutrophils exposed to JE2 and its mutants. Pictures were taken after 3 hours of incubation. Green: Calcein AM, Red: Ethidium Bromide, scale bar: 500 µm.

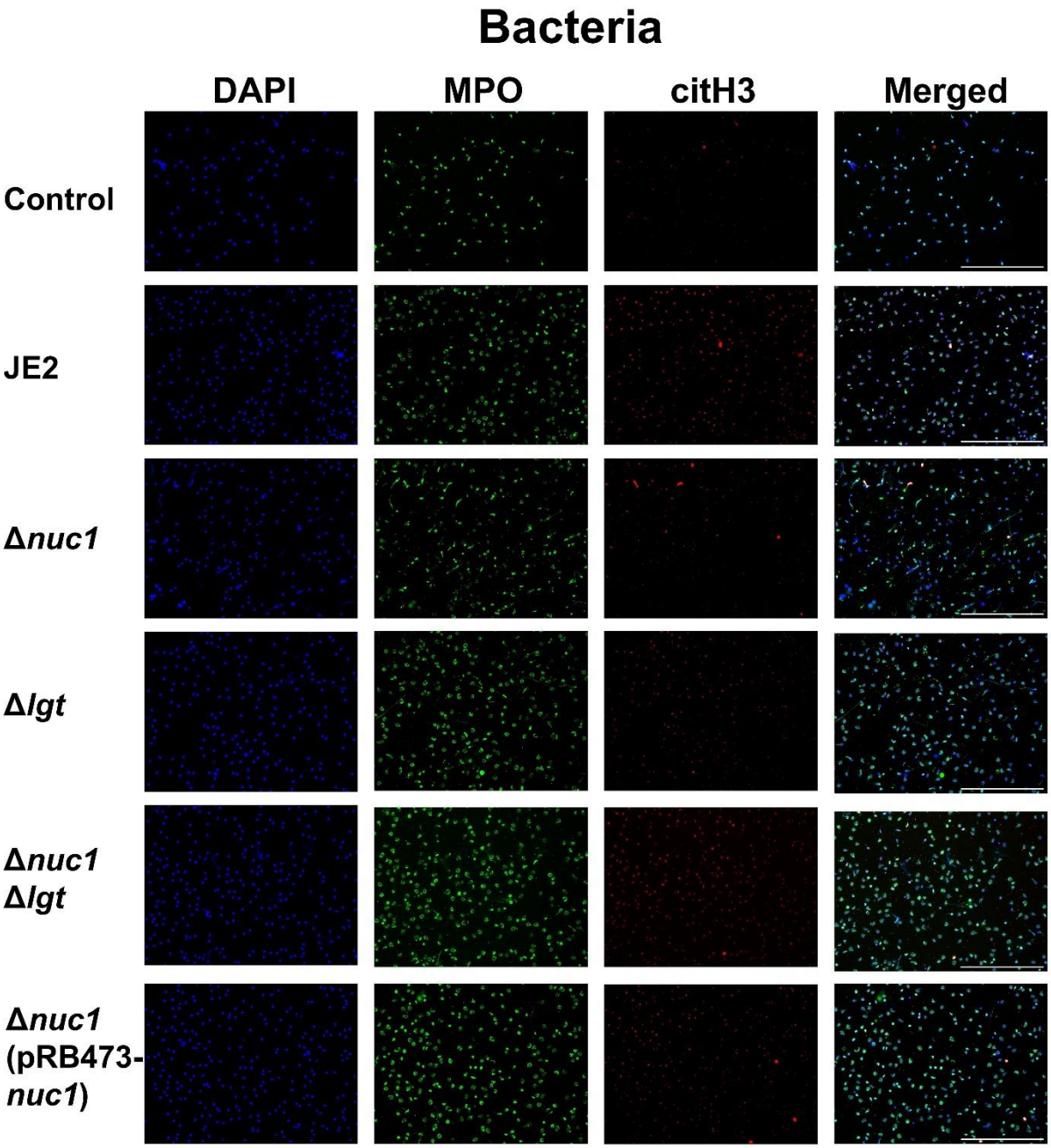

Supplementary Figure 5. Exemplary images of immunofluorescent staining of live bacteria (MOI=2) incubated with neutrophils at 1 h incubation. Blue: DNA (Hoechst 33342); Green: myeloperoxidase, MPO; Red: citrullinated histone H3, citH3, scale bar: 500 µm.

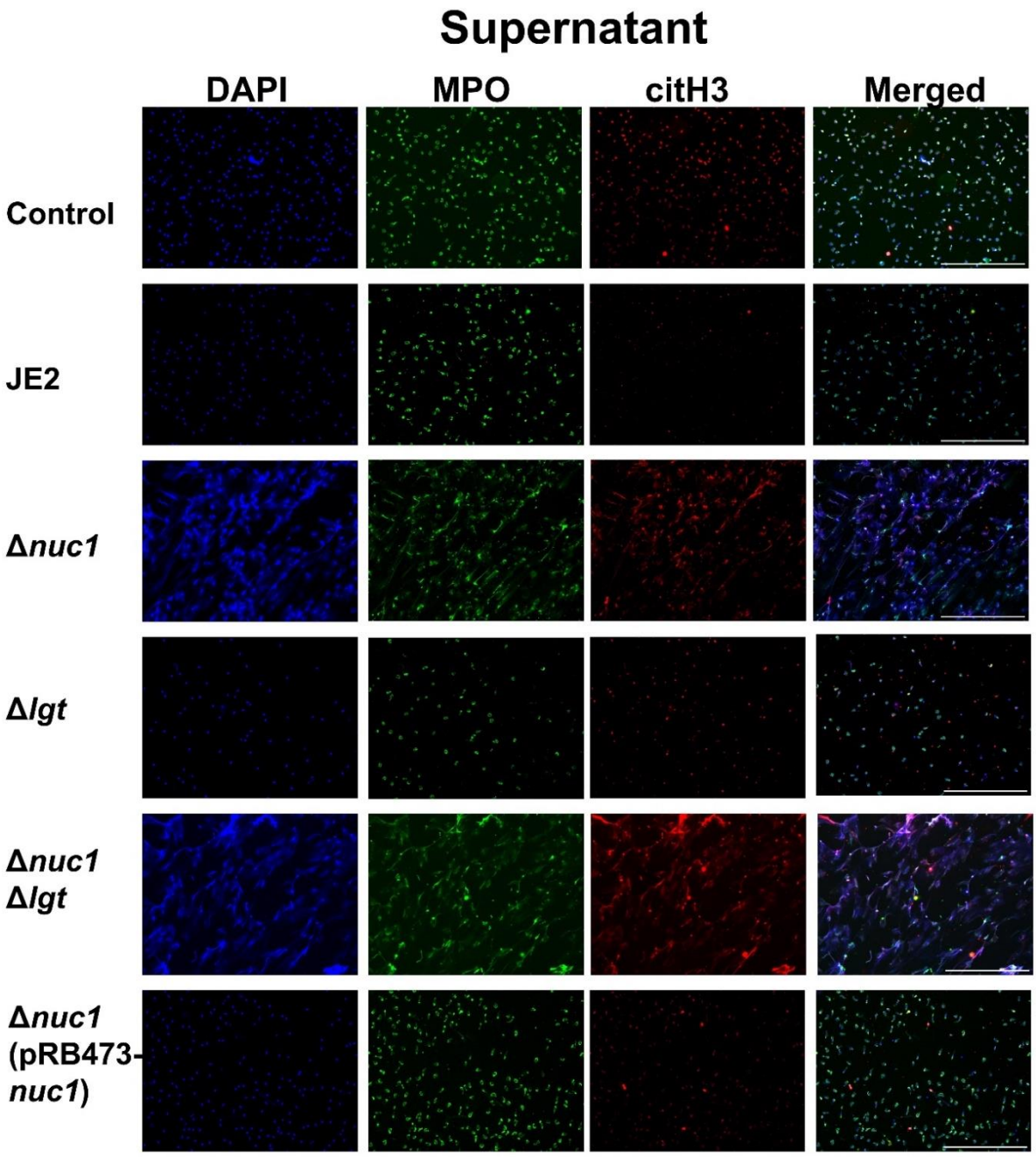

Supplementary Figure 6. Exemplary images of immunofluorescent staining of overnight supernatant (2% volume) incubated with neutrophils at 1 h incubation. Blue: DNA (Hoechst 33342); Green: myeloperoxidase, MPO; Red: citrullinated histone H3, citH3, scale bar: 500 µm.

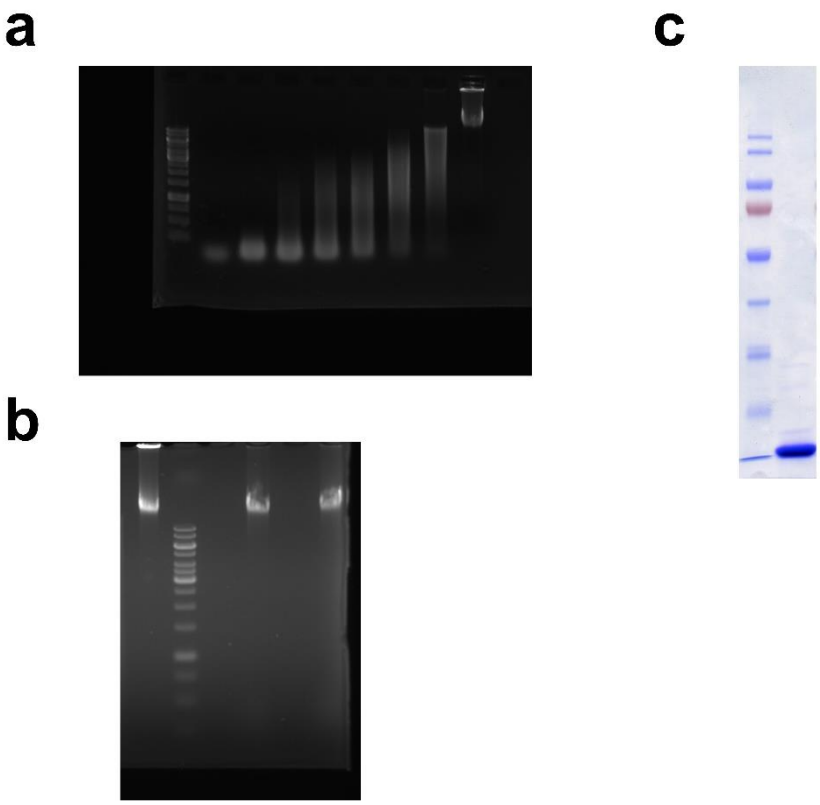

Supplementary Figure 7. **Unedited agarose gel or SDS-PAGE gel images. a** Unedited image for Fig. 3b. **b** Unedited agarose gel image for Supplementary Figure 1b. **c** Unedited SDS-PAGE gel image for Supplementary Figure 2b.

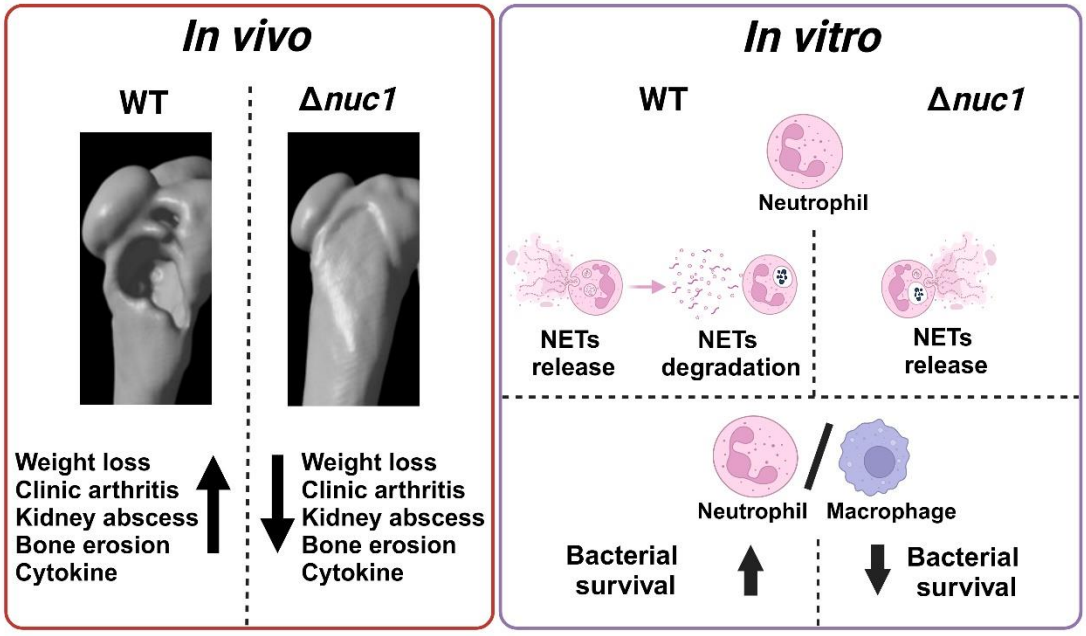

Supplementary Figure 8 (Graphical Abstract). Schematic representation of the differences in pathogenicity between the *S. aureus* wild-type strain (WT) and its Δ*nuc1* mutant in the mouse model for septic arthritis and under *in vitro* conditions. *In vivo*, WT-infected mice showed marked weight loss, increased clinical arthritis frequency, higher kidney abscess score, severe bone erosions, and higher cytokine levels than the Δ*nuc1*-infected mice. *In vitro*, the WT effectively digests NETs formed by neutrophils, which increases bacterial survival. This image is created in BioRender. Götz, F. (2025) https://BioRender.com/w43z906

Supplementary References

1. Studier, F. W. & Moffatt, B. A. Use of bacteriophage T7 RNA polymerase to direct selective high-level expression of cloned genes. *J Mol Biol* **189**, 113-130 (1986).
2. Monk, I. R., Shah, I. M., Xu, M., Tan, M. W. & Foster, T. J. Transforming the untransformable: application of direct transformation to manipulate genetically *Staphylococcus aureus* and *Staphylococcus epidermidis*. *mBio* **3** (2012).
3. Fey, P. D. *et al.* A genetic resource for rapid and comprehensive phenotype screening of nonessential *Staphylococcus aureus* genes. *mBio* **4**, e00537-00512 (2013).
4. Duthie, E. S. & Lorenz, L. L. Staphylococcal coagulase; mode of action and antigenicity. *J Gen Microbiol* **6**, 95-107 (1952).
5. Kreiswirth, B. N. *et al.* The toxic shock syndrome exotoxin structural gene is not detectably transmitted by a prophage. *Nature* **305**, 709-712 (1983).
6. Geiger, T. *et al.* The stringent response of *Staphylococcus aureus* and its impact on survival after phagocytosis through the induction of intracellular PSMs expression. *PLoS Pathog* **8**, e1003016 (2012).
7. Bruckner, R. A series of shuttle vectors for *Bacillus subtilis* and *Escherichia coli*. *Gene* **122**, 187-192 (1992).

AMERICAN SOCIETY FOR MICROBIOLOGY | mBio®

RESEARCH ARTICLE

Molecular Basis of Rhodomyrtone Resistance in *Staphylococcus aureus*

Li Huang,[a,d] Miki Matsuo,[a] Carlos Calderón,[b*] Sook-Ha Fan,[a] Aparna Viswanathan Ammanath,[a] Xiaoqing Fu,[b] Ningna Li,[a] Arif Luqman,[a§] Marvin Ullrich,[c] Florian Herrmann,[c] Martin Maier,[c] Anchun Cheng,[d] Fajun Zhang,[e] Filipp Oesterhelt,[f] Michael Lämmerhofer,[b] Friedrich Götz[a,g]

[a]Microbial Genetics, Interfaculty Institute of Microbiology and Infection Medicine Tübingen (IMIT), University of Tübingen, Tübingen, Germany
[b]Institute of Pharmaceutical Sciences, University of Tübingen, Tübingen, Germany
[c]Institute of Organic Chemistry, University of Tübingen, Tübingen, Germany
[d]Institute of Preventive Veterinary Medicine, College of Veterinary Medicine, Sichuan Agricultural University, Chengdu, China
[e]Institute of Applied Physics, University of Tübingen, Tübingen, Germany
[f]Microbial Bioactive Compounds, Interfaculty Institute of Microbiology and Infection Medicine Tübingen (IMIT), University of Tübingen, Tübingen, Germany
[g]Excellence Cluster 2124 'Controlling Microbes to Fight Infections' (CMFI), University of Tübingen, Tübingen, Germany

Li Huang, Miki Matsuo, and Carlos Calderón contributed equally to this work. Author order was determined by the principal investigator.

ABSTRACT Rhodomyrtone (Rom) is a plant-derived broad-spectrum antibiotic active against many Gram-positive pathogens. A single point mutation in the regulatory *farR* gene (*farR**) confers resistance to Rom in *Staphylococcus aureus* (RomR). The mutation in *farR** alters the activity of the regulator, FarR*, in such a way that not only its own gene, *farR**, but also the divergently transcribed *farE* gene and genes controlled by the global regulator, *agr*, are highly upregulated. Here, we show that mainly the upregulation of the fatty acid efflux pump FarE causes the RomR phenotype, as *farE* deletion in either the parent or the RomR strain (RomR Δ*farE*) yielded hypersensitivity to Rom. Comparative lipidome analysis of the supernatant (exolipidomics) and the pellet fraction revealed that the RomR strain excreted about 10 times more phospholipids (PGs) than the parent strain or the Δ*farE* mutants. Since the PG content in the supernatant (2,244 ng/optical density [OD]) was more than 100-fold higher than that of fatty acids (FA), we assumed that PG interacts with Rom, thereby abrogating its antimicrobial activity. Indeed, by static and dynamic light scattering (SLS and DLS) and isothermal titration calorimetry (ITC) analyses, we could demonstrate that both PG and Rom were vesicular and reacted with each other in milliseconds to form a 1:1.49 [Rom-PG(32:0), where PG(32:0) is PG with C32:0 lipids] complex. The binding is entropically driven and hence hydrophobic and of low specificity in nature. Our results indicate that the cytoplasmic membrane is the actual target of Rom, which is also in agreement with Rom's induced rapid collapse of the membrane potential and decreased membrane integrity.

IMPORTANCE Antibiotic resistance is a growing public health problem, and alternative antibiotics are urgently needed. Rhodomyrtone (Rom), an antimicrobial compound originally isolated from *Rhodomyrtus tomentosa*, is active against multidrug-resistant Gram-positive pathogens. However, Rom-resistant (RomR) mutants occur with low frequency. In this study, we unraveled the underlying resistance mechanism, which is based on a point mutation in the *farR* regulator gene, causing overexpression of FarE, which most likely acts as a phospholipid (PG) efflux pump, as large amounts of PG were found in the supernatant and the pellet fraction. We show that PG can bind to Rom, thereby abrogating its antimicrobial activity. The direct interaction of Rom with PG suggests that Rom's actual target is the cytoplasmic membrane. Antibiotics that interact with PG are rare. Since Rom can be chemically synthesized, it serves as a lead compound for synthesis of improved variants.

Editor Tarek Msadek, Institut Pasteur

Address correspondence to Friedrich Götz, friedrich.goetz@uni-tuebingen.de, or Anchun Cheng, chenganchun@vip.163.com.

*Present address: Carlos Calderón, Escuela de Química, Universidad de Costa Rica, San José, Costa Rica.

§Present address: Arif Luqman, Biology Department, Institut Teknologi Sepuluh Nopember, Surabaya, Indonesia.

The authors declare no conflict of interest.

Received 4 January 2022
Accepted 12 January 2022
Published 15 February 2022

KEYWORDS FarR, FarE, isothermal titration calorimetry, lipidomic analysis, P-lipids, rhodomyrtone, Rom, resistance mechanism, *Staphylococcus*, *farR*

Bacterial infections and particularly antimicrobial resistance to antibiotics are worldwide problems. A crucial point is therefore the development of new antimicrobial strategies against drug-resistant Gram-positive and Gram-negative bacteria that cause acute or chronic infections. While many antibiotics are derived from bacteria and fungi, there is a growing trend of looking more closely to the antimicrobial potential of plant-derived compounds. One such compound is rhodomyrtone (Rom), originally isolated from plant extracts of *Rhodomyrtus tomentosa* (1). Rom has good antimicrobial activity against a wide range of Gram-positive bacteria, including multidrug-resistant *Enterococcus faecalis*, *Propionibacterium acnes*, *Staphylococcus aureus*, *Streptococcus pneumoniae*, and *Streptococcus pyogenes* (2–6). In a mouse model of skin infection with methicillin-resistant *Staphylococcus aureus* (MRSA), it has been shown that rhodomyrtosone B prevents skin ulcer formation and reduces the incidence of infection-related morbidity; its activity was comparable to that of vancomycin (7). Structural analysis revealed that Rom belongs to the acylphloroglucinol class (1). The elaboration of a chemical synthesis route of Rom and thus the production of larger quantities enabled the study of the mode of action (8, 9).

Rom interferes with none of the classical antibiotic targets, such as peptidoglycan biosynthesis, DNA replication, translation, and transcription, but targets the cell membrane by causing a strong dissipation of the membrane potential and release of ATP and cytoplasmic proteins (10). Rom does not seem to be a typical membrane-inserting molecule, but it disrupts the membrane by inducing the formation of large invaginations and transiently binding to phospholipid (P-lipid) (phosphatidylglycerol [PG]) head groups (11). Interestingly, the antimicrobial activity of Rom could be counteracted by supplementing the medium with certain fatty acids (FAs) (pentadecylic acid, palmitic acid, and stearic acid) (10).

In our previous study, we were able to isolate Rom-resistant mutants by subculturing *S. aureus* HG001 in medium supplemented with Rom (12) and to attribute Rom resistance to a single point mutation in the coding region of *farR* (regulator of fatty acid resistance). FarR belongs to the TetR family of regulators (TFRs), which are widely associated with antibiotic resistance and the regulation of genes encoding small-molecule exporters, but they are also involved in controlling many other aspects of prokaryotic physiology (13). In *S. aureus* the divergently transcribed genes *farR-farE*, first described by Alnaseri et al. in 2015 (14), encode the regulator (FarR) and the efflux pump (FarE) that confer resistance to the antimicrobial fatty acids linoleic and arachidonic acids (14).

The Rom-resistant mutant *S. aureus* HG001 $farR_{Cys116Arg}$, henceforth referred to as RomR, exhibited an increase in the MIC from 0.5 μg/mL to $>$128 μg/mL (12). A comparative transcriptome analysis revealed that many genes were differentially expressed in wild-type *S. aureus* HG001 and the isogenic RomR mutant, suggesting that the mutant $FarR_{Cys116Arg}$ (FarR*) displays an altered regulatory activity. In particular, *farR*, *farE*, *agr* (accessory gene regulator), and the Agr-controlled virulence genes were upregulated in the RomR mutant, the latter explaining the increased pathogenicity of the RomR mutant (12). We speculated that the upregulation of *farE* is likely to play a crucial role in Rom resistance, as a *farE* deletion mutant strain (Δ*farE*) became hypersensitive to Rom.

In this study, we demonstrated by qualitative and quantitative lipidomic analyses that the RomR strain releases large amounts of PGs into the supernatant and cell envelope, suggesting that FarE acts as a PG efflux pump. Rom resistance is mediated by interaction of PG with Rom, thereby abrogating its antimicrobial activity.

RESULTS

Deletion of *farE* in *S. aureus* HG001 and its isogenic RomR mutant renders the mutants hypersensitive to Rom. To investigate whether *farE* is responsible for Rom resistance in RomR, we constructed markerless *farE* deletion mutants in the *S. aureus* HG001 wild-type and RomR mutant strains (HG001 Δ*farE* and RomR Δ*farE*, respectively).

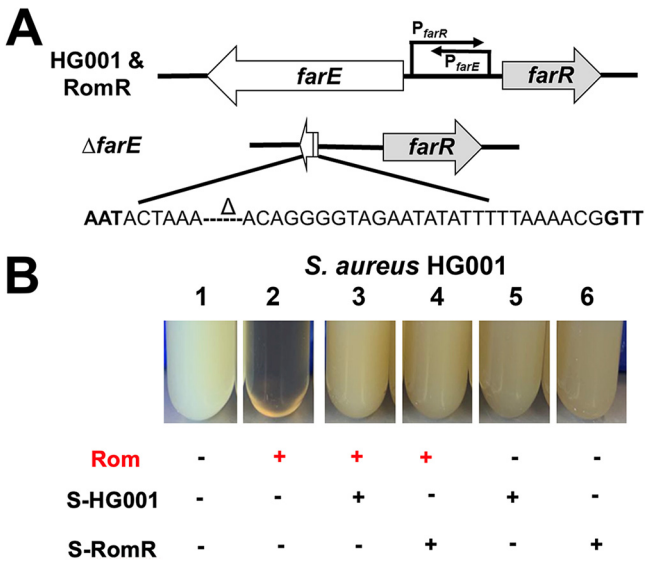

FIG 1 Rom susceptibility and growth of *farE* deletion mutants. (A) Overview of the strategy used to generate the Δ*farE* deletion mutants in HG001 and RomR strains. The delta symbol in the sequence indicates a deleted region. (B) Rom's antimicrobial activity can be abrogated by addition of culture supernatant of HG001 and the RomR mutant from the end of the exponential phase. Growth of *S. aureus* HG001 was inhibited by Rom (2 μg/mL) (compare tubes 1 and 2). The addition of 20-times-concentrated supernatant (1:20 [vol/vol]) of HG001 (tube 3) and 2-times-concentrated supernatant (1:2 [vol/vol]) of RomR (tube 4) rescued the growth, while supernatants alone (tubes 5 and 6) had no impact on growth. Cells were grown in BM for 12 h.

Since the promoters of *farE* and *farR* are divergent and the corresponding transcripts overlapped as described by the group of Martin McGavin (15), we were cautious not to disrupt any of the promoter regions and constructed an internal deletion in *farE* leaving the first 10 codons and the last codons, including the stop codon TAA, intact (Fig. 1A). Deletion of *farE* led to a decrease in the MIC values even in the RomR mutant, with a drop from >128 to 0.5 μg/mL (Table 1).

Next, we examined the impact of Rom on the growth of HG001 and RomR and their respective Δ*farE* mutants. Rom (8 μg/mL) was added to basic medium (BM) 1 h after starting the incubation, and the growth of *S. aureus* clones was followed for 20 h. Growth of HG001 was inhibited for the first 12 h but resumed thereafter. Growth of HG001 Δ*farE* was inhibited for the whole period. Growth of RomR mutant was unaffected in the presence of Rom (completely resistant to Rom), while growth of RomR Δ*farE* was inhibited for about 15 h and resumed thereafter (see Fig. S1 in the supplemental material). We assume that during the 12-h lag phase, HG001 accumulated sufficient PGs to neutralize Rom, allowing it to grow.

Furthermore, we investigated the effect of Rom on the killing of HG001 and RomR and their respective Δ*farE* mutants. The killing of the *S. aureus* clones in BM supplemented with Rom (8 μg/mL) was followed for 8 h. HG001 and HG001 Δ*farE* were almost completely killed after 7 to 8 h, while the growth of the RomR mutant continued. With RomR Δ*farE*, mutant killing was also observed, but it was markedly delayed compared to the case with HG001 and HG001 Δ*farE* (Fig. S2). Together, these results show that deletion of *farE* in both HG001 and RomR rendered the strains hypersensitive to Rom, indicating that FarE is crucial for Rom resistance. We also observed that in

TABLE 1 MICs of Rom

Strain	MIC (μg/mL)
HG001	1.0
RomR	>128.0
HG001 Δ*farE*	0.5
RomR Δ*farE*	0.5

RomR Δ*farE*, the killing rate was lower and the strain even started to regrow after 7 h, suggesting that FarR* regulates some other genes apart from *farE* that contribute to the revival of the mutant.

Concentrated supernatant of HG001 and RomR can neutralize Rom's antimicrobial activity. One of our main questions was whether Rom resistance was due to Rom being expelled from the cell by the efflux pump FarE or whether the excreted PGs and fatty acids neutralized Rom. While two-times-concentrated supernatant of RomR strains grown to the end of the exponential phase was already able to protect HG001 from Rom, the supernatant of HG001 needed to be concentrated 20 times to achieve similar protection (Fig. 1B). This suggests that the substances leading to Rom resistance are the same in the parental strain and the RomR mutant but that their concentrations are different. Since we have previously shown that certain fatty acids can partially abolish the antibiotic activity of Rom (12), we assumed that FarE secreted FAs and lipids to neutralize Rom's activity. To verify this hypothesis, we carried out qualitative and quantitative lipid and FA analyses of the supernatant of parent strain HG001 as well as RomR and Δ*farE* mutants.

Determination of excreted lipids/FAs in the supernatant and pellet wash of HG001 and its mutants. For lipidomic analysis of secreted as well as cell-bound lipids/FAs, we used a chemically defined minimal medium (38) which is free of fatty acids and lipids. When grown in BM, HG001, RomR, HG001 Δ*farE*, and RomR Δ*farE* showed no discernible differences. However, their growth in the defined minimal medium was generally decreased and growth of the two Δ*farE* mutants was somewhat delayed (Fig. S3). The cultures were harvested when they reached the end of the exponential growth phase (optical density at 578 nm [OD_{578}] = 0.9 to 1.0). For the calculation of the sample concentration and the structure, internal standards (ISs) as well as the TripleTOF system and liquid chromatography-electrospray ionization-tandem mass spectrometry (LC-ESI-MS/MS) were used. We analyzed not only the lipid/FAs in the culture supernatant but also those that were loosely bound to the cell wall, referred to as "pellet wash," by detaching them from the cell wall with 90% isopropanol treatment. Absolute amounts of FAs/lipids were calculated in nanograms/OD_{578} and adjusted to the corresponding OD_{578} of 1.0. As described earlier, *S. aureus* synthesizes mainly saturated FAs (16), and in this study, too, we detected only saturated FAs in free or lipid-bound form, suggesting that unsaturated FAs were not synthesized.

Free FAs. Exolipidomic analyses of the supernatant and pellet wash showed that there were no large differences in the majority of even-numbered FAs (C16:0 and C18:0) between HG001 and the mutants. However, the RomR mutant excreted about 2-fold more odd-numbered FAs (C15:0, C17:0, C19:0, and C21:0) than HG001 and the two Δ*farE* mutants (Fig. 2A). If we add up all the FAs in the supernatant and pellet wash, the following values were achieved: 22 ng/OD for RomR, 8 ng/OD for HG001, 9 ng/OD for RomR Δ*farE*, and 15 ng/OD for HG001 Δ*farE*. The distributions of FAs in supernatant and pellet wash were roughly comparable, with only approximately 4 times more C15:0 in the pellet wash than in the supernatant. Since there was only a 4-fold difference in secreted FAs between the parental strain and the RomR mutant, we hypothesized that secreted lipids might be responsible for the Rom resistance in RomR.

PG. Phosphatidylglycerol (PG) was the most excreted lipid in terms of quantity, and it is in the levels of PG that we observed the greatest difference between RomR and HG001 and the Δ*farE* mutants. On average, the RomR strain released about 8 to 10 times more lipids than HG001 and the Δ*farE* mutants. The most abundant lipids ranged from C29:0 to C34:0, with a peak from C30:0 to C32:0 (Fig. 2B). If we add up all the lipid structures in the supernatant and pellet wash, we come to about 2,244 ng/OD for RomR, 268 ng/OD for HG001, 332 ng/OD for RomR Δ*farE*, and 448 ng/OD for HG001 Δ*farE*.

Lys-PG. With respect to the distribution of the chain length of the esterified FAs, we observed a pattern similar to that of PG except for the amount of released lysyl phosphatidylglycerol (Lys-PG), which was about 30-fold lower than for PG (Fig. 2C). If we add up all the Lys-PG structures in the supernatant and pellet wash, we come to about 59 ng/OD for RomR, 8 ng/OD for HG001, 9 ng/OD for RomR Δ*farE*, and 16 ng/OD

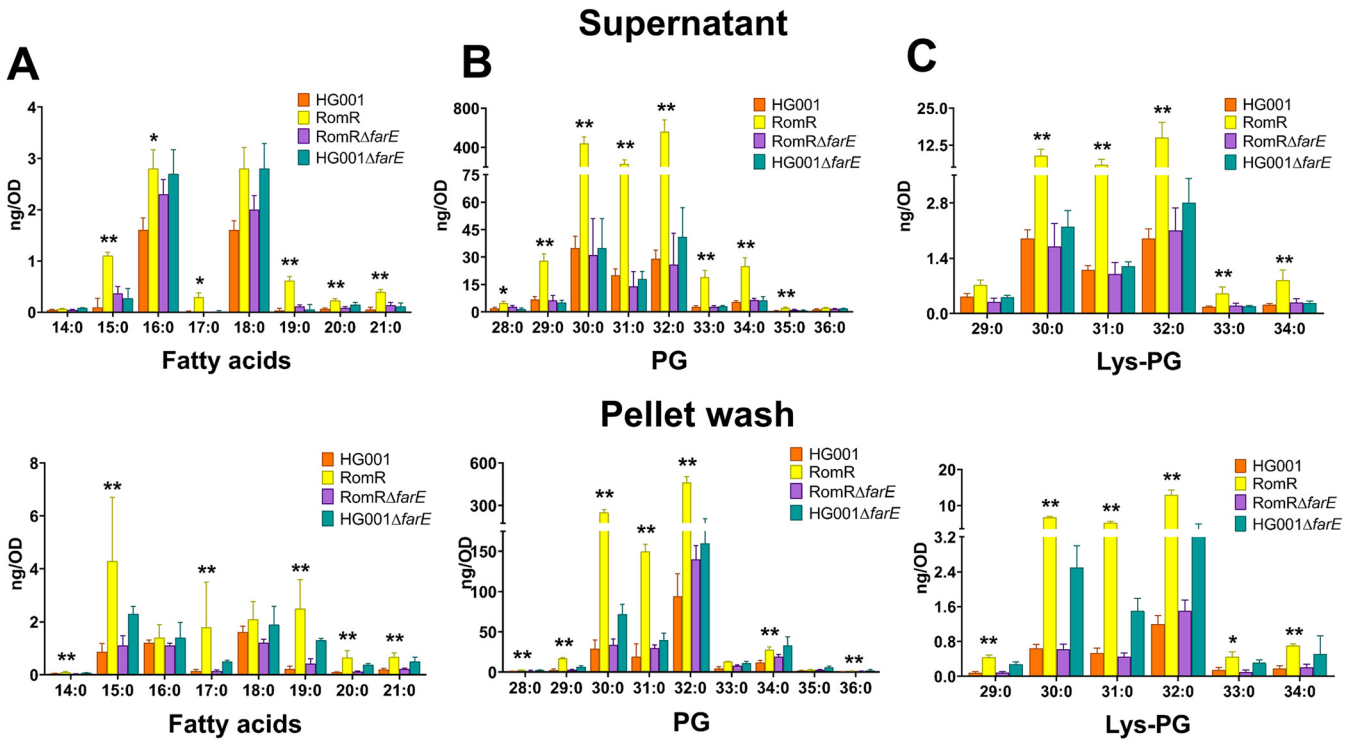

FIG 2 Lipidomic analysis in supernatants (upper row) and pellet wash (lower row) of HG001, RomR, HG001 Δ*farE*, and RomR Δ*farE*. The bar charts show the amounts of FAs ranging from C14:0 to C21:0 (A), phosphatidylglycerols (PGs) ranging from C28:0 to C36:0 (B), and lysyl phosphatidylglycerol (Lys-PG) (C) ranging from C29:0 to C34:0. Absolute amounts of FAs and lipids were calculated in nanograms per OD_{578} of the bacterial cultures grown until the end of the exponential phase and adjusted to the corresponding OD_{578} of 1.0. The supernatant and pellet were separated by centrifugation for lipidomic analyses. The pellet wash was obtained by treating the pellets with 90% isopropanol to remove the fatty acids and lipids from the surface of cells. Each bar represents the mean ± SD from five independent biological replicates. *P* values were obtained using the Mann-Whitney U test for the comparison between HG001 and RomR, with *P* values of <0.05 and <0.01 shown with "*" and "**," respectively.

for HG001 Δ*farE*. It is reasonable that only a small amount (about 3%) of the PG is lysylated, since expression of MprF (multiple peptide resistance factor) is inducible (17) and cells were not grown under conditions that are optimal for MprF expression or harvested at an optimal time point for MprF expression.

DG and MGDG. Only trace amounts of diacylglycerol (DG) and monogalactosyldiacylglycerol (MGDG) were released by all strains, and there was no remarkable difference between RomR and HG001 or the Δ*farE* mutants (Fig. 3). The total amount of DG in the supernatant per strain was on the order of about 1 ng/OD, and that in the pellet wash was about 5 ng/OD (Fig. 3A); the total amounts of MGDG were on the same order, i.e.,1 to 2 ng/OD in the supernatant and about 5 to 8 ng/OD in the pellet wash (Fig. 3B). These results indicate that FarE does not really contribute to the release of DG or MGDG.

DGDG. Digalactosyldiacylglycerol (DGDG) was found in substantial levels in the supernatant, amounting to about 110 ng/OD for each strain, and there were no significant differences among the four strains, except for HG001 and RomR (Fig. 3C). Only in the pellet fraction did we see an approximately 4-fold-larger amount of DGDG in RomR than in the other strains.

Summarizing the lipidomic results, we can say that the RomR strain excreted multiple amounts of PG and Lys-PG, compared to the other strains (Table 2). By far the most abundant lipid structure released was PG, followed by Lys-PG and FAs. DG and MDG were released in only tiny amounts, and we found no indication for a higher release in the RomR strain. DGDG was released in larger amounts than DG and MDG, but only in the pellet wash did we observe a 2-times-higher content in the RomR strain than in the others. The overexpression of FarE in the RomR mutant (12) led the mutant to become a hyperreleaser of PG. Deletion of the *farE* gene in the RomR mutant reversed the

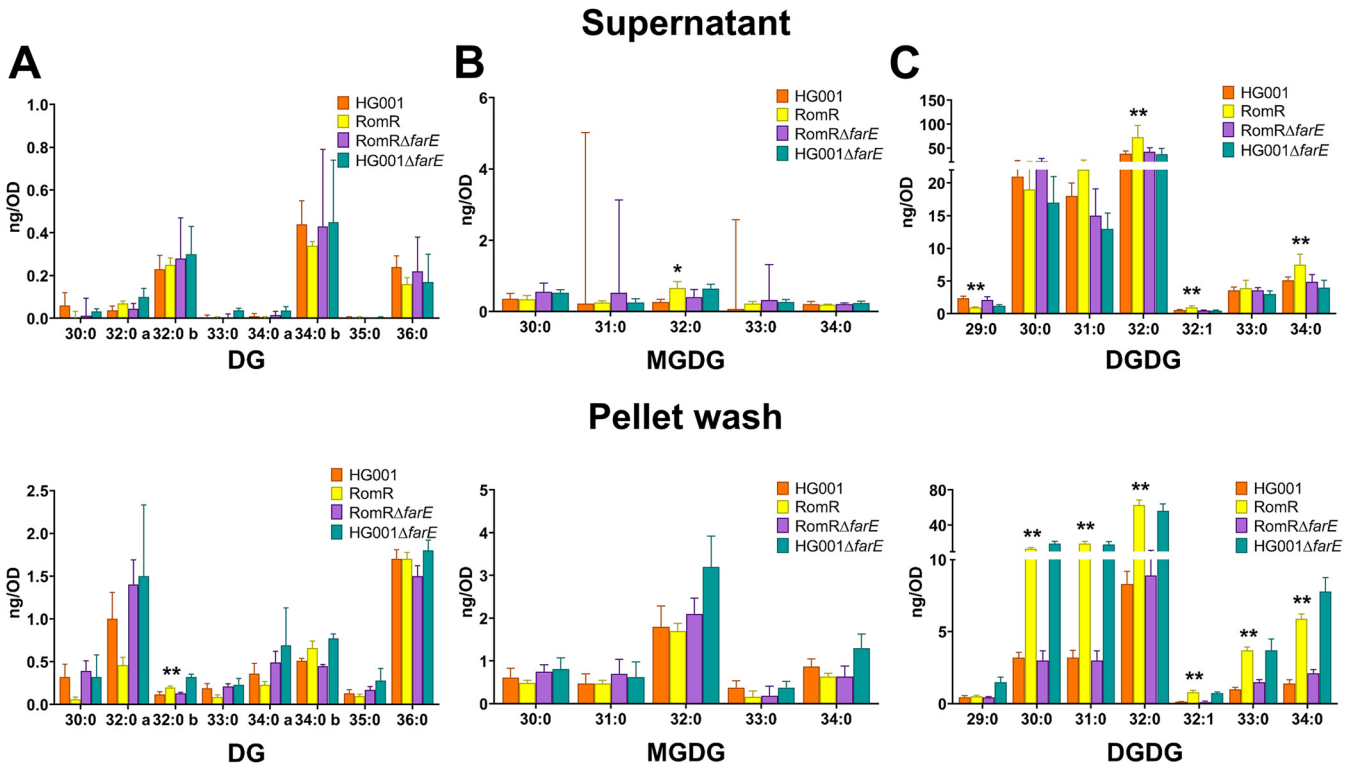

FIG 3 Lipidomic analysis of diacylglycerol (DG), monogalactosyldiacylglycerol (MGDG), and digalactosyldiacylglycerol (DGDG) in supernatants (upper row) and pellet wash (lower row). The bar charts show the amounts of DGs ranging from 30:0 to 36:0 (A), MGDGs ranging from 30:0 to 34:0 (B), and DGDGs ranging from 29:0 to 34:0 (C). *P* values were obtained using the Mann-Whitney U test for the comparison between HG001 and RomR, with *P* values of <0.05 and <0.01 shown with "*" and "**," respectively.

phenotype. This appears to represent direct evidence that overexpression of FarE is responsible for release of PGs.

Rom does not induce the release of fatty acids or PG. To investigate the effects of Rom treatment on the release of lipids by the parent strain HG001 and the mutant strain RomR (Fig. S4), Rom was added at a sublethal concentration (0.3 μg/mL) at early growth phase, and samples were harvested and processed as described above for untreated cultures. The lipidomic analysis showed essentially the same pattern as for the untreated samples. There was no significant difference in the release of FAs, PG, and Lys-PG in the presence of Rom (Fig. S4), indicating that Rom does not induce the release of these compounds in *S. aureus*.

Certain FAs and PGs can neutralize the activity of Rom. Next, we investigated which of the lipid components exported by FarE can most effectively neutralize the antimicrobial activity of Rom. For this, we supplied the medium (BM) with Rom (8 μg/mL $\approx$ 18 μM) and different lipid components in approximately the same molarity. Rom alone completely inhibited growth (Fig. 4). Among the FAs tested, C15:0 was the most efficient in rescuing growth in the presence of Rom; however, the onset of growth was

TABLE 2 Contents of FAs, lipids, PGs, sugar lipids in supernatant of *Staphylococcus aureus*

		Total amt (ng/OD)	
Compound(s)	Most abundant FAs (from high to low)	HG001	RomR
FAs	C18:0, C16:0, C15:0, C19, C21:0, C20:0, C17:0, C14:0	8	22
PG	C32:0, C30:0, C31:0, C34:0, C29:0, C33:0, C28:0, C35:0, C36:0	268	2,244
Lys-PG	C32:0, C30:0, C31:0, C29:0, C34:0, C33:0	8	59
DG	C36:0, C32:0a, C34:0b	5	4
MGDG	C32:0, C34:0, C30:0, C31:0, C33:0	5	5
DGDG	C32:0, C30:0, C31:0, C34:0, C33:0, C29:0, C32:1, C33:1	107	233

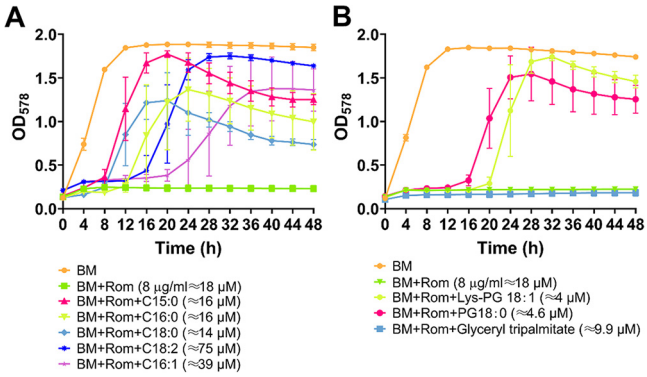

FIG 4 Impact of exogenous supplementation of fatty acids and phospholipids on the activity of Rom. *S. aureus* HG001 was grown in BM with Rom (8 μg/mL) and various supplementations. For panel A, supplementations included the following FAs: 4 μg/mL of C15:0 (≈16 μM), 4 μg/mL of C18:0 (≈14 μM), 4 μg/mL of C16:0 (≈16 μM), 10 μg/mL of C16:1 (≈39 μM), and 21 μg/mL of C18:2 (≈75 μM). For panel B, supplementations included 8 μg/mL of the lipid glyceryl tripalmitate (≈9.9 μM) and phospholipids as follows: 4 μg/mL of PG 18:0 (≈4.6 μM) and 4 μg/mL of Lys-PG 18:1 (≈4 μM). Wells containing tryptic soy broth (TSB) only and bacteria with Rom (8 μg/mL) alone were included as negative and positive controls, respectively. Growth of the bacteria was measured at OD_{578} every 4 h for 48 h using a Varioskan Lux microplate reader (Thermo Scientific) in a 48-well plate. Each point in the graph is the mean ± SD from three independent biological replicates.

delayed by 8 h. Unsaturated FAs like C18:2 and C16:1 had a much smaller effect than C15:0 (Fig. 4A). The P-lipids PG(18:0) [where PG(18:0) is PG with C18:0 lipids] and Lys-PG(18:1) also could abrogate Rom's antimicrobial activity but only after a lag phase of 16 to 20 h (Fig. 4B). Interestingly, triacylglyceride showed no effect. As a control, we also tested whether exogenous supplementation of FAs/lipids/PGs had an effect on growth of HG001. However, neither the tested FAs nor Lys-PG or PG affected growth (Fig. S5A and B).

MprF has no effect on Rom resistance. MprF encodes a bifunctional membrane protein that synthesizes the positively charged lipid Lys-PG and subsequently translocates it from the inner to the outer membrane leaflet (18). Therefore, MprF serves as bacterial resistance factor protecting MRSA from cationic antimicrobial peptides (CAMPs) and the lipopeptide antibiotic daptomycin (18). To investigate whether the biosynthesis of Lys-PG plays a role in Rom resistance, we deleted *mprF* in the RomR strain, generating the strain RomR Δ*mprF* (Fig. S5C). However, when we treated the RomR strain and its Δ*mprF* mutant with Rom, we observed no difference in the MIC values of the two strains (both still >128 μg/mL), suggesting that *mprF* does not play a role in Rom resistance.

In summary, our results show that essentially only the compounds most abundantly released by the RomR strain (PGs) can neutralize the activity of Rom. To demonstrate the postulated interaction of Rom with PGs, we used two methods: static and dynamic light scattering (SLS/DLS) and isothermal titration calorimetry (ITC).

SLS/DLS indicate that Rom interacts with phospholipid PG(32:0). DLS is a frequently used technique for measuring the size distribution of dispersed particles in the range of 1 to 3,000 nm. For studies of interaction of Rom with P-lipids, we have chosen PG(32:0), 1,2-dipalmitoyl-*sn*-glycero-3-phospho-(1′-rac-glycerol) (sodium salt), as a model PG that is also produced by *S. aureus*. Both Rom and PG(32:0) are almost insoluble in water. Therefore, we needed to find a common solvent for both compounds. We overcame the problem by dissolving PG(32:0) first in a chloroform/methanol/water mixture, and then we prepared vesicles formed in 10% dimethyl sulfoxide (DMSO)/phosphate-buffered saline (PBS) (pH 7.2), which is the same solvent as used for Rom.

DLS analysis with 1 mM PG(32:0) (diluted from a 5 mM sample solution) showed that the mean size at a 90° angle was 90.8 nm (Fig. 5A). This size did not change much over time, meaning that PG(32:0) was present as a vesicle under these conditions. Next, we analyzed 0.1 mM Rom solution from a freshly prepared sample and after a 1-h interval.

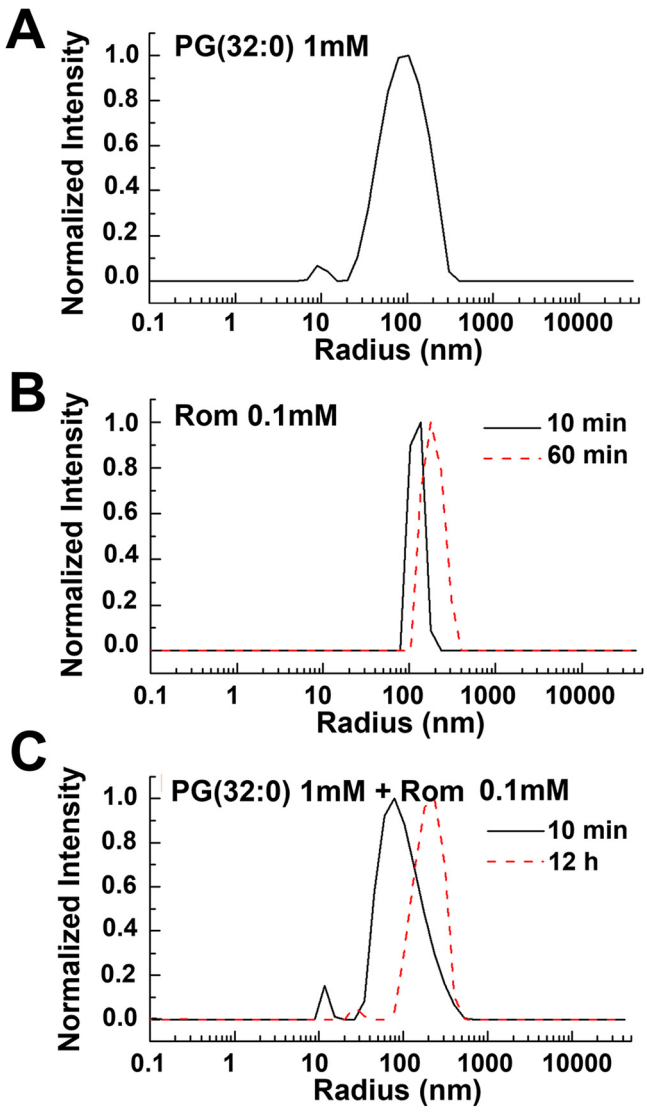

FIG 5 Static and dynamics light scattering (SLS/DLS) of PG(32:0), Rom, and mixed compounds. (A) DLS results for PG(32:0) alone. PG(32:0) at 1 mM was diluted from a 5 mM sample solution. The mean size determined at 90° was 90.8 nm. Further study demonstrated that the size of PG(32:0) vesicles did not change much over time when the concentration was below a certain threshold. (B) DLS results for Rom (0.1 mM) solution. The mean size of nanoclusters was about 120 nm for the freshly prepared sample. The 2nd measurement after 60 min showed an increase in size to 190 nm. For long-time incubation (overnight), visible Rom aggregates appeared. This result suggests that Rom forms nanoclusters after preparation that slowly agglomerate into large aggregates. (C) DLS results for Rom and PG mixture. Rom (0.1 mM) and PG(32:0) (1.0 mM) were mixed in a volume ratio of 1:1. The 1st measurement yielded a mean size of 100 nm, similar to the original size shown in Fig. 1. The 2nd measurement, after overnight incubation, yielded a mean size of about 200 nm, nearly double the size. This result demonstrates that Rom indeed interacts with PG vesicles, leading to an increase of vesicle size.

Rom formed nanoclusters with a mean size of 120 nm for the freshly prepared sample. The 2nd measurement after 60 min showed an increase of size to 190 nm (Fig. 5B). After a long incubation (overnight), visible Rom aggregates appeared. These results suggest that Rom forms nanoclusters after preparation and then slowly agglomerates into large aggregates. Finally, we analyzed a mixture of Rom (0.1 mM) and PG(32:0) (1.0 mM) with a volume ratio of 1:1. After 10 min of treatment, the mixture sample was filtered with a 1.6-μm filter. The 1st measurement yielded a mean size of 100 nm (Fig. 5C). The 2nd measurement after an overnight incubation yielded a mean size of about 200 nm, which is double the size. This result is a first hint that Rom indeed interacts with PG(32:0) vesicles, leading to an increase of vesicle size.

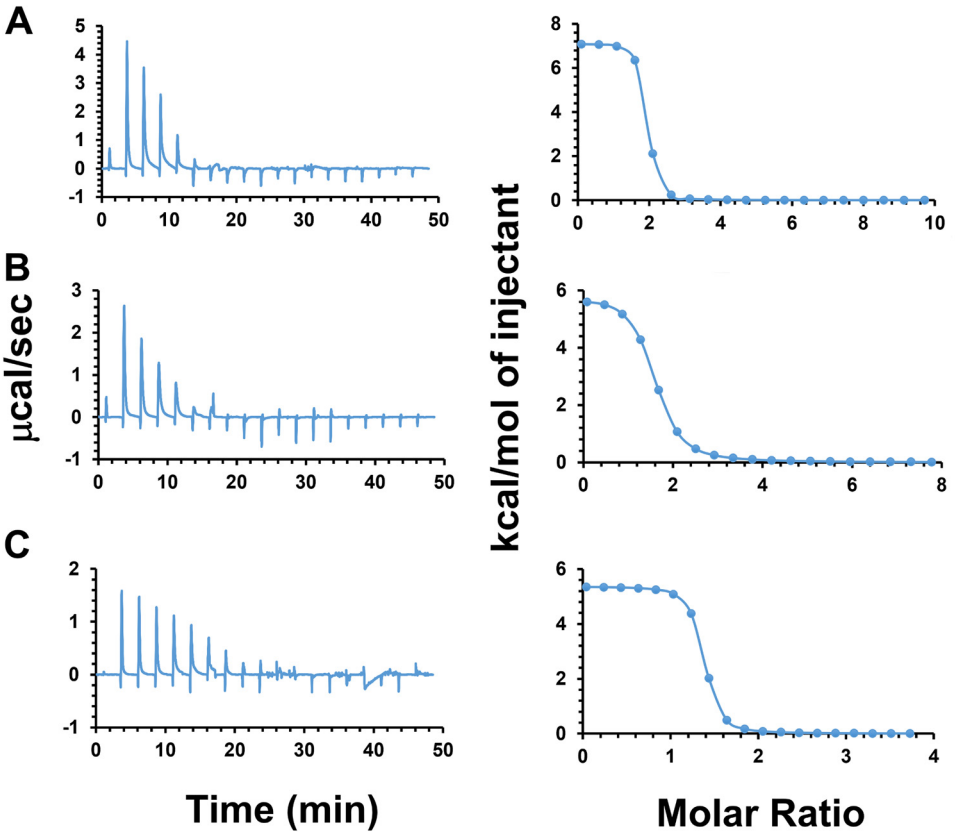

FIG 6 Isothermal titration calorimetry (ITC) of Rom with titrated PG(32:0). Panels A, B, and C present results from three independent experiments with slight changes of injection volume and PG(32:0) concentration. The left side shows the heat change with time. (A) Injection of 2-μL aliquots of 5 mM PG(32:0) into 100 μM Rom. (B) Injection of 2-μL aliquots of 4 mM PG(32:0) into 100 μM Rom. (C) Injection of 1-μL aliquots of 4 mM PG (32:0) into 100 μM Rom. The right side shows the enthalpy change of the binding for each condition. The free energy and entropy were calculated with software provided by Malvern.

Confirmation of the interaction of Rom with PG(32:0) by ITC. To gain further evidence for neutralization of Rom's activity by the released PGs into the medium, we determined the enthalpy change (ΔH), equilibrium binding constant (K_D), and stoichiometry of the reaction (n) involved in the interaction between Rom and PG(32:0) using ITC. The binding of Rom and PG(32:0) was determined titrating PG(32:0) into Rom solution at pH 7.2 in 10% DMSO/PBS buffer at 37°C. Three experiments were conducted with different conditions, all of which resulted in similar heat flows (Fig. 6): (i) injection of 2-μL aliquots of 5 mM PG(32:0) into 100 μM Rom (Fig. 6A), (ii) injection of 2-μL aliquots of 4 mM PG(32:0) into 100 μM Rom (Fig. 6B), and (iii) injection of 1-μL aliquots of 4 mM PG(32:0) into 100 μM Rom (Fig. 6C). The interaction was found to be endothermic, as the titration peaks showed the upward position and the corresponding integrated heat was positive ($\Delta H > 0$). The contribution of the entropy change (ΔS) to the binding was favorable and large ($-T\Delta S < 0$, where T is absolute temperature). In other words, binding is entropically driven and hence hydrophobic and of low specificity in nature. The n and K_D were 1.49 ($\pm$0.0478) and 2.30 ($\pm$0.747) μM, respectively. The interaction of Rom with PG(32:0) was fast and occurred within milliseconds. The data are summarized in Table 3.

RomR shows no cross-resistance to various tested classical antibiotics. Another interesting question was whether the massive excretion of lipids/fatty acids in RomR also causes cross-resistance to other antibiotics. For this reason, we compared the MICs for HG001 and its RomR mutant with those of 21 other antibiotics. As shown in Table 4, we observed no cross-resistance with any of the tested antibiotics. Therefore,

TABLE 3 Thermodynamic parameters obtained by ITC for Rom binding to PG(32:0) vesicles[a]

	System							
Expt	Syringe	Cell	Injection vol	*n*, sites	K_D (mM)	ΔH (kcal/mol)	ΔG (kcal/mol)	$(-T)\Delta S$ (kcal/mol)
1	PG, 5 mM	Rom, 100 μM	2 μL	1.72 ($\pm$0.048)	0.743 ($\pm$0.656)	7.09	−8.7	−15.8
2	PG, 4 mM	Rom, 100 μM	2 μL	1.45 ($\pm$0.0094)	5.61 ($\pm$0.525)	5.83	−7.45	−13.3
3	PG, 4 mM	Rom, 100 μM	1 μL	1.29 ($\pm$0.086)	0.542 ($\pm$1.06)	5.37	−8.89	−14.3
Avg				1.49 ($\pm$0.047)	2.30 ($\pm$0.747)	6.10	−8.35	−14.47

[a]*n*, binding stoichiometry of the interaction of the two molecules; K_D, dissociation constant; ΔH, enthalpy changes; ΔG, Gibbs free energy changes; ΔS, entropy changes.

Rom appears to have a unique ability to interact with PGs, resulting in the abrogation of its antimicrobial activity.

DISCUSSION

The main goal of this work was to further decipher the mechanism of high Rom resistance in the RomR mutant. Originally, we thought that the point mutation in *farR* causing the amino acid change Cys116Arg would inactivate FarR* (12). But here we show that this is apparently not the case. FarR* still acts as a regulator, however, with altered activity. Transcriptome sequencing (RNA-seq) analysis showed that *farE* and the *farR** gene are upregulated in RomR, thus resulting in a positive-feedback loop in which FarR* increases its own and FarE expression (12). In a closed system like a cell, such a hypercycle cannot continue endlessly. Therefore, the question arises as to the possible limiting factors. We assume that FarE, as a transmembrane protein, cannot be highly expressed without causing membrane jamming and cell damage. Therefore, we assume that FarE expression is tightly controlled to counteract the threat of cell damage by unlimited FarE expression. However, FarE appears to be advantageous for growth under certain conditions since in defined minimal medium, growth of the HG001 Δ*farE* and RomR Δ*farE* mutants was somewhat delayed (Fig. S5). Furthermore, FarR* upregulates not only *farE* and *farR** but also several *agr*-controlled genes, which in addition could contribute to some of the effects observed.

There are two pieces of evidence that overexpression of FarE is responsible for the resistance to Rom: (i) upregulation of FarE and Rom resistance is correlated, and (ii) de-

TABLE 4 MICs of various antibiotics for *S. aureus* HG001 and its RomR mutant

	MIC (μg/mL)	
Antibacterial agent	HG001	RomR
Rhodomyrtone	1	>128
Bacitracin	32	32
Benzalkonium chloride	2	2
Chloramphenicol	32	32
Daptomycin	1	1
Ethambutol	>32	>32
Gallidermin	2	2
Gentamicin	2	2
Gramicidin S	4	4
Hygromycin B	32	32
Kanamycin	8	8
Methicillin	4	4
Neomycin	0.5	0.5
Norfloxacin	1	1
Oxacillin	0.25	0.25
Penicillin G	0.03125	0.03125
Polymyxin B	256	256
Spectinomycin	>32	>32
Streptomycin	16	16
Sulfamethoxazole	32	32
Tunicamycin	>32	>32
Vancomycin	1	1

letion of *farE* resensitizes the RomR mutant to Rom (Table 1). However, what we did not fully understand was the underlying mechanism: does FarE act as an efflux pump for Rom as described for the antimicrobial FAs (14), or is FarE rather an efflux pump of PGs in such large amounts that they can cause neutralization the antimicrobial activity of Rom?

To answer this question, we carried out comparative exolipidome analyses in *S. aureus* strains HG001, RomR, HG001Δ*farE*, and RomR Δ*farE* by analyzing the FAs, lipids, PG, Lys-PG, DG, MGDG, and DGDG both analytically and quantitatively. Since we know that *S. aureus* is able to take up and incorporate unsaturated FAs present, for example, on human skin (C16:1, C18:1, or C18:2) into PGs and the lipid moiety of lipoproteins (16), we cultivated the cells in defined minimal medium to exclude medium-derived FAs/lipids and their potential incorporation. We observed an enormous difference particularly in the release of PG and Lys-PG between RomR and its Δ*farE* mutant or HG001 (Fig. 2 and Table 2), with 10 times more excretion in the RomR strain than in the others. Therefore, we assume that FarE is primarily an efflux pump for PGs. We also observed an approximately 3- to 4-fold increase of FAs in RomR; however, the total amount of released FAs was >100 times lower than that of PGs. Our data suggest that FarE functions primarily as an exporter (efflux pump) of PGs.

There are other examples in the literature describing efflux pumps that excrete larger compounds. In *Pseudomonas fluorescens*, EmhABC excretes hydrophobic antibiotics, dyes, and polycyclic aromatic hydrocarbons, including phenanthrene (19). Two possible functions were discussed: that the efflux of FAs is a result of membrane damage or that the primary physiological role of the EmhABC efflux pump is the PG turnover. For *Acinetobacter baumannii*, a novel membrane protection system has been described, the AdeIJK efflux system, which modulates the lipid content of the membrane via direct efflux of lipids, probably contributing to membrane maintenance (20). The papers allude to the possibility that the efflux pumps might have PG as a substrate but did not explicitly state so.

While DG and MGDG were also present in the exolipidome, no difference was observed between RomR and RomR Δ*farE* or HG001. Similarly, only slightly larger amounts of DGDG were observed in the supernatant of RomR (Table 2). In *S. aureus*, DGDG serves as a membrane anchor molecule for lipoteichoic acid (LTA) (21, 22). The membranes of *S. aureus* contain 8 mol% of the free glycolipid, and the ratio of MGDG to DGDG may play an important role in determining bilayer stability, with only the latter forming a bilayer (23).

We could only detect saturated FAs in the exolipidome analysis, which is consistent with the absence of a fatty acid desaturase (24, 25). We could not discriminate between straight-chain saturated fatty acids (SCSFAs) and branched-chain fatty acids (BCFAs), with the latter playing a critical role in maintaining membrane fluidity (24, 26). Although *S. aureus* encodes cardiolipin synthases 1 and 2, we did not detect cardiolipin, most likely because we harvested the supernatant at the end of the exponential growth phase and it has been reported that cardiolipin is produced mainly in the stationary phase (27).

Although we had ample evidence that Rom can be neutralized by PGs, we attempted to show a direct interaction. This experiment was complicated by the fact that both compounds were insoluble in water. As a model PG, we chose PG(32:0). Using the methods described, it was finally possible to dissolve both compounds in 10% DMSO/PBS (pH 7.2). Using SLS/DLS analysis, we could demonstrate that in freshly prepared solutions, both components formed vesicles with mean sizes at a 90° angle of 90.8 nm for PG(32:0) and of 120 nm for Rom. When the two components were mixed, the mean size of 100 nm at the beginning increased with time to 200 nm (Fig. 5C), which is a first hint that Rom and PG(32:0) vesicles interact with each other. So far it is unknown in what form the secreted PG(32:0) is present in the culture supernatant. However, since the environment is predominantly aqueous, PG(32:0) should also form vesicles with time. The vesicle formation is most likely concentration

dependent, similar to the case with the critical micelle concentration (CMC) for surfactants, detergents, and PGs. For example, the CMC for various PGs was in the range of 0.6 to 3.7 μM (28). With a concentration of 1.0 mM PG(32:0), this is well above the CMC. In the supernatant of the RomR mutant, we obtained 100 to 200 μM for each of PG(30:0), PG(31:0), and PG(32:0), excluding the less abundant PG(29:0), PG(33:0), and PG(34:0). All PGs together in the culture supernatant of the cells at the end of the exponential growth phase amounted to about 600 μM (Fig. S6). This means that with a concentration of 1 mM PG(32:0), our results were well within a realistic range.

In order to directly analyze the interaction of Rom with PG(32:0), we used isothermal titration calorimetry (ITC). ITC can measure the association constant (K_a), reaction stoichiometry (n), the heat capacity (ΔCp) of the reaction, binding free energy (ΔG), entropy (ΔS), and enthalpy (ΔH). We obtained similar heat fluxes in all three experiments, each with slightly different conditions (Fig. 6). The results indicate that there is a rapid (millisecond) interaction of Rom with PG(32:0) which is entropically driven and hence hydrophobic and of low specificity in nature. The ratio of Rom binding to PG(32:0) was 1:1.49.

Another question is how to explain the high Rom resistance (MIC $>$ 128 μg/mL) in the RomR mutant (Table 1). In the MIC analysis, a high concentration of Rom was added right at the beginning of the diluted cell culture; thus, there was insufficient time for the excretion of PG in the supernatant to reach a concentration high enough to neutralize Rom. Nevertheless, there was hardly a lag phase when Rom was added to the RomR mutant (Fig. S1). This indicates that the Rom resistance acted in the RomR mutant from the beginning. There are two possible explanations for this observation: (i) FarE acts as an efflux pump not only for PG but also for Rom, and (ii) in the RomR mutant, a high concentration of PG is already stored near the membrane and also in the cell wall, providing high resistance from the beginning, and therefore, we see almost no lag phase in the RomR mutant. In fact, the concentration of PG in the pellet wash was almost as high as in the supernatant (Fig. 2), indicating that a high proportion of PG is accumulated in the cell envelope. Therefore, we hypothesize that the second is the most plausible explanation, since it is unlikely that FarE also serves as an efflux pump for Rom; the structures of PG and Rom are too different.

We tested several clinically applied antibiotics and could not detect any cross-resistance (Table 3). There are only a few antimicrobial compounds reported that interact with PGs. One is the positively charged antibiotic gentamicin, which interacts with cell membranes, especially PGs (29–31). This interaction induced membrane permeabilization and depolarization, the same activity as we also observed with Rom (10). The other antibiotic is daptomycin, which is inactivated by the released membrane PGs (32). It was a bit surprising that the MIC and the minimum bactericidal concentration (MBC) were not increased in the RomR mutant, which accumulated a high concentration of PGs ($\approx$600 μM) in the culture supernatant (Fig. S6). The new insight that Rom binds to P-lipids leads us to assume that the cytoplasmic membrane is the actual target of Rom. This is in agreement with our previous findings that Rom causes a collapse of the membrane potential within seconds and induces local membrane damage. Therefore, the actual mechanism of resistance in the RomR mutant is overproduction of the target molecule. Resistance mechanisms based on overexpression of the target molecule are rare but have been described for some antibiotics. For example, one of the several mechanisms of trimethoprim resistance is based on overexpression of the target enzyme dihydrofolate reductase (33). The second main cause of resistance to isoniazid (INH) is the overexpression of enoyl-acyl-carrier protein reductase InhA (34, 35). Overexpression of the D-alanine racemase gene confers resistance to D-cycloserine in *Mycobacterium smegmatis* (36).

So far, plants are not known to produce small antimicrobial compounds that bind PGs. To the best of our knowledge, Rom is a novelty. From the immunology point of view, antibodies that are directed against PGs and PG-binding proteins play a role in certain human diseases. Too much of anti-PG antibodies, such as in lupus anticoagulant, anti-cardiolipin antibodies, and anti-β2-glycoprotein 1 antibodies, can cause the

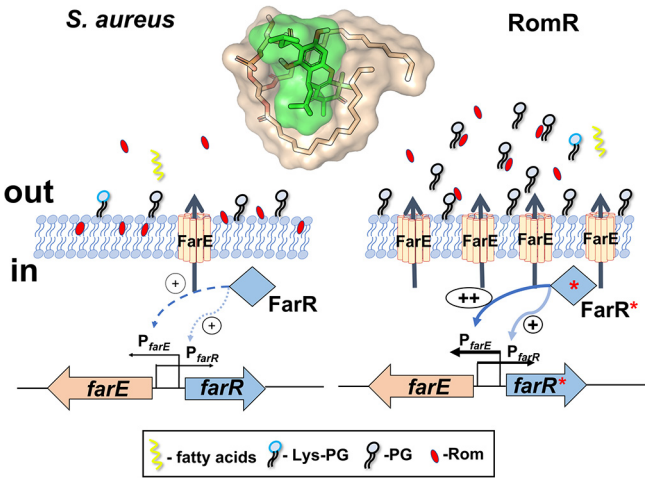

FIG 7 Mechanism of Rom resistance (graphical abstract). The regulation of *farE* and *farR* as well as the secretion of PGs in the parental strain *S. aureus* HG001 in comparison with its RomR mutant is illustrated. In HG001, FarR mildly activates *farE* and *farR* expression. The membrane-localized FarE secretes small amounts of PGs, which are too small to cause resistance to Rom. In the RomR mutant, FarR* becomes a potent activator of *farE* and *farR*. The resulting overexpression of FarE, acting as a PG efflux pump, leads to increased accumulation of PGs in the supernatant and cell envelope. The PG concentration is now high enough to efficiently scavenge Rom, thereby abrogating its antimicrobial activity. Rom binds to PGs at a ratio of 1:1.4. We hypothesize that the resistance results from interaction of Rom with PGs, causing neutralization of Rom's antimicrobial activity. The inserted structure of PG and Rom shows a possible interaction of both compounds.

so-called antiphospholipid syndrome (APS), an autoimmune disease occurring mostly in young women (37). It would be worthwhile to examine the impact of Rom on APS in more detail.

Conclusion. Considering the results of our lipidomic analysis showing that the RomR mutant excretes much larger amounts of PGs than its parent strain and that Rom indeed binds to PG, we provide strong evidence that Rom resistance in the RomR mutant is due to the neutralization of Rom's activity by binding to PGs. Our hypothesis for the *farE-farR* function is the following. In the wild type, *farE* expression is low and FarR acts only as a mild activator. In the RomR mutant, the point mutation in *farR** causes FarR* to become a strong activator of *farE* and its own (*farR**) gene expression. Overexpression of FarE, which acts most likely as a PG efflux pump, causes massive accumulation of PG in the supernatant and the cell envelope area. PG scavenges Rom, thereby abrogating its antimicrobial activity (Fig. 7).

MATERIALS AND METHODS

Bacterial strains and growth conditions. Bacterial strains and plasmids used in this study are listed in Table S1. For cloning procedures, *S. aureus* and *Escherichia coli* strains were grown in basic medium (BM) containing 1% (wt/vol) soy peptone, 0.5% yeast extract, 0.5% NaCl, 0.1% K_2HPO_4, and 0.1% glucose at pH 7.2. Bacteria were cultivated aerobically (200 rpm) at 37°C. For lipidomic analysis, we used a defined minimal medium as described by Rudin et al. (38). To investigate whether Rom has an impact on excretion of lipids/fatty acids in *S. aureus*, we supplemented the medium with sublethal concentrations (0.3 μg/mL) of Rom.

Construction of deletion mutants. The deletion mutants were constructed as markerless deletions as previously described (12). Recombinant knockout plasmids were constructed using the temperature-sensitive plasmid pBASE6, which is a derivative of pBT2 (39, 40). Briefly, ~1,000-bp upstream and ~1,000-bp downstream fragments of SAOUHSC_02866 (*farE*) and SAOUHSC_01359 (*mprF*) were amplified from the genomic DNA of *S. aureus* HG001 and RomR strains, respectively. Then, the fragments were assembled with the EcoRI-linearized pBASE6 using Hi-Fi DNA assembly master mix (New England BioLabs). The ligation mixtures were transformed into *E. coli* DC10B chemically competent cells. The correct plasmids were confirmed by PCR and sequencing before being transformed via electroporation into HG001 and RomR, respectively. Mutagenesis was performed as previously described (41, 42). The mutants were named *S. aureus* HG001 Δ*farE*, RomR Δ*farE*, and RomR Δ*mprF*. All oligonucleotides used in this study are listed in Table S2.

Determination of MIC. MIC values of Rom were determined in 96-well microtiter plates using BM as previously described (43). Briefly, 50 μL of Rom was serially diluted from 128 μg/mL to 0.25 μg/mL.

Then, 50 μL of bacterial culture (10^6 CFU/mL) was added to each well. An inoculated broth without Rom was regarded as a positive control, and the well without bacteria was used as a negative control. The 96-well microtiter plates were incubated at 37°C for 24 h. The MIC values were determined as the lowest concentration that completely inhibited the visible growth of bacteria. The experiments were repeated three times.

Growth studies of staphylococcal strains in defined minimal medium. For lipidomic analysis, bacteria were cultivated with shaking at 37°C in defined medium using a 48-well Varioskan Lux microplate reader (Thermo Scientific). Bacteria were precultured in defined medium inoculated into 500 μL of fresh defined medium at a starting OD_{578} of 0.1, and growth of HG001, HG001 Δ*farE*, RomR, and RomR Δ*farE* was monitored for 48 h (Fig. S3).

Impact of supernatants of HG001 and RomR on Rom activity. HG001 was inoculated into BM and incubated at 37°C with shaking overnight, and the impact of Rom (2 μg/mL) and culture supernatant (S) on growth was monitored. Culture supernatants from the HG001 and RomR strains were harvested at the end of the exponential growth phase, sterile filtered (0.2-μm filter), and concentrated 10 times with a speed vacuum concentrator. The supernatant was applied at 1:10 (vol/vol) (Fig. 1B).

Preparation of the samples for lipidomic analysis. The overnight bacterial cultures (HG001, HG001 Δ*farE*, RomR, and RomR Δ*farE*) were used to inoculate 15 mL of defined minimal medium in 100-mL flasks (OD_{578} = 0.1) and incubated at 37°C with shaking until the end of the exponential phase was reached. Cells were then centrifuged at 8,000 rpm and 4°C for 10 min, and both the supernatants and pellets were collected. The supernatants were filter sterilized and lyophilized. All samples were prepared in five biological replicates and used for subsequent preparation for lipidomic analyses. We also investigated whether sublethal concentrations of Rom can induce lipid/FA release. In this case, the cultures were grown in the presence of 0.3 μg/mL of Rom.

Materials used in the isolation and analyses of lipids and fatty acids (internal standard [IS]). SPLASH LIPIDOMIX mass spectrometry standard, 18:2 cardiolipin-d5 (18:2 CL-d5), 18:0 phosphatidylglycerol-d70 (18:0 PG-d70), and 18:1 lysyl-phosphatidylglycerol (18:1 Lys-PG) were purchased from Avanti Polar Lipids (Alabaster, AL). Arachidonic acid-d11 (AA-d11) and C18-ceramide-d7 (d18:1-d7/18:0) were obtained from Cayman Chemicals (Ann Arbor, MI). Isopropanol (IPA), acetonitrile (ACN), and methanol (MeOH) at ultra-LC-MS grade were from Carl Roth (Karlsruhe, Germany). Ammonium formate, formic acid, and IPA at high-performance liquid chromatography (HPLC) grade were purchased from Merck (Darmstadt, Germany). Purified water was produced by Elga Purelab Ultra (Celle, Germany).

Lipid extractions from bacterial samples. Lipid extraction from bacterial supernatant was performed by a biphasic extraction method following the protocol of Matyash et al. (44). First, the IS mixture was prepared by mixing 75 mL of ice-cold MeOH with 250 μL of LipidoMIX solution, 5 μL of AA-d11 stock solution (1 mg/mL), 50 μL of 18:2 CL-d5 stock solution (1 mg/mL), 50 μL of d18:1-d7/18:0 stock solution (0.25 mg/mL), 50 μL of 18:0 PG-d70 (1 mg/mL), and 50 μL of Lys-PG(18:1) (1 mg/mL) stock solutions. The IS mixture was then fully vortexed, and 1.5 mL of ice-cold methanol containing IS was added to a 50-mL Falcon tube with freeze-dried bacterial supernatant for each sample. The samples were vortexed for 10 s. Afterwards, 5 mL of ice-cold methyl tert-butyl ether (MTBE) was added. Samples were incubated on ice for 1 h, followed by addition of 1.25 mL of H_2O to account for a final ratio of MTBE-MeOH-H_2O of 10:3:2.5 (vol/vol/vol) and incubation at room temperature for another 10 min to induce phase separation. The upper layer was transferred to a new Falcon tube, and the water phase was reextracted by adding 2 mL of the upper phase from a solution of MTBE-MeOH-H_2O (10:3:2.5 [vol/vol/vol]). The upper layer from reextraction was then combined with the phase from first extraction and dried with a Genevac EZ-2 evaporator (SP, Ipswich, UK) with nitrogen protection. Extraction residues after evaporation were reconstituted in 100 μL of MeOH, and after vortexing (10 s), sonication (2 min), and centrifugation (3,500 $\times$ *g*, 10 min), the methanol solutions were transferred to autosampler vials.

For the preparation of bacterial pellet wash, lipid extraction was performed using a monophasic extraction method following the IPA/H_2O protocol (45). An IS mixture was prepared by mixing 450 mL of ice-cold IPA and 50 mL of H_2O with 500 μL of LipidoMIX solution, 10 μL of AA-d11 stock solution (1 mg/mL), 100 μL of CL-d5(18:2) stock solution (1 mg/mL), 100 μL of d18:1-d7/18:0 stock solution (0.25 mg/mL), 100 μL of 18:0 PG-d70 (1 mg/mL), and 100 μL of Lys-PG(18:1) (1 mg/mL) stock solutions. Dry bacterial pellets were suspended in 5 mL of IPA/H_2O (9:1 [vol/vol]) with IS, vortexed for 10 s, and sonicated for 2 min. Then the samples were incubated on ice for 1 h with 2 min of sonication every 12 min during the incubation, which means a total of 5 cycles of sonication (2 min). The samples were centrifuged (3,500 $\times$ *g*, 10 min), pellets were kept, and supernatant (lipid extract) was transferred to fresh Falcon tubes and dried with the Genevac EZ-2 evaporator (SP, Ipswich, UK) with nitrogen protection. Afterwards, the extracts were reconstituted in 100 μL of MeOH, vortexed (10 s), sonicated (2 min), centrifuged (3,500 $\times$ *g*, 10 min), and transferred to autosampler vials.

Lastly, for the extraction from bacterial pellets, 5 mL of IPA/H_2O (9:1 [vol/vol]) with IS was added to the pellets, which were kept after washing from the previous step. Samples were vortexed and sonicated. After adding beads (1-mm diameter) and enzyme (50 μL of lysostaphin at 0.3 mg/mL) to each sample, the pellets were disrupted in a Fastprep-24 (MP Biomedicals) (3 cycles of 30 s each at a speed 6.5 m/s). Samples were then centrifuged (3,500 $\times$ *g*, 10 min), and supernatant was collected for further drying with a Genevac EZ-2 evaporator (Ipswich, UK) with nitrogen protection. The dried extracts were then reconstituted, vortexed, sonicated, and transferred into vials as described above. A pooled quality control (QC) sample was prepared by mixing 15-μL aliquots of each reconstituted sample from three extraction process.

UHPLC-ESI-QTOF-MS/MS method. The analysis of samples was performed with an Agilent 1290 Infinity ultrahigh-performance liquid chromatography (UHPLC) system (Agilent, Waldbronn, Germany)

equipped with a binary pump and a PAL-HTX xt DLW autosampler (CTC Analytics AG, Switzerland) and coupled to a SCIEX TripleTOF 5600+ quadrupole time of flight (QTOF) mass spectrometer with a DuoSpray source (SCIEX, Ontario, Canada). The chromatographic separation was performed on an Acquity UPLC CSH C_{18} column (100 mm by 2.1 mm; 1.7-μm particles; Waters Corporation, Milford, MA) with precolumn (5 mm by 2.1 mm; 1.7-μm particles). The column temperature was 65°C, with a flow rate 0.6 mL/min. Mobile phase A was composed of H_2O/ACN (2:3 [vol/vol]) containing 10 mM ammonium formate and 0.1% (vol/vol) formic acid, while mobile phase B was IPA/ACN/H_2O (90:9:1 [vol/vol/vol]) containing 10 mM ammonium formate and 0.1% (vol/vol) formic acid. A gradient elution started from 15% mobile phase B to 30% mobile phase B in 2 min, followed by an increase of mobile phase B to 48% in 0.5 min. Then mobile phase B was further increased to 82% at 11 min and quickly reached 99% in the next 0.5 min, followed by holding this percentage for another 0.5 min. Afterwards, the percentage of mobile phase B was taken back to starting conditions (15% mobile phase B) in 0.1 min to reequilibrate the column for the next injection (2.9 min).

LC-ESI-MS/MS experiments were operated in both positive and negative modes with injection volumes of 3 μL for positive and 5 μL for negative mode. An MS full-scan experiment with mass range *m/z* of 50 to 1,250 was selected, while different SWATH windows were acquired for MS/MS experiments (Table S3). The ion source temperature was set to 350°C with curtain gas (CUR), nebulizer gas (GS1), and heater gas (GS2) pressures 35 lb/in^2, 60 lb/in^2, and 60 lb/in^2, respectively, for both modes. The ion spray voltage was set to 5,500 V in the positive mode and −4,500 V in negative mode. The declustering potential (DP) was adjusted to 80 V and −80 V for positive and negative polarity modes, respectively. The cycle time was always 720 ms. The collision energy (CE) and collision energy spread (CES) for each experiment are shown in Table S3. The sequence was started with three injections of IS mixture as a system suitability test. The whole sequence was controlled by injection of QC samples after every five samples.

Effects of FAs, lipids, and PGs on Rom activity. The effects of FAs (pentadecanoic acid, palmitic acid, and stearic acid) and PGs [PG(18:0) and Lys- PG(18:1)] on Rom activity were determined in a 48-well microplate reader in BM at 37°C with shaking overnight. The OD_{578} was determined every 2 h for 24 h. All experiments were conducted in three independent biological replicates.

Solubilization of Rom and PG(32:0). Since PG(32:0) was insoluble in all organic solvents tested, an organic solvent mixture (chloroform- methanol-water at 65:35:8 [vol/vol/vol]) was used to dissolve it. However, this solvent mixture was not suitable to be used for ITC because of the volatilization of chloroform; thus, PG(32:0) was prepared as vesicles formed in 10% DMSO/PBS and used for ITC and DLS. Rom, on the other hand, was soluble in all organic solvents tested but not in water; thus, it was first dissolved in 100% DMSO and subsequently diluted in 10% DMSO/PBS. Thus, both compounds were dissolved in the same solvent, which is a prerequisite for ITC studies.

Preparation of PG vesicles and determination of size distribution by DLS. PG(32:0), 1,2-dipalmitoyl-*sn*-glycero-3-phospho-(1′-rac-glycerol) (sodium salt), was purchased from Avanti Polar Lipids Inc. PG powder was dissolved in organic solvent (chloroform-methanol-water at 65:35:8 [vol/vol/vol]) in a glass tube. The lipid was dried completely by evaporator for 2 h and exicator overnight. The dried lipid film was weighed, dissolved in buffer (10% DMSO/PBS), adjusted to a concentration of 5 mM, and treated in an ultrasonic bath for 2 h. The lipid dispersion was transferred to an Eppendorf tube and subjected to ultrasonication (Titan tip) four times, each for 2 min. Subsequently, the size distribution of the vesicles was determined by DLS.

ITC. ITC experiments were performed using a MicroCal PEAQ-ITC calorimeter (Malvern). PG(32:0) vesicles and Rom were dissolved in 10% DMSO/PBS (1:9 [vol/vol]) and degassed via vacuum before titration. An initial volume of 0.4 μL followed by 18 injections of 2 μL of PG(32:0) vesicles was injected into the cell with Rom solution. Injection of PG(32:0) vesicles into 10% DMSO was used as a control to correct the heat of dilution. The measurements were carried out at 37°C with stirring at 750 rpm with 150-s intervals. The final data were analyzed via the "one-site-binding" model to determine the binding affinity (K_D), enthalpy (ΔH) and entropy (ΔS) of binding and stoichiometry (n).

Static and dynamics light scattering (SLS/DLS). The SLS/DLS experiments were performed using an ALVCGS3 setup with a wavelength of 632.8 nm. The CONTIN analysis was performed using the light scattering software provided by ALV. Toluene and water were used as the standard and solvent for all measurements. The hydrodynamic radius obtained at 90° was used to describe the size of PG(32:0) vesicles and Rom clusters.

Data visualization and analysis. The growth curves and bar charts were visualized using GraphPad Prism 6.0 software. Mann-Whitney U test was applied to compare significant differences between HG001 and RomR. R was employed for performing the Mann-Whitney U test.

Data availability. The main data supporting the findings of this work are available within the article and the supplemental material files or from the corresponding author upon request.

SUPPLEMENTAL MATERIAL

Supplemental material is available online only.

FIG S1, PDF file, 0.2 MB.

FIG S2, PDF file, 0.1 MB.

FIG S3, PDF file, 0.1 MB.

FIG S4, PDF file, 0.2 MB.

FIG S5, PDF file, 0.3 MB.

FIG S6, PDF file, 0.1 MB.
TABLE S1, DOCX file, 0.02 MB.
TABLE S2, DOCX file, 0.01 MB.
TABLE S3, DOCX file, 0.02 MB.

ACKNOWLEDGMENTS

This work was supported by funding from the Deutsche Forschungsgemeinschaft (DFG) TRR 261 (project 39896743). L.H. was supported by the Chinese Scholarship Council. We acknowledge the support by Open Access Publishing Fund of University of Tübingen.

We thank Libera Lo Presti for critically reading and editing the manuscript and Frank Böckler for helping to model the Rom-PG interaction. We acknowledge the infrastructural support by Deutsche Forschungsgemeinschaft, Germany's Excellence Strategy—EXC 2124 (project 390838134) "Controlling Microbes to Fight Infections" (CMFI).

F.G., Miki Matsuo, and L.H. conceived the idea and designed the study. L.H., Miki Matsuo, N.L., A.V.A., and S.-H.F. performed most of the experiments. Miki Matsuo, N.L., and F.O. carried out ITC. C.C. and X.F. performed the lipidomic analysis under the supervision of M.L., and these data were analyzed by C.C. M.U., F.H., and Martin Maier synthesized the rhodomyrtone (Rom). A.L. and M.S.W. analyzed the data. F.Z. carried out DLS. F.G., Miki Matsuo, L.H., and S.-H.F. wrote the manuscript.

REFERENCES

1. Salni D, Sargent MV, Skelton BW, Soediro I, Sutisna M, White AH, Yulinah E. 2002. Rhodomyrtone, an antibiotic from *Rhodomyrtus tomentosa*. Aust J Chem 55:229–232. https://doi.org/10.1071/CH01194.
2. Limsuwan S, Hesseling-Meinders A, Voravuthikunchai SP, van Dijl JM, Kayser O. 2011. Potential antibiotic and anti-infective effects of rhodomyrtone from *Rhodomyrtus tomentosa* (Aiton) Hassk. on *Streptococcus pyogenes* as revealed by proteomics. Phytomedicine 18:934–940. https://doi.org/10.1016/j.phymed.2011.02.007.
3. Saising J, Götz F, Dube L, Ziebandt AK, Voravuthikunchai SP. 2015. Inhibition of staphylococcal biofilm-related gene transcription by rhodomyrtone, a new antibacterial agent. Ann Microbiol 65:659–665. https://doi.org/10.1007/s13213-014-0904-1.
4. Saising J, Hiranrat A, Mahabusarakam W, Ongsakul M, Voravuthikunchai SP. 2008. Rhodomyrtone from Rhodomyrtus tomentosa (Aiton) Hassk. as a natural antibiotic for staphylococcal cutaneous infections. J Health Sci 54:589–595. https://doi.org/10.1248/jhs.54.589.
5. Saising J, Voravuthikunchai SP. 2012. Anti *Propionibacterium acnes* activity of rhodomyrtone, an effective compound from *Rhodomyrtus tomentosa* (Aiton) Hassk. leaves. Anaerobe 18:400–404. https://doi.org/10.1016/j.anaerobe.2012.05.003.
6. Voravuthikunchai SP, Dolah S, Charernjiratrakul W. 2010. Control of *Bacillus cereus* in foods by Rhodomyrtus tomentosa (Ait.) Hassk. leaf extract and its purified compound. J Food Prot 73:1907–1912. https://doi.org/10.4315/0362-028x-73.10.1907.
7. Zhao L, Liu H, Huo L, Wang M, Yang B, Zhang W, Xu Z, Tan H, Qiu SX. 2018. Structural optimization and antibacterial evaluation of rhodomyrtosone B analogues against MRSA strains. Medchemcomm 9:1698–1707. https://doi.org/10.1039/c8md00257f.
8. Morkunas M, Dube L, Götz F, Maier ME. 2013. Synthesis of the acylphloroglucinols rhodomyrtone and rhodomyrtosone B. Tetrahedron 69:8559–8563. https://doi.org/10.1016/j.tet.2013.07.091.
9. Morkunas M, Maier ME. 2015. Alternative routes to the acylphloroglucinol rhodomyrtone. Tetrahedron 71:9662–9666. https://doi.org/10.1016/j.tet.2015.10.063.
10. Saising J, Nguyen MT, Härtner T, Ebner P, Al Mamun Bhuyan A, Berscheid A, Muehlenkamp M, Schakermann S, Kumari N, Maier ME, Voravuthikunchai SP, Bandow J, Lang F, Brötz-Oesterhelt H, Götz F. 2018. Rhodomyrtone (Rom) is a membrane-active compound. Biochim Biophys Acta Biomembr 1860:1114–1124. https://doi.org/10.1016/j.bbamem.2018.01.011.
11. Saeloh D, Wenzel M, Rungrotmongkol T, Hamoen LW, Tipmanee V, Voravuthikunchai SP. 2017. Effects of rhodomyrtone on Gram-positive bacterial tubulin homologue FtsZ. PeerJ 5:e2962. https://doi.org/10.7717/peerj.2962.
12. Nguyen MT, Saising J, Tribelli PM, Nega M, Diene SM, Francois P, Schrenzel J, Sproer C, Bunk B, Ebner P, Hertlein T, Kumari N, Härtner T, Wistuba D, Voravuthikunchai SP, Mader U, Ohlsen K, Götz F. 2019. Inactivation of *farR* causes high rhodomyrtone resistance and increased pathogenicity in *Staphylococcus aureus*. Front Microbiol 10:1157. https://doi.org/10.3389/fmicb.2019.01157.
13. Cuthbertson L, Nodwell JR. 2013. The TetR family of regulators. Microbiol Mol Biol Rev 77:440–475. https://doi.org/10.1128/MMBR.00018-13.
14. Alnaseri H, Arsic B, Schneider JE, Kaiser JC, Scinocca ZC, Heinrichs DE, McGavin MJ. 2015. Inducible expression of a resistance-nodulation-division-type efflux pump in *Staphylococcus aureus* provides resistance to linoleic and arachidonic acids. J Bacteriol 197:1893–1905. https://doi.org/10.1128/JB.02607-14.
15. Alnaseri H, Kuiack RC, Ferguson KA, Schneider JET, Heinrichs DE, McGavin MJ. 2019. DNA binding and sensor specificity of FarR, a novel TetR family regulator required for induction of the fatty acid efflux pump FarE in *Staphylococcus aureus*. J Bacteriol 201:e00602-18. https://doi.org/10.1128/JB.00602-18.
16. Nguyen MT, Hanzelmann D, Härtner T, Peschel A, Götz F. 2016. Skin-specific unsaturated fatty acids boost the *Staphylococcus aureus* innate immune response. Infect Immun 84:205–215. https://doi.org/10.1128/IAI.00822-15.
17. Ernst CM, Peschel A. 2011. Broad-spectrum antimicrobial peptide resistance by MprF-mediated aminoacylation and flipping of phospholipids. Mol Microbiol 80:290–299. https://doi.org/10.1111/j.1365-2958.2011.07576.x.
18. Ernst CM, Slavetinsky CJ, Kuhn S, Hauser JN, Nega M, Mishra NN, Gekeler C, Bayer AS, Peschel A. 2018. Gain-of-function mutations in the phospholipid flippase MprF confer specific daptomycin resistance. mBio 9:e01659-18. https://doi.org/10.1128/mBio.01659-18.
19. Adebusuyi AA, Foght JM. 2011. An alternative physiological role for the EmhABC efflux pump in *Pseudomonas fluorescens* cLP6a. BMC Microbiol 11:252. https://doi.org/10.1186/1471-2180-11-252.
20. Jiang JH, Hassan KA, Begg SL, Rupasinghe TWT, Naidu V, Pederick VG, Khorvash M, Whittall JJ, Paton JC, Paulsen IT, McDevitt CA, Peleg AY, Eijkelkamp BA. 2019. Identification of novel *Acinetobacter baumannii* host fatty acid stress adaptation strategies. mBio 10:e02056-18. https://doi.org/10.1128/mBio.02056-18.
21. Fischer W. 1994. Lipoteichoic acid and lipids in the membrane of *Staphylococcus aureus*. Med Microbiol Immunol 183:61–76. https://doi.org/10.1007/BF00277157.
22. Brundish DE, Shaw N, Baddiley J. 1966. Bacterial glycolipids. Glycosyl diglycerides in gram-positive bacteria. Biochem J 99:546–549. https://doi.org/10.1042/bj0990546.

23. Wieslander A, Christiansson A, Rilfors L, Khan A, Johansson LB, Lindblom G. 1982. Lipid phase structure in the regulation of lipid composition in *Acholeplasma laidlawii* membranes. Rev Infect Dis 4(Suppl):S43–S49. https://doi.org/10.1093/clinids/4.supplement_1.s43.
24. Sen S, Sirobhushanam S, Johnson SR, Song Y, Tefft R, Gatto C, Wilkinson BJ. 2016. Growth-environment dependent modulation of *Staphylococcus aureus* branched-chain to straight-chain fatty acid ratio and incorporation of unsaturated fatty acids. PLoS One 11:e0165300. https://doi.org/10.1371/journal.pone.0165300.
25. Parsons JB, Frank MW, Jackson P, Subramanian C, Rock CO. 2014. Incorporation of extracellular fatty acids by a fatty acid kinase-dependent pathway in *Staphylococcus aureus*. Mol Microbiol 92:234–245. https://doi.org/10.1111/mmi.12556.
26. Tiwari KB, Gatto C, Wilkinson BJ. 2020. Plasticity of coagulase-negative staphylococcal membrane fatty acid composition and implications for responses to antimicrobial agents. Antibiotics (Basel) 9:214. https://doi.org/10.3390/antibiotics9050214.
27. Koprivnjak T, Zhang D, Ernst CM, Peschel A, Nauseef WM, Weiss JP. 2011. Characterization of *Staphylococcus aureus* cardiolipin synthases 1 and 2 and their contribution to accumulation of cardiolipin in stationary phase and within phagocytes. J Bacteriol 193:4134–4142. https://doi.org/10.1128/JB.00288-11.
28. Zhang H, Dudley EG, Harte F. 2017. Critical synergistic concentration of lecithin phospholipids improves the antimicrobial activity of eugenol against Escherichia coli. Appl Environ Microbiol 83:e01583-17. https://doi.org/10.1128/AEM.01583-17.
29. Kaloyanides GJ. 1992. Drug-phospholipid interactions: role in aminoglycoside nephrotoxicity. Ren Fail 14:351–357. https://doi.org/10.3109/08860229209106642.
30. Kovács E, Savopol T, Iordache M-M, Săplăcan L, Sobaru I, Istrate C, Mingeot-Leclercq M-P, Moisescu M-G. 2012. Interaction of gentamicin polycation with model and cell membranes. Bioelectrochemistry 87:230–235. https://doi.org/10.1016/j.bioelechem.2012.03.001.
31. Sautrey G, El Khoury M, Dos Santos AG, Zimmermann L, Deleu M, Lins L, Decout JL, Mingeot-Leclercq MP. 2016. Negatively charged lipids as a potential target for new amphiphilic aminoglycoside antibiotics: a biophysical study. J Biol Chem 291:13864–13874. https://doi.org/10.1074/jbc.M115.665364.
32. Pader V, Hakim S, Painter KL, Wigneshweraraj S, Clarke TB, Edwards AM. 2016. *Staphylococcus aureus* inactivates daptomycin by releasing membrane phospholipids. Nat Microbiol 2:16194. https://doi.org/10.1038/nmicrobiol.2016.194.
33. Burchall JJ, Elwell LP, Fling ME. 1982. Molecular mechanisms of resistance to trimethoprim. Rev Infect Dis 4:246–254. https://doi.org/10.1093/clinids/4.2.246.
34. Banerjee A, Dubnau E, Quemard A, Balasubramanian V, Um KS, Wilson T, Collins D, de Lisle G, Jacobs WR, Jr. 1994. inhA, a gene encoding a target for isoniazid and ethionamide in *Mycobacterium tuberculosis*. Science 263:227–230. https://doi.org/10.1126/science.8284673.
35. Fenner L, Egger M, Bodmer T, Altpeter E, Zwahlen M, Jaton K, Pfyffer GE, Borrell S, Dubuis O, Bruderer T, Siegrist HH, Furrer H, Calmy A, Fehr J, Stalder JM, Ninet B, Bottger EC, Gagneux S, Swiss HIV Cohort Study, Swiss Molecular Epidemiology of Tuberculosis Study Group. 2012. Effect of mutation and genetic background on drug resistance in *Mycobacterium tuberculosis*. Antimicrob Agents Chemother 56:3047–3053. https://doi.org/10.1128/AAC.06460-11.
36. Caceres NE, Harris NB, Wellehan JF, Feng Z, Kapur V, Barletta RG. 1997. Overexpression of the D-alanine racemase gene confers resistance to D-cycloserine in *Mycobacterium smegmatis*. J Bacteriol 179:5046–5055. https://doi.org/10.1128/jb.179.16.5046-5055.1997.
37. Schreiber K, Sciascia S, de Groot PG, Devreese K, Jacobsen S, Ruiz-Irastorza G, Salmon JE, Shoenfeld Y, Shovman O, Hunt BJ. 2018. Antiphospholipid syndrome. Nat Rev Dis Primers 4:17103. https://doi.org/10.1038/nrdp.2017.103.
38. Rudin L, Sjöström J-E, Lindberg M, Philipson L. 1974. Factors affecting competence for transformation in Staphylococcus aureus. J Bacteriol 118:155–164. https://doi.org/10.1128/jb.118.1.155-164.1974.
39. Geiger T, Francois P, Liebeke M, Fraunholz M, Goerke C, Krismer B, Schrenzel J, Lalk M, Wolz C. 2012. The stringent response of Staphylococcus aureus and its impact on survival after phagocytosis through the induction of intracellular PSMs expression. PLoS Pathog 8:e1003016. https://doi.org/10.1371/journal.ppat.1003016.
40. Brückner R. 1997. Gene replacement in Staphylococcus carnosus and Staphylococcus xylosus. FEMS Microbiol Lett 151:1–8. https://doi.org/10.1111/j.1574-6968.1997.tb10387.x.
41. Bae T, Schneewind O. 2006. Allelic replacement in Staphylococcus aureus with inducible counter-selection. Plasmid 55:58–63. https://doi.org/10.1016/j.plasmid.2005.05.005.
42. Luqman A, Nega M, Nguyen M-T, Ebner P, Götz F. 2018. SadA-expressing staphylococci in the human gut show increased cell adherence and internalization. Cell Rep 22:535–545. https://doi.org/10.1016/j.celrep.2017.12.058.
43. Wang H, Kraus F, Popella P, Baykal A, Guttroff C, Francois P, Sass P, Plietker B, Götz F. 2019. The polycyclic polyprenylated acylphloroglucinol antibiotic PPAP 23 targets the membrane and iron metabolism in Staphylococcus aureus. Front Microbiol 10:14. https://doi.org/10.3389/fmicb.2019.00014.
44. Matyash V, Liebisch G, Kurzchalia TV, Shevchenko A, Schwudke D. 2008. Lipid extraction by methyl-tert-butyl ether for high-throughput lipidomics. J Lipid Res 49:1137–1146. https://doi.org/10.1194/jlr.D700041-JLR200.
45. Calderón C, Sanwald C, Schlotterbeck J, Drotleff B, Lämmerhofer M. 2019. Comparison of simple monophasic versus classical biphasic extraction protocols for comprehensive UHPLC-MS/MS lipidomic analysis of Hela cells. Anal Chim Acta 1048:66–74. https://doi.org/10.1016/j.aca.2018.10.035.

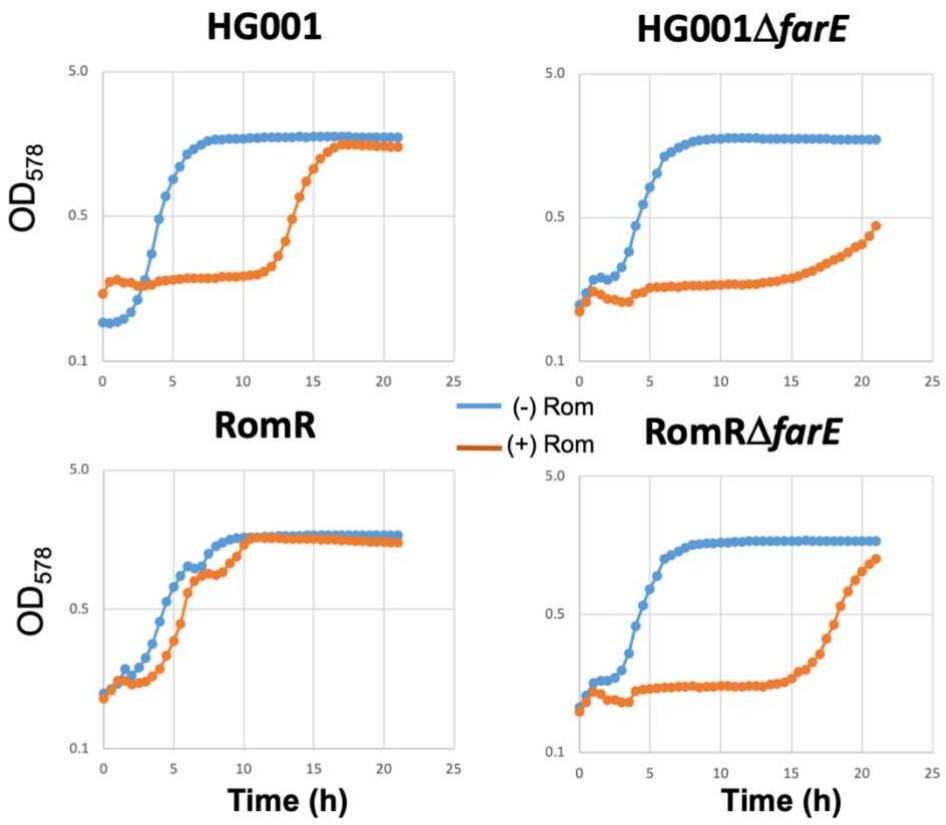

Figure S1. Impact of Rom on the growth of HG001 and RomR and their respective Δ*farE* mutants. The growth of the *S. aureus* clones in BM supplemented with Rom (8 μg/ml) was followed for 24 h. Growth of HG001 was inhibited for about 12 h but resumed thereafter; growth of HG001Δ*farE* was inhibited for the whole period. Growth of RomR mutant was unaffected in the presence of Rom (completely resistant to Rom), while the growth of RomRΔ*farE* was inhibited for about 15 h, and resumed thereafter. The result indicate that FarE is crucial for Rom resistance. The graph shown here is a representative of one of the triplicates growth studies performed.

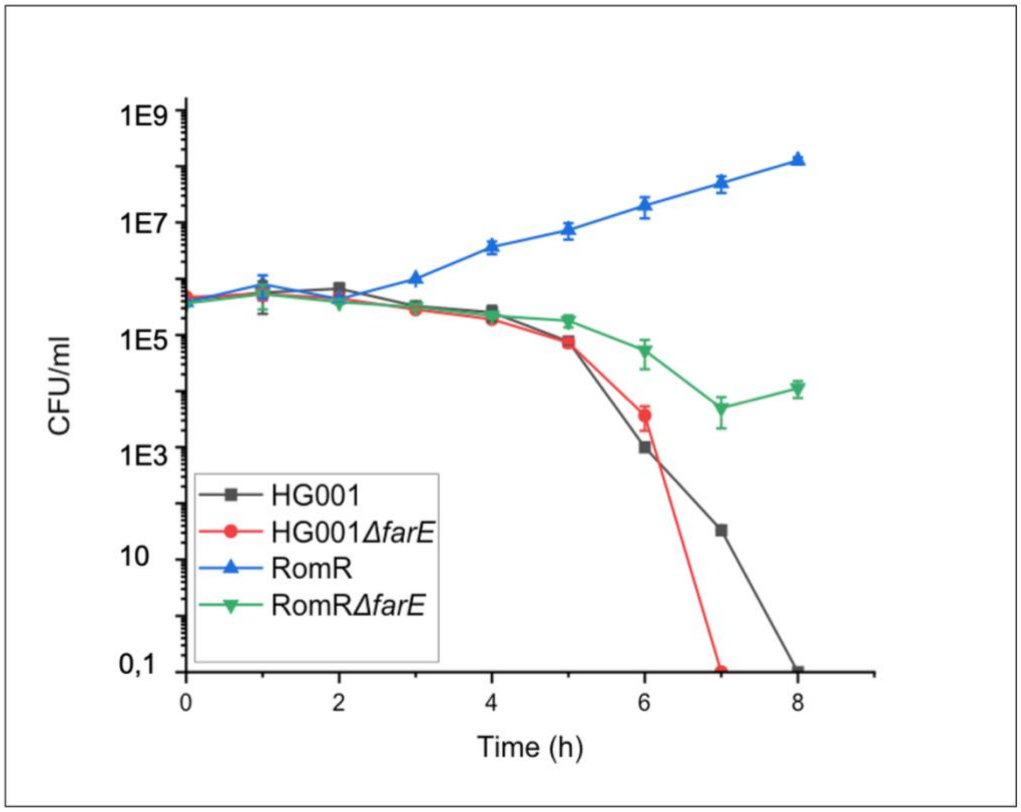

Figure S2. Impact of Rom on the killing of HG001 and RomR and their respective Δ*farE* mutants. The killing of the *S. aureus* clones in BM supplemented with Rom (8 μg/ml) was followed for 8 h. Cells were inoculated to a cell concentration of about 6 x 10^5 cfu/ml. HG001 and HG001Δ*farE* were almost completely killed after 7-8 h, while growth of the RomR mutant continued. With RomRΔ*farE* mutant, killing was also observed, but it was markedly delayed compared to HG001 and HG001Δ*farE*. Each bar represents the mean ± SD from three independent biological replicates.

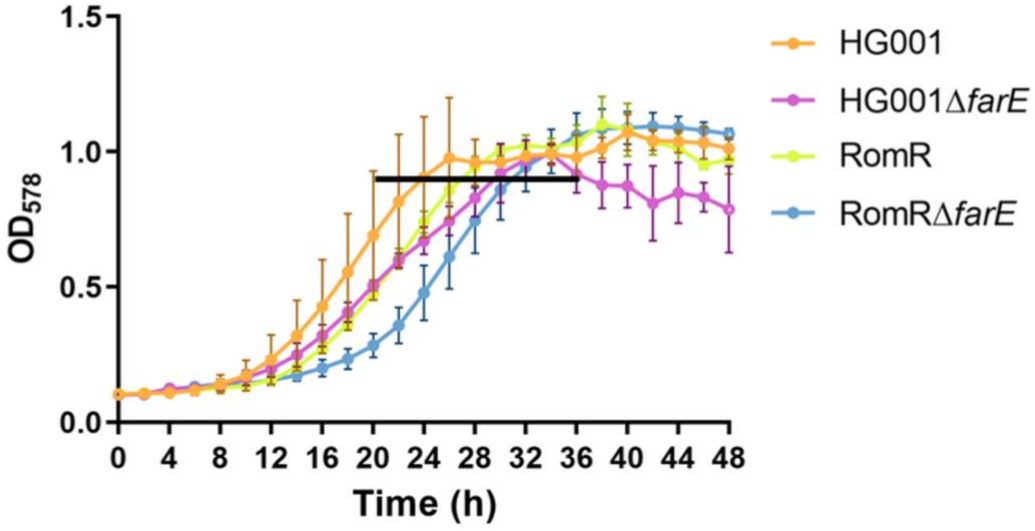

Figure S3. Comparative growth of HG001 and its mutants in defined minimal medium (AAM) using a microplate reader. Each point in the graph is the mean ± SD of three independent biological replicates; bar, indicates end-exponential phase (OD_{578} ≈ 0.9) at which the cells were harvested for lipidomic analysis.

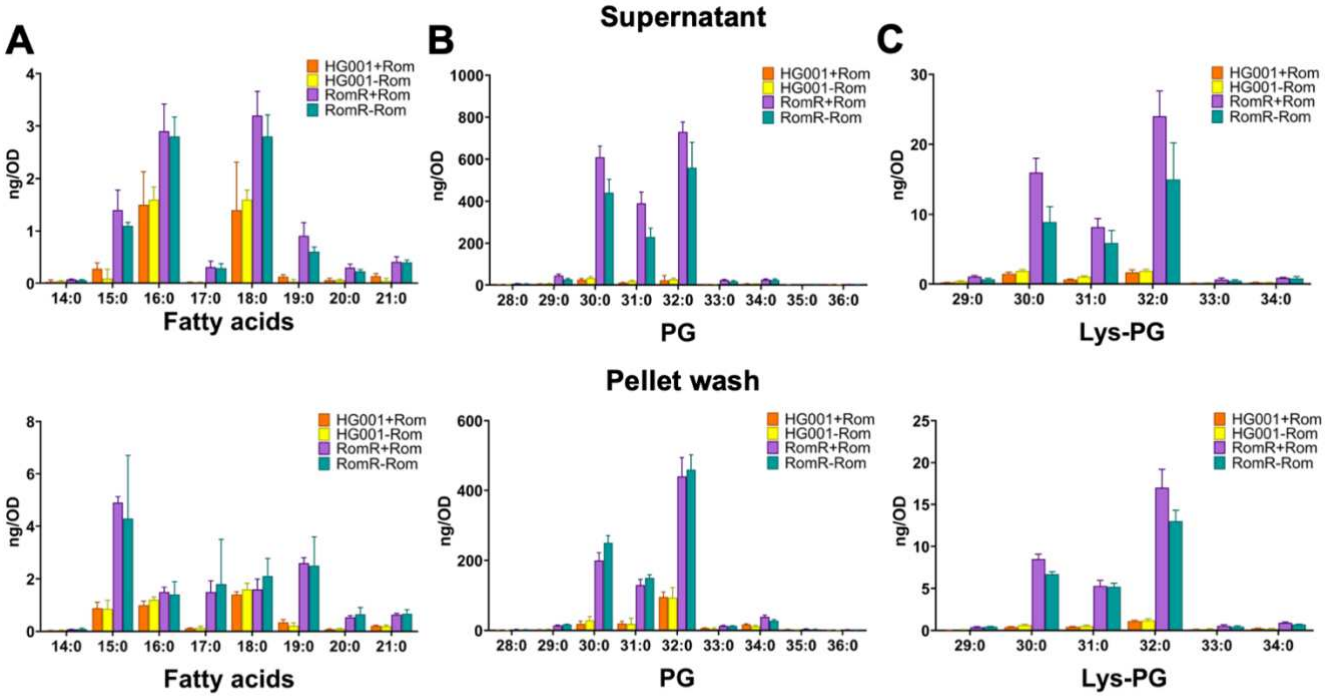

Figure S4. Effect of sub-inhibitory concentrations of Rom on the release of fatty acids and lipids by the *S. aureus* HG001 and RomR strains in the supernatant (above) and pellet wash (below). The bar charts show the amount of (**A**) fatty acids ranging from C14:0 to C21:0 (**B**) phosphatidylglycerol (PG) ranging from C28:0 to C36:0 and (**C**) lysyl phosphatidylglycerol (Lys-PG) ranging from C29:0 to C:34 detected in both the strains in the presence of sub-inhibitory concentration of Rom at 0.3 µg/ml. All absolute amounts of FAs and lipids were reported in ng/OD_{578} of the bacterial cultures grown until end exponential phase and adjusted to the corresponding OD_{578} = 1.0. The supernatant and pellet were separated by centrifugation for lipidomic analyses. The pellet wash was obtained by treating the pellets with 90% isopropanol to remove the fatty acids and lipids from the surface of cells. Each bar shown in the chart represents the mean ± SD from five independent biological replicates.

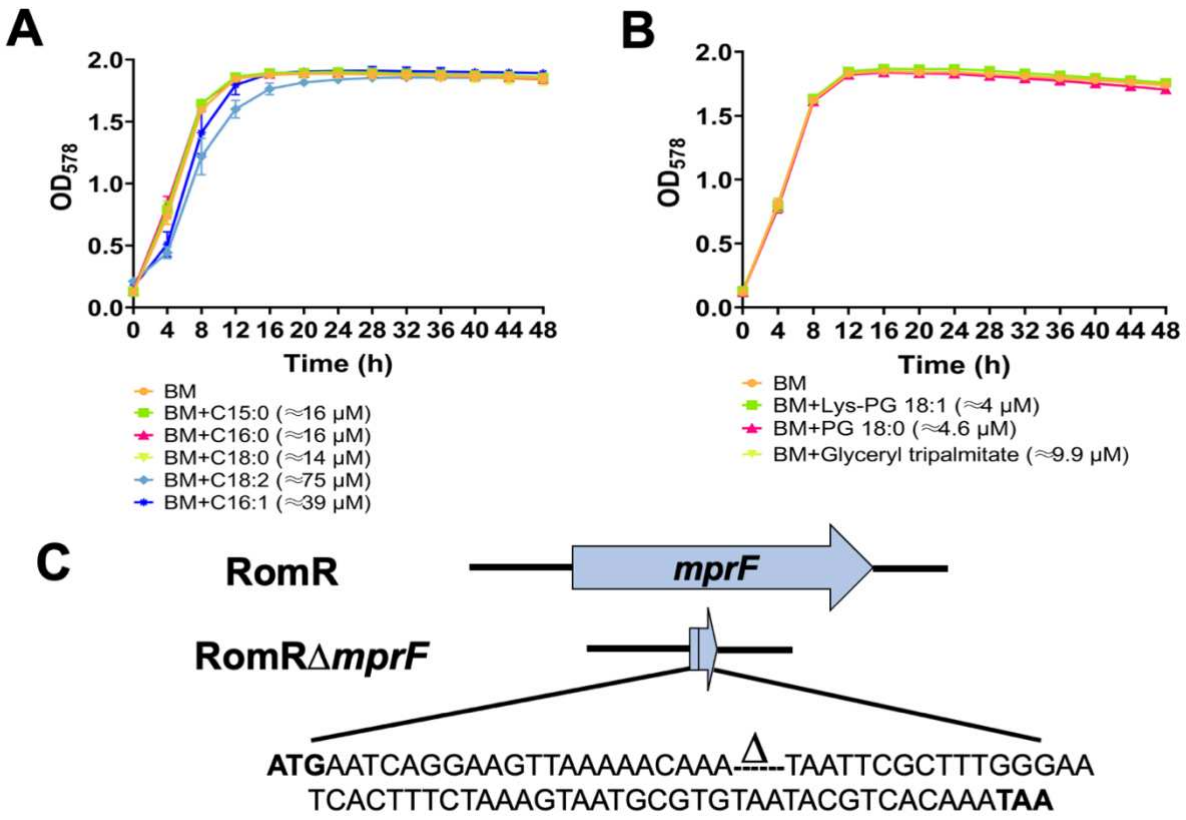

Figure S5. Impact of exogenous supplementation of FAs / lipids on the growth of HG001 and construction of RomRΔ*mprF*. The growth of *S. aureus* HG001 in BM with supplementations of (**A**) fatty acids at 4 μg/ml C15:0 (≈16 μM), 4 μg/ml C18:0 (≈14 μM), 4 μg/ml C16:0 (≈16 μM), 10 μg/ml C16:1 (≈39 μM) 21 μg/ml C18:2 (≈75 μM); (**B**) lipids at 4 μg/ml PG 18:0 (≈4.6 μM), 4 μg/ml Lys-PG 18:1 (≈4 μM). Well containing BM only and bacteria was regarded as positive control. Growth of the bacteria was measured at OD_{578} every 4 h for 48 h using a microplate reader Varioskan Lux (Thermo Scientific) in a 48 wells plate. Each point in the graph is the mean ± SD from three independent biological replicates. (**C**) Illustration of RomRΔ*mprF* deletion mutant.

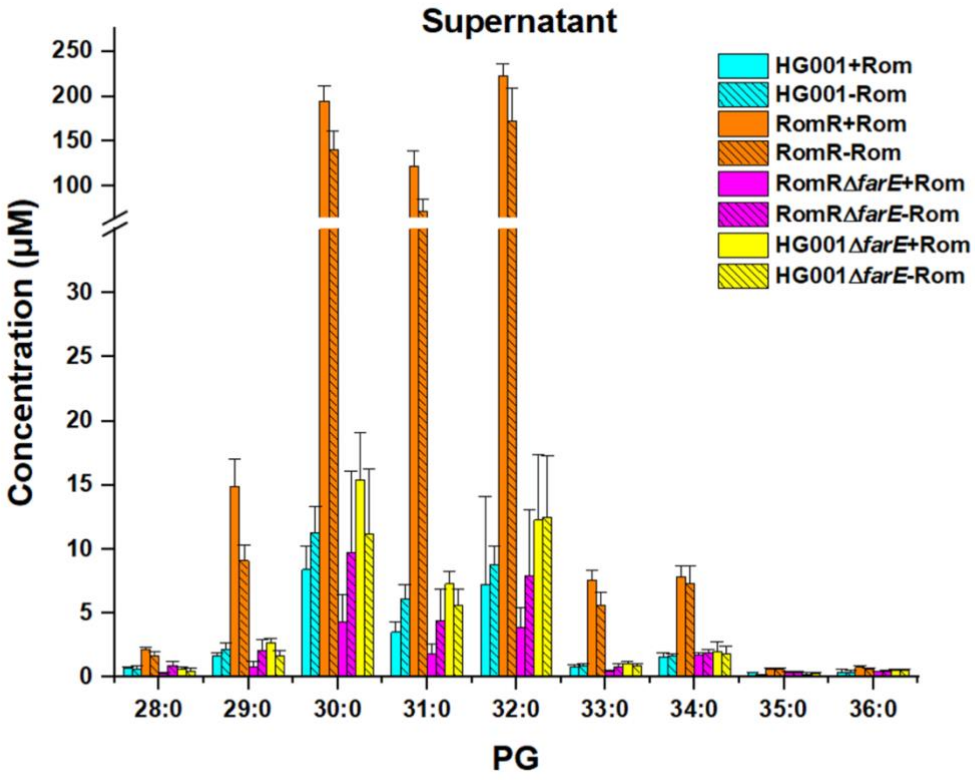

Figure S6. Lipidomic analysis in supernatants only for PGs in HG001, RomR, HG001Δ*farE* and RomRΔ*farE* in the absence and presence of Rom. This illustration is similar to the one in Fig. 2. The only difference is that here, we show the molarity (and not ng/OD) of PGs in the supernatant. The PGs ranged from C28:0 to C36:0. It is observed that the presence of sublethal concentration of Rom did not alter much the PG release.